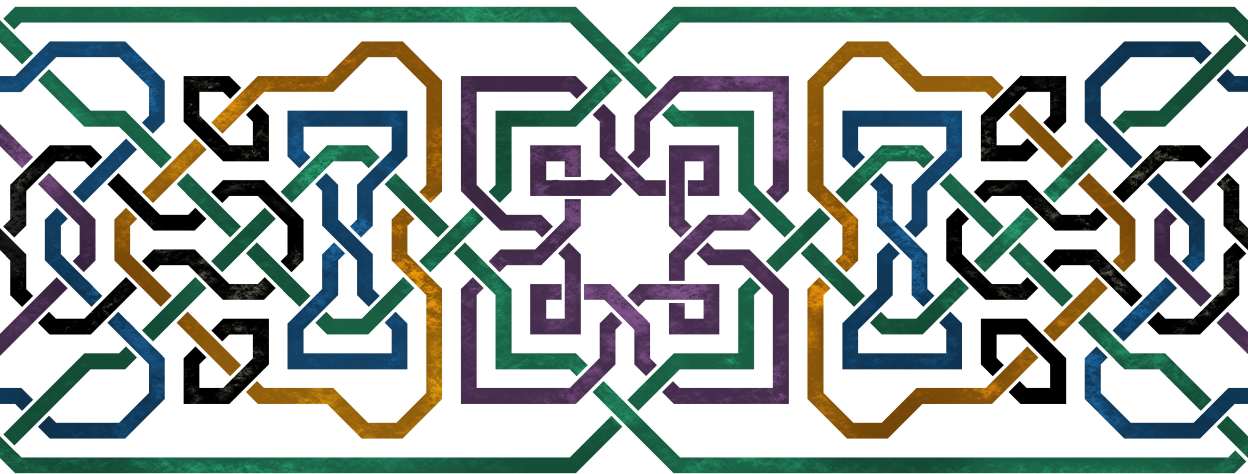# Topology off the beaten path

From critical to non-Hermitian systems

Carlos Ortega-Taberner

Topology off the beaten path
From critical to non-Hermitian systems

Carlos Ortega-Taberner

Abstract
A central topic in condensed matter research during the last decades has been the study and classification of topological phases of matter. Topological insulators in particular, a subset of symmetry protected topological phases, have been investigated for over a decade. In recent years, several extensions to this formalism have been proposed to study more unconventional systems.In this thesis we explore two of these extensions, where key assumptions in the original formalism are removed. The first case is critical systems, which have no energy gap. Conventional topological invariants are discontinuous at topological transitions, and therefore not well-defined for critical systems. We propose a method for generalizing conventional topological invariants to critical systems and show robustness to disorder that preserves criticality. The second case involves non-Hermitian systems, which appear in effective descriptions of dissipation, where we study the entanglement spectrum and its connection to topological invariants. Furthermore, by introducing non-Hermiticity to critical systems we show how the winding numbers that characterize some topological phases of the non-Hermitian system, as well as topological signatures in the entanglement spectrum, can be obtained from the related critical model.

Keywords: *Topological phases, Critical systems, Non-Hermitian systems.*

Department of Physics

Stockholm University, 106 91 Stockholm

TOPOLOGY OFF THE BEATEN PATH

Carlos Ortega-Taberner

Topology off the beaten path

From critical to non-Hermitian systems

Carlos Ortega-Taberner

Cover art by Ana Romero Aranda

Abstract

A central topic in condensed matter research during the last decades has been the study and classification of topological phases of matter. Topological insulators in particular, a subset of symmetry protected topological phases, have been investigated for over a decade. In recent years, several extensions to this formalism have been proposed to study more unconventional systems. In this thesis we explore two of these extensions, where key assumptions in the original formalism are removed. The first case is critical systems, which have no energy gap. Conventional topological invariants are discontinuous at topological transitions, and therefore not well-defined for critical systems. We propose a method for generalizing conventional topological invariants to critical systems and show robustness to disorder that preserves criticality. The second case involves non-Hermitian systems, which appear in effective descriptions of dissipation, where we study the entanglement spectrum and its connection to topological invariants. Furthermore, by introducing non-Hermiticity to critical systems we show how the winding numbers that characterize some topological phases of the non-Hermitian system, as well as topological signatures in the entanglement spectrum, can be obtained from the related critical model.

Svensk sammanfattning

Klassificering av topologiska materiefaser har under de senaste decennierna varit ett centralt tema i forskningen om kondenserad materia. I synnerhet topologiska isolatorer, en undergrupp av symmetriskyddade topologiska faser, har studerats i över ett decennium. Under senare år har flera utvidgningar av denna formalism föreslagits för att studera mer okonventionella system.

I denna avhandling utforskar vi tvåav dessa utvidgningar, där antaganden som är viktiga i den ursprungliga teorin tagits bort. Det första fallet vi studerar är kritiska system utan energigap. Konventionella topologiska invarianter är diskontinuerliga vid topologiska övergångar och är därför inte väldefinierade för kritiska system. Vi föreslår en metod för att generalisera konventionella topologiska invarianter till kritiska system och visar att dessa är robusta mot störningar som bevarar kritikalitet. Det andra fallet vi studerar handlar om icke-Hermitiska system, som beskriver dissipation, där vi undersöker sammanflätningsspektrumet och dess koppling till topologiska invarianter. Dessutom visar vi, genom att introducera icke-Hermiticitet till kritiska system, hur de omloppstal som kännetecknar vissa topologiska faser av det icke-Hermitiska systemet, samt topologiska signaturer i sammanflätningsspektrumet, kan erhållas från den relaterade kritiska modellen.

List of accompanying papers

The following papers are included in this dissertation:

Paper I **Relation of the entanglement spectrum to the bulk polarization**
Carlos Ortega-Taberner and Maria Hermanns
Phys. Rev. B 103, 195132 - Published 17 May 2021

Paper II **Polarization and entanglement spectrum in non-Hermitian systems**
Carlos Ortega-Taberner, Lukas Rødland, and Maria Hermanns
Phys. Rev. B 105, 075103 - Published 2 February 2022

Paper III **Quantization of topological indices in critical chains at low temperatures**
Oleksandr Balabanov, Carlos Ortega-Taberner, and Maria Hermanns
Phys. Rev. B 106, 045116 - Published 13 July 2022

Paper IV **From Hermitian critical to non-Hermitian point-gapped phases**
Carlos Ortega-Taberner and Maria Hermanns
arXiv:2211.13721

Additional papers written by the author during the PhD that are not included in this thesis:

Paper A **Anomalous Josephson current through a driven double quantum dot**
Carlos Ortega-Taberner, Antti-Pekka Jauho, Jens Paaske
arXiv:2207.06152

My contributions

Paper I   The study of the polarization and the proof of the relation to the entanglement occupancy spectrum was done by me, as well as the calculations and plots. I also wrote the initial draft of the manuscript.

Paper II   The extension of the proof to non-Hermitian systems was done mostly by me. The numerical calculations and plots were also done by me. I contributed to the writing of the paper.

Paper III   I contributed to the discussion regarding polarization. I carried out the numerical calculation in close collaboration with Oleksandr Balavanov and did all the figures. I studied the effects of disorder on the central charge and contributed to the writing of the paper.

Paper IV   I suggested the idea for the project. I carried out most of the calculations and wrote the initial draft.

Paper A   This paper is an extension of the work from my Master thesis. I proposed the idea leading to the project, performed all numerical calculations and contributed to the writing of the paper. The paper was finished during my PhD.

Note: Parts of this dissertation are based on my licentiate thesis [1]. In particular, Chapter 2 is heavily inspired by Chapters 2, 3 and 4 of the licentiate thesis. Parts of Chapter 1 in this thesis are also based on Chapter 1 in the licentiate thesis.

Acknowledgements

First and foremost, I want to thank Maria, my supervisor, for giving me the opportunity of embarking on this PhD, and for her invaluable guidance and support throughout this time. I am grateful for all the discussions we had and everything that I have learned from her, for constantly managing to make time for me and all my questions, and always answering them with good insight. I also want to thank her for the time dedicated to give me feedback on the few talks I had, as well as thoroughly proofreading this thesis. Thanks to everyone in Maria's group, Oleksandr, Lukas, Megha and Anna, for all our discussions and collaborations. Specially to Lukas, for all our conversations on non-Hermitian physics, and for proofreading parts of this thesis. I am also grateful to everyone that passed through KOF during my stay for always making the corridor a good work environment, including the faculty, postdocs, other students and the cleaning workers. Special thanks to my office mates before *the event*, Yoran, Iman and Axel, for answering all my physics and administrative questions when I first arrived and for making me feel welcomed. Thanks also to my office mates after *the event*, Carlos, Ilaria and Anna for all the great chats we had and for encouraging me during the writing of this thesis. Finally, I would like to thank Elisabet and Ahmed, who shared this journey with me, for all the conversations we had, and for their encouragement and support throughout this time.

I wish to express my gratitude to family, friends and others too: First to my parents, for always being supportive. Thanks to my friends Raffa and Laura, for making Copenhagen still feel hygge, as well as Roula and Lena, for making Hugin truly feel like a home. I am extremely grateful to my friend Ana, for always being there for me, and for helping me birth the cover art. I also wish to thank Facu and Ashewyn, for being my office mates during *the event* and for making working from home tolerable. Last but not least I want to express my deep gratitude to Carole and Lillemor, whom without their help this dissertation would have not been possible.

Contents

Chapter 1

Introduction

A recurrent problem in physics is that of classifying phases of matter. For the most part of last century, *Landau's theory of phase transitions* [2] was thought to provide a complete description of continuous phase transitions. In this formalism, phases are described by a local order parameter associated with a symmetry that is broken. This is the case, for example, with ferromagnets where a non-zero magnetization emerges below the Curie temperature, associated with a broken rotational symmetry of the spins [3].

The discovery of the integer quantum Hall effect [4–6] challenged this paradigm. A two dimensional electron gas under a strong perpendicular magnetic field was shown to have a transverse conductance quantized to integers of e^2/h, carried by gapless edge states. However, no local order parameter or symmetry breaking can be assigned to the different phases. The quantized conductance in these systems was found to be related to a topological quantity [7–9], the Chern number. Another important step towards understanding phases like the integer quantum Hall was taken by Haldane in 1988 [10]. He showed that the physics of the quantum Hall effect is not due to the Landau levels, but due to time-reversal symmetry being broken. He showed that a lattice model of free electrons with intrinsically broken time-reversal symmetry presented the same features as the integer quantum Hall effect, i.e. gapless edge states and quantization of the transverse conductance. Such systems are nowadays referred to as *Chern insulators.*

In the following decades many lattice models of free fermions were shown to have similar features. Systems such as the Su-Schrieffer-Heeger (SSH) chain [11, 12], or the quantum spin Hall (QSH) liquid [13, 14] cannot be described by Landau's theory. They host gapless edge modes and quantized observables which are characterized by topological invariants — objects computed from the bulk that characterize the topological phase. In particular the topological invariants give the number of topological gapless edge states found by imposing open boundary conditions.

This relation was coined the *bulk-boundary correspondence*. Unlike Chern insulators, however, these systems are not inherently robust and require the presence of symmetries. These phases are known as *symmetry protected topological phases* (SPT) [15]. A particular subset of these, known as topological insulators and superconductors, have been widely studied. The classification of these is now fully understood with the framework of *the ten-fold way* [16, 17], based on the classification of random matrices developed by Altland and Zirnbauer [18–21]. This formalism classifies Hamiltonians into different classes depending on their symmetries, and for each class and dimension tells us how many non-trivial topological phases are allowed, if any.

There are many different signatures of non-trivial topology that can be studied. Two important ones are the existence of gapless edge states and quantized observables which can be measured in transport experiments, such as the transverse conductance described above. The observable which we focus on in this thesis is the bulk polarization, which is a topological invariant in one dimension under certain symmetries. The polarization is a very simple physical observable when considering finite systems, where it is related to the accumulated surface charge. However, things become challenging when periodic boundary conditions are considered. A coherent description of the bulk polarization was not obtained until the development of the *modern theory of polarization* in the early 90's [22–27]. This theory has two important consequences. First, it was able to express the polarization as the geometric phase of the ground state. Furthermore, the resulting bulk polarization is only defined mod e. An important remark is that the bulk polarization cannot be understood as an absolute quantity. Only changes in the polarization, which generate measurable currents, are a physical quantity. However, three decades after the development of the modern theory of polarization the bulk polarization remains a source of confusion. It was only recently that an exhaustive study was done looking at the physical significance of different definitions of the bulk polarization that can be found in the literature, and the relations between them [28].

Another physical property that has been useful in the study of topology has been entanglement. It played an important role in understanding strongly correlated topological phases of matter [29]. In particular the entanglement entropy [30, 31] was shown to have a universal term that depends on the topology of the system, although it does not fully characterize the topological phase. Later on, the spectrum of the reduced density matrix, the *entanglement spectrum*, was shown to provide more information about the topology of the ground state in some cases [32,33]. For non-interacting topological insulators the entanglement spectrum is also known to provide knowledge about the edge spectrum [34], which in turn provides information about the topology of the system. It was shown by Peschel [35–37] that in

non-interacting systems the entanglement spectrum could be obtained from the spectrum of the subsystem correlation matrix, the *entanglement occupancy spectrum*. The entanglement occupancy spectrum has been used as a topological signature [38–40], however, it is still not fully understood how much information it encodes. In Chapter 2 we show an explicit connection to the bulk polarization.

One of the hallmarks of symmetry protected topological phases is that they are robust against perturbations unless they drive the system into a phase transition or they break the symmetries protecting the phase [15]. However, the fate of topological features becomes less clear as soon as one removes some of the prerequisites used to define conventional topological insulators. Examples include studies of amorphous systems [41, 42], topological crystalline insulators [43, 44], systems with criticality [45–50] or systems described by a non-Hermitian Hamiltonian [51–53]. In Chapters 3 and 4 we focus on the latter two, respectively.

For a long time critical systems were thought to be topologically trivial, in the sense that they could not hosts topological gapless edge modes. At the critical point, the correlation length diverges, thus allowing the topological edge states of the two edges to hybridize with each other and split from zero energy. This question was revisited recently [45, 46], showing that this is not correct and that systems at a critical point can indeed host topological edge states. Such systems, however, lie outside those studied by the ten-fold way, which explicitly assumes the existence of a gap. Furthermore, conventional topological invariants are not well-defined at critical points, as they must change by an integer value between two topological phases at both sides of the critical point. Therefore it seems that one needs new topological invariants to characterize these phases, as well as a new classification scheme. In Chapter 3 we explore how one can generalize conventional topological invariants to critical systems.

Non-Hermitian Hamiltonians have been used in physics to describe systems interacting with an environment [54–62]. Processes of dissipation and gain as the system exchanges energy or particles with the environment can be described effectively with non-Hermitian Hamiltonians, once the details about the environment are forgotten. Some examples are classical mechanical systems [62], photonic lattices [54–56] or quantum optics setups [61]. The study of topology in non-Hermitian systems has been a very active field in recent years [53,63–74], and a complete classification of topological phases was recently achieved [52]. However, the field is still somewhat new and many feautres known from Hermitian systems are not yet understood in the presence of Hermiticity. The two objects we focus on in this thesis, the entanglement occupancy spectrum and the bulk polarization have not yet been studied in depth. In this thesis we studied the entanglement occupancy spectrum of non-Hermitian systems and how it relates to their bulk topology, as discussed in

Chapter 4. We showed how the relation to the polarization we previously obtained for Hermitian systems, discussed in Chapter 1, still applies for some non-Hermitian phases. In addition, we showed that topological signatures are present for certain non-Hermitian phases which were previously overlooked [75, 76]. Furthermore, we show how some non-Hermitian phases and critical systems, which seem initially totally unrelated, share certain topological features. We showed how to obtain features of the non-Hermitian system from the critical system and vice versa. This might improve our understanding of topology in critical systems by using notions of non-Hermitian topology. Finally, in Chapter 5 we discuss the results in this thesis and comment on possible future directions.

Chapter 2

Topological insulators

As mentioned in the introduction, this thesis focuses on the study of *symmetry protected topological* (SPT) phases [15, 20, 77]. In particular, this chapter focuses on a subset of these, topological insulators of non-interacting fermions. The bulk of topological insulators is described by a gapped Hamiltonian. That is, it has a gap in its energy spectrum separating the occupied and empty bands where there are no states present. In the mathematical field of topology two objects, e.g. a sphere and a torus, are topologically distinct if they cannot be deformed into one another without tearing and gluing. These objects are characterized by a topological invariant, the genus, which counts the number of "holes" (0 for the sphere and 1 for the torus). Similarly, in the context of condensed matter and SPT phases, two gapped Hamiltonians are said to be topologically distinct if they cannot be adiabatically deformed into each other unless the symmetries of the system are broken or the bulk gap closes, such that the system undergoes a quantum phase transition. Topological invariants are also defined for the Hamiltonians. These are objects computed from the bulk that take discrete values for distinct topological phases and thus identify the topology of the system.

One characteristic property of topological insulating phases is that their boundary is gapless [15]. In 1D this translates to zero-energy edge modes, while in 2D the edge-modes connect the occupied and empty bands. Due to the symmetries these edge-modes are robust, i.e. they are not sensitive to symmetry-conserving disorder unless the disorder closes the bulk gap. In some exceptional cases, the boundary of a SPT phase can also be gapped, in which case it must have topological order [15], or it spontaneously breaks the symmetry that protects the topological phase. The classification of non-interacting topological insulators protected by non-unitarily realized symmetries is fully understood with the *ten-fold way* framework [15, 20], which we discuss in section 2.2.

After the discovery of the integer quantum Hall effect, Haldane took an impor-

tant step towards understanding topological insulators [10]. He showed that the topological properties of the integer quantum Hall effect do not require Landau levels by constructing a lattice model with intrinsically broken time reversal symmetry and similar topological properties. Two decades later, Kane and Mele [13] proposed a similar phase, the quantum spin hall effect. They predicted this phase to appear in graphene with spin-orbit coupling, a model similar to the one considered by Haldane. However, spin-orbit coupling in graphene turned out to be too small for this phase to be observable. Bernevig, Hughes and Zhang [78] predicted the existence of the quantum spin Hall effect in 2D HgCdTe quantum well heterostructures under a strain. Transport experiments were later shown to be consistent with this prediction [79], having a quantized conductance as expected for a bulk insulator with gapless edge states. Other candidates for 2D topological insulators have also been confirmed experimentally, such as InAs/GaSb quantum wells [80], mono and bi-layer Bismuth [81, 82] or layered transition metal dichalcogenides [83, 84].

Soon after the discovery of the quantum spin Hall effect in 2D, generalizations to 3D were proposed [85–87] and the term "topological insulator" was coined [87]. This was followed by the experimental confirmation of a topological phase in the 3D semiconducting alloy $Bi_{1-x}Sb_x$ [88]. In 3D materials transport experiments are more difficult to realize. However, by using angle resolved photoemission spectroscopy (ARPES) the surface of the material could be studied and gapless edge states were shown occur. Several other materials followed, such as Bi_2Se_3 [89], $BiTe_3$ [90, 91] and many others [92]. However, as opposed to $Bi_{1-x}Sb_x$, most of the other materials are not strictly insulators. They are metals or semimetals that can host topological gapless edge states in parts of their Brillouin zone which are gapped.

There are other materials which are also not topological insulators but share some of their topological properties. This is the case of topological superconductors [93], which are not insulators but present a gap in the spectrum. Topological superconductors are classified with the same *ten-fold way* that classifies topological insulators. Of particular importance are 1D topological superconductors, introduced first by Kitaev [94]. Signatures consistent with a topological superconducting phase were later found in hybrid superconductor-semiconductor nanowires [95]. Another relevant class of materials are Weyl semimetals [96–98]. These are 3D materials with topologically protected band crossings, known as Weyl points. Cuts through the Brillouin zone avoiding these points can be interpreted as Chern insulators. The Chern number of the two-dimensional cuts can only change when crossing a Weyl point. As a whole, Weyl semimetals are topologically trivial. However, the non-trivial topology of the lower dimensional cuts leads to the existence of gapless edge states, known as Fermi arcs, which connect pairs of Weyl points.

In 1D one of the prototypical examples of a topological insulator, and one of the most studied due to its simplicity, is the Su-Schrieffer-Hegger (SSH) chain [11, 12] — a model inspired by polyacetylene that describes spinless electrons in a chain of one orbital sites with staggered hopping. It has two topological phases that can be distinguished by the bulk polarization, which is quantized and takes only two values. Both the topological edge states and a quantized topological invariant have been observed experimentally [99, 100]. Throughout this thesis we employ an extension of this model, which we introduce in Section 2.1.1.

2.1 Tight-binding Hamiltonian and Bloch states

In this thesis we employ tight-binding Hamiltonians to describe the systems we study. In this section we introduce the tight-binding Hamiltonian and set the notation we will use throughout the rest of the thesis. We will also present the Bloch Hamiltonian for systems with translational invariance with the same purpose.

Consider the general second-quantized quadratic Hamiltonian

$$\mathcal{H} = \sum_{ij=1}^{L} \sum_{\alpha\beta=1}^{M} c_{i\alpha}^{\dagger} H_{i\alpha,j\beta} c_{j\beta}, \tag{2.1}$$

where unless we say otherwise, we use latin indices for the position of the L sites and greek indices to label the M orbitals at each site. Writing the fermionic operators as vector $c = (c_{11}, ...c_{1M}, ..., c_{L1}, ..., c_{LM})^T$ the Hamiltonian is $\mathcal{H} = c^{\dagger} H c$, which can be diagonalized by a transformation $c = U\gamma$, where U is a unitary matrix such that $U^{\dagger} H U = \hat{E}$ is diagonal. The matrix H is called the first-quantized Hamiltonian or single-particle Hamiltonian. Defining the unitary matrix elements as $(U)_{p\mu,i\alpha} = \psi_{i\alpha}^{p\mu}$ the transformation between the different fermionic operators is

$$\gamma_{p\mu}^{\dagger} = \sum_{i\alpha} c_{i\alpha}^{\dagger} \psi_{p\mu}^{i\alpha}, \quad \gamma_{p\mu} = \sum_{i\alpha} \psi_{p\mu}^{i\alpha *} c_{i\alpha}$$

$$c_{i\alpha}^{\dagger} = \sum_{p\mu} \gamma_{p\mu}^{\dagger} \psi_{p\mu}^{* i\alpha}, \quad c_{i\alpha} = \sum_{p\mu} \psi_{p\mu}^{i\alpha} \gamma_{p\mu}. \tag{2.2}$$

We can define now the single-particle eigenstates

$$\begin{aligned} |\psi_{p\mu}\rangle &= \gamma_{p\mu}^{\dagger} |0\rangle \\ &= \sum_{i\alpha} c_{i\alpha}^{\dagger} \psi_{p\mu}^{i\alpha} |0\rangle, \end{aligned} \tag{2.3}$$

that have the components $\langle i\alpha|\psi_{p\mu}\rangle = \psi_{p\mu}^{i\alpha}$. The condition that $U^\dagger H U$ is diagonal gives the eigenvalue equation

$$\sum H_{i\alpha,j\beta}\psi_{p\mu}^{j\beta} = E_{p\mu}\psi_{p\mu}^{i\alpha} \tag{2.4}$$

or $H\,|\psi_{p\mu}\rangle = E_{p\mu}\,|\psi_{p\mu}\rangle$.

Assuming now that the Hamiltonian H is translational invariant, the single-particle eigenstates $|\psi_{k\mu}\rangle$ are labeled by their momentum $k = n2\pi/L$, with the integer $n = [1, L]$, and their components can be written as $\psi_{k\mu}^{j\alpha} = e^{ikj}u_{k\mu}^{\alpha}$.

The eigenvalue equation for the single-particle eigenstates then becomes

$$\sum_{j\beta} H_{lj,\alpha\beta}e^{ikj}u_{k\mu}^{\beta} = E_{k\mu}e^{ikl}u_{k\mu}^{\alpha}$$

$$\sum_{\beta} H_{k,\alpha\beta}u_{k\mu}^{\beta} = E_{k\mu}u_{k\mu}^{\alpha}, \tag{2.5}$$

where the Fourier transformed H_k is the Bloch Hamiltonian. Our single particle eigenstates $|\psi_{k\mu}\rangle$ are the Bloch waves and the states $|u_{k\mu}\rangle$ are their periodic part. In the following we will consider a model with a single-site unit cell, this makes these states periodic in momentum as well, $|u_{k+2\pi,\mu}\rangle = |u_{k,\mu}\rangle$.

2.1.1 SSH and Shockley models

At the beginning of this chapter we mentioned the SSH chain, describing spinless electrons in a chain of one orbital sites with staggered hopping, see Fig.2.1.(a). This is one of the most widely studied models for topological insulators, given by the Hamiltonian

$$H = \sum_j (t + (-1)^j\delta)c_{j+1}^\dagger c_j. \tag{2.6}$$

Throughout this thesis and in the accompanying papers we use a similar model where instead of having one orbital per site and two sites per unit cell, we have two orbitals per site and one site per unit cell. This is known as the Shockley model [101, 102], a model describing electrons in a one dimensional chain of atoms with orbitals s and p_x, see Fig.2.1.(b). The two models have equivalent Hamiltonians except for the spacial distribution of their eigenstates. This, however, makes a key difference when considering the polarization, which we study in Section 2.3.2. We nevertheless refer to the models used as SSH, as it is more widely known in the community. In order to realize a larger variety of topological phases we employ
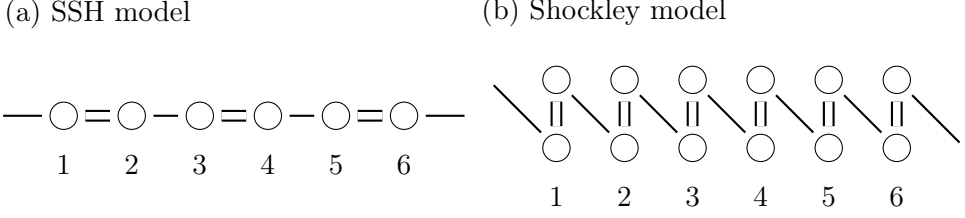
(a) SSH model

(b) Shockley model

Figure 2.1: Diagram of the (a) SSH model and (b) Shockley model . Circles represent different orbitals with the staggered hopping represented by single and double lines. The numbers represent the position of each site in real space. While the SSH chain consists of single orbital sites, the Shockley model corresponds to two states per site. Apart from their spatial distribution the models are otherwise equivalent.

an extension to the model by adding a second neighbour hopping, see Fig. 2.2. We refer to this as *long-range SSH model*, given by the Hamiltonian

$$H = \sum_{i\alpha, j\beta} c^\dagger_{i\alpha} H_{ij,\alpha\beta} c_{j\beta}. \tag{2.7}$$

The elements of the single-particle Hamiltonian, H_{ij}, are

$$\begin{aligned}
H_{ij} =& (t_0\sigma_x + \kappa\sigma_z)\delta_{ij} + \frac{1}{2i}\kappa'\sigma_z(\delta_{i-j,1} - \delta_{i-j,-1}) \\
&+ \frac{1}{2}t_1\left[(\sigma_x + i\sigma_y)\delta_{i,j+1} + (\sigma_x - i\sigma_y)\delta_{i,j-1}\right] \\
&+ \frac{1}{2}t_2\left[(\sigma_x + i\sigma_y)\delta_{i,j+2} + (\sigma_x - i\sigma_y)\delta_{i,j-2}\right],
\end{aligned} \tag{2.8}$$

where σ_α are the Pauli matrices,

$$\sigma_x = \begin{pmatrix} 0 & 1 \\ 1 & 0 \end{pmatrix}, \quad \sigma_y = \begin{pmatrix} 0 & -i \\ i & 0 \end{pmatrix}, \quad \sigma_z = \begin{pmatrix} 1 & 0 \\ 0 & -1 \end{pmatrix}. \tag{2.9}$$

The corresponding Bloch Hamiltonian is

$$\begin{aligned}
H(k) =& \begin{pmatrix} \kappa + \kappa'\sin(k) & t_0 + t_1 e^{ik} + t_2 e^{2ik} \\ t_0 + t_1 e^{-ik} + t_2 e^{-2ik} & -\kappa - \kappa'\sin(k) \end{pmatrix} \\
=& (t_0 + t_1\cos(k) + t_2\cos(2k))\sigma_x \\
&+ (-t_1\sin(k) - t_2\sin(2k))\sigma_y + (\kappa + \kappa'\sin(k))\sigma_z.
\end{aligned} \tag{2.10}$$

We will employ this model to illustrate the concepts we introduce in the two following chapters.
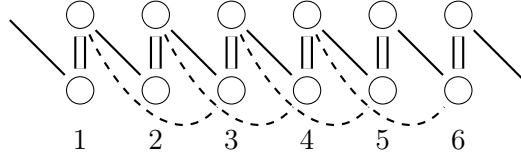
Figure 2.2: Diagram of the model used throughout this thesis, consisting of two orbitals per site, with hopping between orbitals of the same site t_0 (double line), hopping between adjacent sites (continuous line) and hopping between next to nearest neighbors (dashed line)

2.2 Symmetries and the classification of topological insulators and superconductors, the ten-fold way

The framework of the *ten-fold way* [15, 20], based on the random matrix classification developed by Altland and Zirnbauer [18, 19], aims to give a most fundamental classification of topological insulator and superconductor phases, for systems where no unitarily realized symmetry on the first quantized Hamiltonian is required to protect the topological phase. *Ordinary* symmetries, e.g. inversion symmetry or spin-rotation symmetries, are unitary, commute with the Hamiltonian and are typically easily broken.

If a certain first quantized Hamiltonian is invariant under a unitarily realized symmetry, one can always define a basis for which the Hamiltonian is block-diagonal and these blocks do not have any constraint imposed by the unitarily realized symmetry [15]. Since the topological phase is not protected by this unitarily realized symmetry the topology of the Hamiltonian must come from the topology of these general block Hamiltonians. The ten-fold way deals with classifying these general blocks.

There are three symmetries that do not act as the ordinary symmetries described above, those are time-reversal, charge conjugation (or particle-hole), and chiral (or sublattice) symmetries. The first two act on the first quantized Hamiltonian as anti-unitary operators. The latter is a unitary operator but it does not commute the Hamiltonian, it anti-commutes. In the literature, these symmetries are defined in several different ways, we will use the convention found in reference [15], which is one of the most accessible reviews on the topic.

Time-reversal symmetry is defined acting on the second-quantized operators as

$$\mathcal{T}c_i\mathcal{T}^{-1} = \sum_j (U_T^\dagger)_{ij}c_j, \quad \mathcal{T}c_i^\dagger\mathcal{T}^{-1} = \sum_j c_j^\dagger(U_T)_{ji}, \tag{2.11}$$

where the indices i, j can label lattice sites, orbitals, spins, momentum, or any

combination of them. The time-reversal operator is anti-unitary, $\mathcal{T}i\mathcal{T}^{-1} = -i$. Defining the time-reversal operator acting on the first quantized Hamiltonian as $T = U_T K$, where K is the complex conjugation operator, time-reversal symmetry is imposed by

$$THT^{-1} = H, \quad TH(k)T^{-1} = H(-k), \tag{2.12}$$

for position and momentum space. Due to unitarity we have $U_T U_T^* = e^{i\gamma}\mathcal{I}$. Considering $(U_T U_T^*)U_T = U_T(U_T^* U_T)$, so that $e^{i\gamma}U_T = U_T e^{-i\gamma}$, it implies that $T^2 = U_T U_T^* = \pm 1$. There are therefore three ways a general Hamiltonian can respond to time-reversal symmetry. It can be not time-reversal invariant or it can be time-reversal invariant with either $T^2 = 1$ or $T^2 = -1$.

The same analysis can be done with charge conjugation. This is defined as

$$\mathcal{C}c_i\mathcal{C}^{-1} = \sum_j (U_C^{*\dagger})_{ij}c_j^\dagger, \quad \mathcal{C}c_i^\dagger\mathcal{C}^{-1} = \sum_j c_j(U_C^*)_{ji}, \tag{2.13}$$

where $\mathcal{C}$ is a unitary operator. Defining the first-quantized charge conjugation operator as $C = U_C K$, it acts as

$$CHC^{-1} = -H, \quad CH(k)C^{-1} = -H(-k). \tag{2.14}$$

Similar to time-reversal symmetry, $C^2 = \pm 1$. So far these lead to 9 different ways a Hamiltonian can respond to both time-reversal and charge conjugation symmetries.

The last symmetry to consider, chiral symmetry, is a combination of the previous two, $\mathcal{S} = \mathcal{T} \cdot \mathcal{C}$. It acts on the second-quantized operators as

$$\mathcal{S}c_i\mathcal{S}^{-1} = \sum_j (U_S^{*\dagger})_{ij}c_j^\dagger, \quad \mathcal{S}c_i^\dagger\mathcal{S}^{-1} = \sum_j c_j(U_S^*)_{ji}. \tag{2.15}$$

We can write the first-quantized chiral symmetry operator as $S = U_S = U_T U_C^* = TC$, which anticommutes with the Hamiltonian,

$$SHS^{-1} = -H, \quad SH(k)S^{-1} = -H(k). \tag{2.16}$$

Since the phases of U_C and U_T are completely arbitrary, one can change them so that $S^2 = +1$. There are therefore only two ways a Hamiltonian can respond to chiral symmetry, it is either invariant under it, or it is not. Furthermore, the way a Hamiltonian responds to chiral symmetry is constrained by how it responds to time-reversal and charge-conjugation. A Hamiltonian cannot be invariant under chiral symmetry unless it is invariant to either both, time-reversal and charge conjugation, or none of them. This leads to a total of ten ways a Hamiltonian can respond to these symmetries. These correspond to the ten different *Cartan classes.*

Symmetries				Spatial dimension			
Class	T	C	S	1	2	3	...
A	0	0	0	0	$\mathbb{Z}$	0	...
AIII	0	0	1	$\mathbb{Z}$	0	$\mathbb{Z}$	...
AI	1	0	0	0	0	0	...
BDI	1	1	1	$\mathbb{Z}$	0	0	...
D	0	1	0	$\mathbb{Z}_2$	$\mathbb{Z}$	0	...
DIII	-1	1	1	$\mathbb{Z}_2$	$\mathbb{Z}_2$	$\mathbb{Z}$	...
AII	-1	0	0	0	$\mathbb{Z}_2$	$\mathbb{Z}_2$	...
CII	-1	-1	1	$\mathbb{Z}$	0	$\mathbb{Z}_2$	...
C	0	-1	0	0	$\mathbb{Z}$	0	...
CI	1	-1	1	0	0	$\mathbb{Z}$	...

Table 2.1: Cartan-Altland-Zimbauer (CAZ) table that shows the classification of non-interacting topological insulator and superconductor phases protected by not unitarily realized symmetries.

The ten-fold way formalism aims at answering the questions: what non-trivial topology, if any, can be found in each of these classes for different spatial dimensions and what kind of topological invariant characterizes these topological phases? The results of the ten-fold way [15, 20] are summarized in the periodic table of topological insulators and superconductors found in Table 2.1. It can also be found referred to as the Cartan-Altland-Zimbauer (CAZ) table. For each of the Cartan classes defined by the symmetries of the Hamiltonian, and for each possible spatial dimension, there are three possible outcomes. Either the class is trivial (0), there can be two topologically distinct phases ($\mathbb{Z}_2$), or there can be infinite distinct topological phases ($\mathbb{Z}$).

Unitary symmetries can lead to additional topological classes. Although, as mentioned before, in practice they are more fragile. One particularly interesting case is that of spatial symmetries [103]. In the following we will also briefly consider one of these symmetries, namely inversion symmetry, defined by

$$U_P\hat{x}U_P = -\hat{x}. \qquad (2.17)$$

A system is inversion symmetric if it holds that

$$U_P H U_P = H, \quad U_P H(k) U_P = H(-k). \tag{2.18}$$

Symmetries of the model Hamiltonian: We can now test the symmetries of the model Hamiltonian, Eq.(2.8). Time-reversal is given by $T = K$, where K is the conjugation operator. Acting on the Bloch Hamiltonian of the model, Eq. (2.10), we have

$$T H(k) T^{-1} - H(-k) = \begin{pmatrix} 2\kappa' \sin(k) & 0 \\ 0 & -2\kappa' \sin(k) \end{pmatrix}, \tag{2.19}$$

and time-reversal is broken by the κ' term. Particle-hole is given by $C = \sigma_z K$,

$$C H(k) C^{-1} + H(-k) = \begin{pmatrix} 2\kappa & 0 \\ 0 & -2\kappa \end{pmatrix}, \tag{2.20}$$

and is broken by the κ term. As for the chiral symmetry, $S = TC = \sigma_z$ gives

$$S H(k) S^{-1} + H(k) = \begin{pmatrix} 2(\kappa + \kappa' \sin(k)) & 0 \\ 0 & -2(\kappa + \kappa' \sin(k)) \end{pmatrix}, \tag{2.21}$$

broken by either κ or κ'. Finally, let us consider inversion symmetry, given by $U_P = \sigma_x$. Acting on the Bloch Hamiltonian,

$$U_P H(k) U_P^{-1} - H(-k) = \begin{pmatrix} -2\kappa & 0 \\ 0 & 2\kappa \end{pmatrix}, \tag{2.22}$$

shows that inversion symmetry is also broken by κ. To summarize, without the symmetry breaking terms, κ and κ', the Hamiltonian has time-reversal, particle-hole, chiral and inversion symmetries. It is therefore in the BDI class, with a $\mathbb{Z}$ topological invariant in one dimension, which we will introduce below. The κ' term breaks time-reversal and chiral symmetries, leaving the system in the D class, with a $\mathbb{Z}_2$ invariant in one dimension. The κ term breaks particle-hole, chiral and inversion symmetries, leaving the system in the AI class, which is topologically trivial in one dimension. The same holds for class A (a class without any symmetries), obtained when both κ, κ' terms are non-zero.

2.3 Topological invariants

As mentioned in the begining of this chapter, topological invariants are bulk quantities that characterize the topology of the system. There are many ways the

information about the topology is encoded on the system and, therefore, there are multiple ways these topological invariants are defined. These can be quantized observables, such as the bulk polarization or the transverse conductance, or mathematical objects borrowed from topology, such as the winding number or the Chern number.

For topological insulators and superconductors one must consider two different types of invariants. $\mathbb{Z}_2$ invariants can only take two values and therefore distinguish between two phases, a trivial one and a non-trivial one. The trivial phase is defined as the one that can be adiabatically connected to the atomic insulator phase, where there is no hopping or hybridization between different sites. A $\mathbb{Z}$ invariant can take any integer value and therefore distinguishes between a trivial phase and multiple distinct non-trivial phases. In a class characterized by a $\mathbb{Z}$ invariant it might still be useful to consider $\mathbb{Z}_2$ invariants that distinguish between two sets of phases.

In the following we introduce the topological invariants that are relevant for this thesis. First we introduce a useful concept, the geometric phase [26, 104–106]. Then we introduce the bulk polarization and the Zak phase [107], two equivalent $\mathbb{Z}_2$ topological invariants in 1D [23,26,28]. Next we introduce the winding number [15], a $\mathbb{Z}$ invariant defined in odd dimensions and the Chern number [15], which is also a $\mathbb{Z}$ topological invariant, most relevant in 2D systems although it has applications in 1D systems that we will discuss. We will also discuss how the winding and Chern numbers are related to the polarization.

2.3.1 Geometric phases for adiabatic evolution

Consider a Hamiltonian $H(\boldsymbol{R})$ and a particular eigenstate $|n(\boldsymbol{R})\rangle$ with a set of parameters $\boldsymbol{R}(t)$ that are varied adiabatically over a closed path C in parameter space. After this evolution is completed at time T the final eigenstate might differ from the original one by a phase factor, $|n(\boldsymbol{R}(T))\rangle = e^{i\gamma_C} |n(\boldsymbol{R}(0))\rangle$. Consider first that the path C_N is discretized into N different points, where N can be later taken to infinity to ensure adiabaticity. The phase between the eigenstate at two adjacent points will be

$$\gamma_{j,j+1} = -\text{Im} \ln[\langle n(\boldsymbol{R}_j)|n(\boldsymbol{R}_{j+1})\rangle]. \tag{2.23}$$

Therefore the total phase acquired by the eigenstate is given by

$$\gamma_{C_N} = -\text{Im} \ln \left[\prod_{j=1}^{N} \langle n(\boldsymbol{R}_j)|n(\boldsymbol{R}_{j+1})\rangle \right], \tag{2.24}$$

where $\boldsymbol{R}_{N+1} = \boldsymbol{R}_1$. For a continuous path the phase acquired by the eigenstates results in

$$\exp[i\gamma_C] = \exp\left[i\int_C d\boldsymbol{R}\,i\left\langle n(\boldsymbol{R})\right| \nabla_{\boldsymbol{R}}\left|n(\boldsymbol{R})\right\rangle\right], \qquad (2.25)$$

where the Berry connection

$$\boldsymbol{A}(\boldsymbol{R}) = i\left\langle n(\boldsymbol{R})\right|\nabla_{\boldsymbol{R}}\left|n(\boldsymbol{R})\right\rangle, \qquad (2.26)$$

is always real. While the Berry connection depends on the choice of gauge, the geometric phase is gauge invariant.

One might be interested in expressing the geometric phase as a surface integral instead. To do that, we must introduce the Berry curvature, $\boldsymbol{\Omega} = \nabla \times \boldsymbol{A}$, or

$$\begin{aligned}\Omega_{\mu\nu} =& \partial_\mu A_\nu(\mu,\nu) - \partial_\nu A_\mu(\mu,\nu)\\ =& -2\,\mathrm{Im}\left\langle\partial_\mu n(\mu,\nu)|\partial_\nu n(\mu,\nu)\right\rangle.\end{aligned} \qquad (2.27)$$

In general one finds the relation [26]

$$\exp\left[-i\oint_{\partial_S}\boldsymbol{A}\cdot d\boldsymbol{R}\right] = \exp\left[-i\int_S\Omega_{\mu\nu}dS_{\mu\nu}\right]. \qquad (2.28)$$

In the case where the Berry connection is smooth over the whole surface one can directly invoke Stoke's theorem to show that

$$\oint_{\partial_S}\boldsymbol{A}\cdot d\boldsymbol{R} = \int_S\Omega_{\mu\nu}dS_{\mu\nu}. \qquad (2.29)$$

If the Berry connection is instead piecewise smooth one has to divide the surface of integration into different smooth parts and apply Stoke's theorem independently in each surface. The discussion above describes the evolution of an isolated eigenstate. The extension to multiple states is straight-forward [26].

2.3.2 Polarization

Attempts to adapt the formulation of polarization from finite systems to bulk systems proved elusive until the development of the modern theory of polarization [22–27]. A crucial characteristic of the bulk polarization is that it is not itself a physical observable. Only changes in the bulk polarization can be measured, in the form of currents. An important step in this direction was taken by King-Smith and Vanderbilt [27]. Using perturbation theory they computed the change of polarization when a parameter (λ) is changed adiabatically. They found that

the derivative of the polarization is given by the integral of a Berry curvature in the (λ, k) space,

$$\partial_\lambda \mathcal{P}^{\text{Bloch}} = -\sum_{\mu \in \text{occ}} \int_0^{2\pi} \frac{dk}{2\pi} 2\text{Im} \langle \partial_\lambda u_{k\mu} | \partial_k u_{k\mu} \rangle, \qquad (2.30)$$

where $|u_{k\mu}\rangle$ are the eigenstates of the Bloch Hamiltonian. The polarization obtained using these eigenstates is denoted as $\mathcal{P}^{\text{Bloch}}$, following the notation in reference [28].

The total change in the bulk polarization by the adiabatic evolution of λ is therefore given by the Berry flux inside the region $\{\lambda \in [\lambda_i, \lambda_f], k \in [0, 2\pi)\}$. Using the fact that the Berry curvature is gauge-invariant we can find the path-independent expression for the change of the bulk polarization between two states λ_i and λ_f as

$$\Delta \mathcal{P}^{\text{Bloch}}_{\lambda_i, \lambda_f} = \frac{1}{2\pi} \sum_{\mu \in occ} [\gamma_\mu(\lambda_f) - \gamma_\mu(\lambda_i)], \qquad (2.31)$$

where

$$\gamma_\mu(\lambda) = \int_0^{2\pi} dk \, A_\mu(k, \lambda) \qquad (2.32)$$

is known as the Zak phase [26, 107] for band μ and $A_\mu(k, \lambda) = i \langle u_{k\mu}(\lambda) | \partial_k u_{k\mu}(\lambda) \rangle$ is the Berry connection. We can therefore identify the polarization with the total Zak phase,

$$\mathcal{P}^{\text{Bloch}} = \frac{1}{2\pi} \sum_{\mu \in occ} \gamma_\mu. \qquad (2.33)$$

Note that, unless one knows the complete evolution of the phase along the path, the total change in the phase can only be known up to a 2π factor, and the change of the polarization can only be defined modulo 1.

One of the challenges that appears when trying to adapt the formulation from finite systems to periodic systems is that the position operator is not periodic itself. Resta [24] proposed that when dealing with bulk systems, the position should be treated as an angle instead, defining a meaningful average of the many-body position operator as

$$\left\langle \hat{X} \right\rangle_\Psi \equiv \frac{L}{2\pi} \text{Im} \ln \langle \Psi | e^{-i\frac{2\pi}{L}\hat{X}} | \Psi \rangle, \qquad (2.34)$$

for any general state $|\Psi\rangle$, where the many-body position operator can be computed from the single-particle ones by $\hat{X} = \sum_i \hat{x}_i \hat{n}_i$. Based on this position average, one

can define a bulk polarization as

$$\mathcal{P} = \lim_{L \to \infty} \frac{1}{L} \left\langle \hat{X} \right\rangle_0, \tag{2.35}$$

which is now naturally defined modulo 1.

The definition of polarizations $\mathcal{P}^{\text{Bloch}}$, Eq. (2.33), and $\mathcal{P}$, Eq. (2.35), have different motivation, but we now show that they are in fact equivalent. Consider the many-body ground state, a Slater determinant of the occupied single particle eigenstates

$$|\Psi_0\rangle = A \prod_{\mu=1} |\psi_\mu\rangle, \tag{2.36}$$

where A stands for antisymmetrized. We can now define the state $|\Psi_0'\rangle = e^{-i\frac{2\pi}{L}\hat{X}} |\Psi_0\rangle$, or equivalently $\left|\psi_{p\mu}'\right\rangle = e^{-i\frac{2\pi}{L}\hat{x}} |\psi_{p\mu}\rangle$, so that the expectation value of the position is given by

$$\left\langle \hat{X} \right\rangle_0 = \frac{L}{2\pi} \mathrm{Im} \ln \langle \Psi_0 | \Psi_0' \rangle. \tag{2.37}$$

A well-known theorem states that the overlap of two determinants is equal to the determinant of the overlap matrix among the orbitals [108, 109], so that

$$\left\langle \hat{X} \right\rangle_0 = \frac{L}{2\pi} \mathrm{Im} \ln \det S, \tag{2.38}$$

where the matrix S is given by

$$S_{\mu\nu} = \sum_{j\alpha} \langle \psi_\mu | e^{-i\frac{2\pi}{L}\hat{x}} |\psi_\nu\rangle, \tag{2.39}$$

with the indices μ, ν going only over the occupied subspace. The polarization can then be computed as

$$\mathcal{P} = \lim_{L \to \infty} \frac{1}{2\pi} \mathrm{Im} \ln \det S. \tag{2.40}$$

In order to simplify the calculation above, consider the operator, $P_{occ} e^{-i\frac{2\pi}{L}\hat{x}}$, where $P_{occ} = \sum_{\mu \in occ} |\psi_\mu\rangle \langle \psi_\mu|$ is the projector onto the occupied subspace. It can be written in block form using the basis $\{|\psi_{occ}\rangle, |\psi_{emp}\rangle\}$ as

$$P_{occ} e^{-i\frac{2\pi}{L}\hat{x}} = \begin{pmatrix} S & 0 \\ M & 0 \end{pmatrix}, \tag{2.41}$$

where S is the matrix defined above and M is some other matrix. The determinant of this operator vanishes because it vanishes for the empty subspace. Instead, we

consider the operator

$$I - P_{occ} + P_{occ}e^{-i\frac{2\pi}{L}\hat{x}} = \begin{pmatrix} S & 0 \\ M & I \end{pmatrix}, \tag{2.42}$$

such that the polarization can now be expressed as

$$\mathcal{P} = \lim_{L\to\infty} \frac{1}{2\pi} \text{Im} \ln \det[I - P_{occ} + P_{occ}e^{-i\frac{2\pi}{L}\hat{x}}]. \tag{2.43}$$

This expression simplifies numerical computations as well as certain analytical calculations. In the translationally invariant case, using the Bloch states one arrives to

$$\mathcal{P} = \lim_{L\to\infty} \frac{1}{2\pi} \text{Im} \ln \left\{ (-1)^{\nu(L-1)} \prod_k \det'[S_{k,k+2\pi/L}] \right\}$$

$$= \lim_{L\to\infty} \frac{1}{2\pi} \text{Im} \ln \left\{ \prod_k \det'[S_{k,k+2\pi/L}] \right\} + \nu \frac{L-1}{2}. \tag{2.44}$$

Taking the continuous limit, the first term results in the Zak phase, defined in Eq. (2.32). Therefore, in the thermodynamic limit the polarization is given by

$$\mathcal{P} = \frac{1}{2\pi}\gamma_Z + \nu \frac{L-1}{2}. \tag{2.45}$$

Indeed, the polarization introduced by Resta can be regarded as a generalization of the Zak phase to position space. Note that, since only changes in the polarization are physical, the constant term is irrelevant.

Using the expression in Eq. (2.43) we can now show how symmetries quantize the polarization. Consider first particle-hole symmetry, see Eq. (2.14). Acting on the projector gives

$$U_C P_{occ}^* U_C^{-1} = 1 - P_{occ}, \tag{2.46}$$

so that

$$\det\left[I - P_{occ} + P_{occ}e^{-i\frac{2\pi}{L}\hat{x}}\right] = \det\left[I - U_C P_{occ} U_C^{-1} + U_C P_{occ}e^{-i\frac{2\pi}{L}\hat{x}}U_C^{-1}\right]$$

$$= \det\left[P_{occ}^* + (I - P_{occ}^*)e^{-i\frac{2\pi}{L}\hat{x}}\right], \tag{2.47}$$

where we assume that the symmetry does not affect the position operator, $U_C \hat{x} U_C^{-1} = \hat{x}$. Taking the exponential out we have

$$\det\left[P_{occ}^* + (I - P_{occ}^*)e^{-i\frac{2\pi}{L}\hat{x}}\right] = \det\left[P_{occ}^* e^{i\frac{2\pi}{L}\hat{x}} + (I - P_{occ}^*)\right]\det\left[e^{-i\frac{2\pi}{L}\hat{x}}\right]$$

$$= \det\left[I - P_{occ} + P_{occ}e^{-i\frac{2\pi}{L}\hat{x}}\right]^* \tag{2.48}$$

where we used that $\det\left[e^{i\frac{2\pi}{L}\hat{x}}\right] = 1$. This implies that the polarization fulfills $\mathcal{P} = -\mathcal{P}$. Since it is defined modulo 1, this leads to only two possible values, $\mathcal{P} = 0, 1/2$. A similar calculation can be done for the chiral symmetry,

$$SP_{occ}S = 1 - P_{occ}, \qquad (2.49)$$

and

$$\det\left[I - P_{occ} + P_{occ}e^{-i\frac{2\pi}{L}\hat{x}}\right] = \det\left[I - SP_{occ}S + SP_{occ}e^{-i\frac{2\pi}{L}\hat{x}}S\right]$$
$$= \det\left[P_{occ} + (I - P_{occ})e^{-i\frac{2\pi}{L}\hat{x}}\right], \qquad (2.50)$$

where once again we assume that the position operator commutes with the symmetry, $[S, \hat{x}] = 0$. We again take the exponential out,

$$\det\left[P_{occ} + (I - P_{occ})e^{-i\frac{2\pi}{L}\hat{x}}\right] = \det\left[P_{occ}e^{i\frac{2\pi}{L}\hat{x}} + (I - P_{occ})\right]\det\left[e^{-i\frac{2\pi}{L}\hat{x}}\right]$$
$$= \det\left[I - P_{occ} + P_{occ}e^{i\frac{2\pi}{L}\hat{x}}\right]$$
$$= \det\left[I + (-I + e^{-i\frac{2\pi}{L}\hat{x}})P_{occ}\right]^{*}, \qquad (2.51)$$

where in the last step we have used $\det[A] = \det\left[A^{\dagger}\right]^{*}$ and the fact that the projector is Hermitian. This is almost the same result as for particle-hole, with the exception that the exponential and the projector are commuted. To get the same form we make use of Sylvester's identity, $\det[I + AB] = \det[I + BA]$, such that

$$\det\left[I - P_{occ} + P_{occ}e^{-i\frac{2\pi}{L}\hat{x}}\right] = \det\left[I + P_{occ}(-I + e^{-i\frac{2\pi}{L}\hat{x}})\right]^{*}$$
$$= \det\left[I - P_{occ} + P_{occ}e^{-i\frac{2\pi}{L}\hat{x}}\right]^{*}, \qquad (2.52)$$

recovering the same quantization of the polarization. Finally we consider the case of inversion symmetry. Consider the projector matrix in position space, $\overline{\overline{P}}_{occ}$,

$$U_P\overline{\overline{P}}_{occ}U_P^{-1} = \overline{\overline{P}}_{occ}^{T}, \qquad (2.53)$$

$$\det\left[I - \overline{\overline{P}}_{occ} + \overline{\overline{P}}_{occ}e^{-i\frac{2\pi}{L}\overline{\overline{x}}}\right] = \det\left[I - U_P\overline{\overline{P}}_{occ}U_P^{-1} + U_P\overline{\overline{P}}_{occ}e^{-i\frac{2\pi}{L}\overline{\overline{x}}}U_P^{-1}\right]$$
$$= \det\left[I - \overline{\overline{P}}_{occ}^{*} + \overline{\overline{P}}_{occ}^{*}e^{i\frac{2\pi}{L}\overline{\overline{x}}}\right]$$
$$= \det\left[I - \overline{\overline{P}}_{occ} + \overline{\overline{P}}_{occ}e^{-i\frac{2\pi}{L}\overline{\overline{x}}}\right]^{*}, \qquad (2.54)$$

where we used that $\overline{\overline{P}}_{occ}$ is Hermitian. We recover quantization as well. Note that as opposed to particle-hole and chiral symmetry, there is no assumption other than the existence of the symmetry. In both particle-hole and chiral symmetry, quantization is conditional to the commutation of the symmetry with the position operator. This, however, is a relatively common situation in simple models and it applies to the model used throughout this thesis, see Eq. (2.20).

Another way of defining a polarization that does not rely on translational invariance is by computing the geometric phase for $U(1)$ flux insertion for a periodic system [28]. If the flux is introduced homogeneously, through a vector potential $A_x = \Phi/L$ along the chain, a polarization can be defined as

$$\mathcal{P} = \int_0^{2\pi} \frac{d\Phi}{2\pi} i \left\langle \Psi^\Phi \middle| \partial_\Phi \middle| \Psi^\Phi \right\rangle + \frac{1}{2\pi} \operatorname{Im} \ln \left\langle \Psi^0 \middle| e^{2\pi i \hat{P}} \middle| \Psi^{2\pi} \right\rangle, \qquad (2.55)$$

where $\left| \Psi^\Phi \right\rangle$ is the ground state in the presence of a flux Φ and $\hat{P} = \frac{1}{L} \sum_{j\alpha} j \hat{n}_{j\alpha}$ is the polarization operator. The second term is needed since the ground state is not periodic in Φ, consequence of $A_x(\Phi + 2\pi) \neq A_x(\Phi)$. This polarization is equivalent in the thermodynamic limit to the one introduced by Resta in Eq. (2.44) [28].

Instead of introducing the flux homogeneously one can also introduce it by imposing a twisted boundary condition between sites $i = 1$ and $i = L$. This is equivalent to performing the gauge transformation

$$\left| \tilde{\Psi}^\Phi \right\rangle = e^{i\Phi\hat{P}} \left| \Psi^\Phi \right\rangle, \qquad (2.56)$$

which makes $\left| \tilde{\Psi}_0^\Phi \right\rangle$ fully periodic in Φ. We can now define the bulk polarization

$$\tilde{\mathcal{P}} = \int_0^{2\pi} \frac{d\Phi}{2\pi} i \left\langle \tilde{\Psi}^\Phi \middle| \partial_\Phi \middle| \tilde{\Psi}^\Phi \right\rangle. \qquad (2.57)$$

Changes in this bulk polarization are related to charge transported across the twisted boundary [28], while changes in $\mathcal{P}$ give the total charge transported through the system. This bulk polarization is related to the homogeneous bulk polarization [28] by

$$\mathcal{P} = \tilde{\mathcal{P}} + \tilde{\mathcal{P}}_0, \qquad (2.58)$$

where

$$\tilde{\mathcal{P}}_0 = \int_0^{2\pi} \frac{d\Phi}{2\pi} \left\langle \tilde{\Psi}^\Phi \middle| \hat{P} \middle| \tilde{\Psi}^\Phi \right\rangle. \qquad (2.59)$$

2.3.3 Winding number

The winding number is a $\mathbb{Z}$ topological invariant defined for systems with chiral symmetry [20] in odd dimensions. In the diagonal basis of the chiral symmetry operator the chiral symmetric Bloch Hamiltonian can be written in block form as

$$H(k) = \begin{pmatrix} 0 & h(k) \\ h^{\dagger}(k) & 0 \end{pmatrix}, \tag{2.60}$$

where $h(k)$ can be a matrix. It is more useful to work with the flat-band Hamiltonian, defined as

$$\begin{aligned} Q(k) =& H(k)(H(k)^2)^{-1/2} \\ =& \begin{pmatrix} 0 & q(k) \\ q^{\dagger}(k) & 0 \end{pmatrix}. \end{aligned} \tag{2.61}$$

Note that since Q only has eigenvalues ± 1, $Q^2 = I$ and therefore $q^{\dagger} = q^{-1}$ is a unitary matrix. The determinant of the off-diagonal block, $q(k)$, is a phase. The winding number is the number of times that this phase winds along the Brillouin zone,

$$\nu = \int_{-\pi}^{\pi} \frac{dk}{2\pi} \partial_k \mathrm{Im} \log \det[q(k)], \tag{2.62}$$

which is by definition an integer, as opposed to the polarization. Alternatively, using that $\log \det M = \mathrm{Tr} \log M$, it can also be written as

$$\nu = \int_{-\pi}^{\pi} \frac{dk}{2\pi i} \mathrm{Tr}[q(k)^{\dagger} \partial_k q(k)], \tag{2.63}$$

which is another form typically used. There are also generalizations of the winding number for systems without translational invariance [51, 110, 111] which will be discussed in section 3.4.

In particular, for a two-band system with chiral symmetry, $S = \sigma_z$, the Bloch Hamiltonian is given by $H(k) = \boldsymbol{h}(k) \cdot \boldsymbol{\sigma}$, with $h_z(k) = 0$. The winding number is then given by

$$\begin{aligned} \nu =& \int_{-\pi}^{\pi} \frac{dk}{2\pi} \partial_k \mathrm{Im} \log \left[\frac{h_x(k) - i h_y(k)}{\sqrt{h_x(k)^2 + h_y(k)^2}} \right] \\ =& \int_{-\pi}^{\pi} \frac{dk}{2\pi} \partial_k \mathrm{Im} \log[h_x(k) - i h_y(k)] \end{aligned} \tag{2.64}$$

i.e. the winding number is the number of times the complex number $h_x(k) - ih_y(k)$ winds around the origin on the complex plane, which is the same as the number of times $\boldsymbol{h}(k)$ winds around the origin in the $x - y$ plane. The winding number is also found in the literature expressed as

$$\nu = \frac{1}{2\pi} \oint dk \, \frac{(\partial_k h_x(k))h_y(k) - h_x(k)\partial_k h_y(k)}{h_x(k)^2 + h_y(k)^2}. \tag{2.65}$$

All the different expressions for the polarization given here, which are equivalent to each other for gapped systems, will be used in the accompanying papers.

The winding number is also related to the Zak phase. In the case of the two-band model introduced above, this is easy to show. The eigenstates of a chiral-symmetric two-band system can be expressed as

$$|u_{k\pm}\rangle = \frac{1}{\sqrt{2}} \begin{pmatrix} \pm q(k) \\ 1 \end{pmatrix}. \tag{2.66}$$

Using these eigenstates, the Zak phase can be now computed as

$$\begin{aligned} \gamma_Z &= \int_{-\pi}^{\pi} dk \, i \, \langle u_{k-}| \, \partial_k \, |u_{k-}\rangle \\ &= \frac{1}{2} \int_{-\pi}^{\pi} dk \, iq^*(k)\partial_k q(k) \\ &= \pi\nu \bmod 2\pi. \end{aligned} \tag{2.67}$$

Winding number of the model Hamiltonian

For $\kappa = \kappa' = 0$ the system has time-reversal, particle-hole and chiral symmetries. It is therefore in the BDI class, and has the phase diagram shown in Fig. 2.3, presenting phases with winding number $\nu = 0, 1$ and 2, the latter being fundamental to showcase our results. The κ term breaks particle-hole and chiral symmetries, while the κ' term breaks time-reversal and chiral symmetries.

In Fig.2.3(b-e) we show the energy spectrum of the corresponding open system (surface spectrum) for the dashed line in the phase diagram for different values of the symmetry breaking terms, κ, κ'. The edge states are plotted in red and blue, to show their degeneracy. For the case with $\kappa = \kappa' = 0$ (a) we see that the winding number is equal to the number of zero-energy modes in each phase. For $\kappa = 0, \kappa' \neq 0$ (b) the system is in the D class, with only a $\mathbb{Z}_2$ invariant. All the phases with an even winding number in the BDI class now become indistinguishable from the trivial phase. Accordingly, the κ term allows the former two zero-energy modes to hybridize and split from zero energy. For $\kappa \neq 0, \kappa' = 0$ ($\neq 0$)the system is in the AI (A) class, which is trivial for 1D, and no zero-energy states are found anywhere.
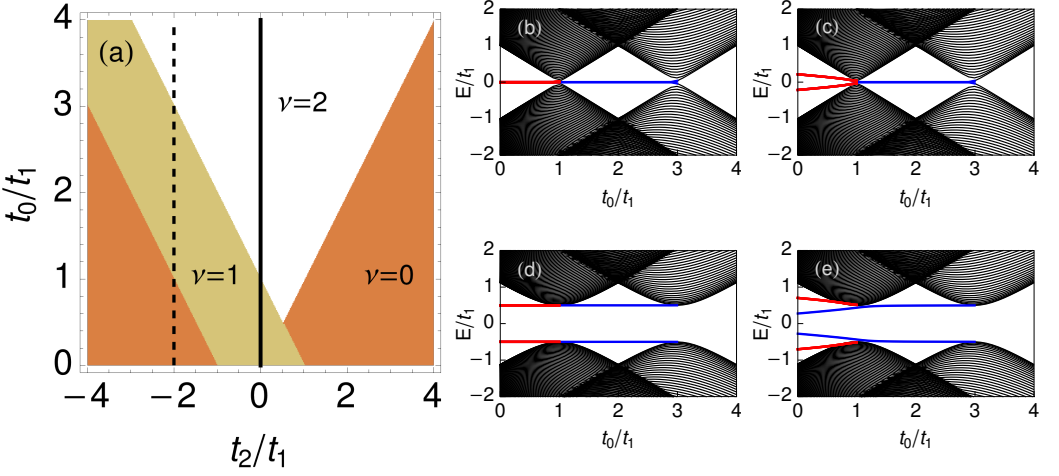
Figure 2.3: (a) Phase diagram for the model we use (see Eq. (2.8)) in the BDI class (for $\kappa = \kappa' = 0$) showing the winding number of each region. (b-e) Edge spectrum along the dashed line in the phase diagram (i.e. $t_2 = -2t_1$) for different values of κ and κ'. The edge states are plotted in blue and red, to show their degeneracy.

2.3.4 Chern number

In 2D the relevant $\mathbb{Z}$ invariant is the Chern number. The Chern number is defined as the total geometric flux piercing a closed surface. In translationally invariant systems in 2D, this surface corresponds to the torus defined by the two momentum variables,

$$C = \frac{1}{2\pi} \int_{S_{\boldsymbol{k}^2}} \boldsymbol{\Omega} \cdot d\boldsymbol{k}^2, \tag{2.68}$$

where $\boldsymbol{\Omega}$ is the Berry curvature defined in equation (2.27). The Chern number is equal to the number of vortices in the surface. As mentioned in section 2.3.1, using Stoke's theorem this computation can be simplified to

$$C = \frac{1}{2\pi} \oint_{\partial S_{\boldsymbol{k}^2}} \boldsymbol{A} \cdot d\boldsymbol{k}, \tag{2.69}$$

given that the Berry connection is smooth over the whole surface. If not, one has to divide it into several surfaces where it is smooth, which is always possible but might not be a trivial task.

Although not as a topological invariant in the sense described in this chapter, the Chern number is also of interest in the adiabatic evolution of 1D systems, where it is computed over the torus defined by the momentum and another variable, λ,
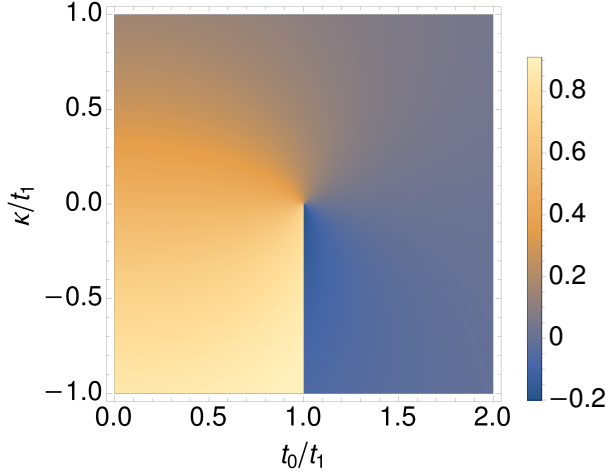
Figure 2.4: $\gamma_Z/2\pi$ calculated for the model in Eq. (2.8) with $t_2 = \kappa' = 0$. Obtained in the smooth gauge where the second element of the occupied eigenstate of the Bloch Hamiltonian is kept real. Other gauge choices simply move the branch cut around. The Zak phase winds once as we go around the gapless point at $t_0 = t_1$ and $\kappa = 0$. Figure equivalent to Fig.9 from paper I.

which the system cycles over,

$$C = \int_{-\pi}^{\pi} \frac{dk}{2\pi} \oint_\lambda d\lambda \, \Omega_{k\lambda}. \tag{2.70}$$

Chern number on the model Hamiltonian: Using the model (see Eq.(2.10)) we can now give an example of the appearance of Chern numbers in 1D systems. Consider the SSH model with the on-site potential κ, $(t_2 = \kappa' = 0)$, known as the Rice-Mele model [12, 112]. We will consider the Chern numbers of loops in the parameter space (t_0, κ) parametrized by θ. Using Stoke's theorem the total geometric flux in a cylinder defined by $(k : -\pi \to \pi, \theta : \theta_i \to \theta_f)$ is given by

$$\Phi = \int_{\theta_i}^{\theta_f} d\theta \, \partial_\theta \gamma_Z(\theta). \tag{2.71}$$

We show the Zak phase in the (t_0, κ) parameter space in Fig. 2.4, where we computed it using a gauge where the second element of $|u_k\rangle$ is real. For $\kappa = 0$ this gauge is equal to the one used in Eq.(2.66). There is a degenerate point at $(t_0 = t_1, \kappa = 0)$ that is reflected in the geometric phase as the origin of a branch cut. We can see that there are two types of loops one can consider. A (counterclockwise) loop around the degenerate point will give $C = 1$ while a loop that does

not enclose the degenerate point will give $C = 0$. The Chern number gives the change in the Zak phase, or Polarization, along the loop, and therefore after a loop is completed C electrons are pumped through the chain. This effect is known as topological charge pumping [7, 113] .

2.3.5 Wannier states

A more intuitive way of understanding the bulk polarization and its relation to the winding and Chern numbers is given in terms of Wannier states [26]. Consider again a system with translational invariance. Wannier states are defined as Fourier transform of Bloch states,

$$|w_{j\mu}\rangle = \frac{1}{\sqrt{L}} \sum_k e^{-ikj} |\psi_{k\mu}\rangle , \qquad (2.72)$$

where μ is the corresponding energy band. However, since there is a gauge freedom in how we choose Bloch states, Wannier states are not unique, and in general they are given by

$$|w_{j\mu}\rangle = \frac{1}{\sqrt{L}} \sum_k e^{-ikj} e^{i\beta_\mu(k)} |\psi_{k\mu}\rangle , \qquad (2.73)$$

where $\beta(k) \in \mathbb{R}$ is a periodic function of the momentum. Independently of $\beta(k)$, Wannier states are orthogonal and related by translation,

$$
\begin{aligned}
w_{j\mu}(l\alpha) &= \frac{1}{\sqrt{L}} \sum_k e^{-ik(j-l)} e^{i\beta_\mu(k)} u_{k\mu}^\alpha \\
&= w_{0\mu}(l - j, \alpha),
\end{aligned}
\qquad (2.74)
$$

where $w_{j\mu}(l\alpha) = \langle l\alpha | w_{j\mu}\rangle$, with l labelling position and α the internal degrees of freedom. All the Wannier states have the same shape but are shifted an integer site from each other. Because of this we can measure their total spreading as

$$\Omega = \sum_\mu [\langle w_{0\mu}| x^2 |w_{0\mu}\rangle - (\langle w_{0\mu}| x |w_{0\mu}\rangle)^2]. \qquad (2.75)$$

Their spreading depends on the choice of $\beta(k)$, but they are always found to be localized. The spread can further be decomposed into $\Omega = \Omega_I + \tilde{\Omega}$ [114] where

$$
\begin{aligned}
\Omega_I &= \sum_\mu [\langle w_{0\mu}| x^2 |w_{0\mu}\rangle - \sum_{j\nu} |\langle w_{j\nu}| x |w_{0\mu}\rangle|^2] \\
\tilde{\Omega} &= \sum_\mu \sum_{j,\nu \neq 0,\mu} |\langle w_{j\nu}| x |w_{0\mu}\rangle|^2.
\end{aligned}
\qquad (2.76)
$$

The first term Ω_I is found to be gauge invariant so in order to obtain maximally localized Wannier states one has to choose a $\beta(k)$ that makes $\tilde{\Omega}$ vanish. The eigenstates of $C\hat{X}C$, where C is the full correlation matrix (the projector onto the occupied bands) and $\hat{X}$ is the many-body position operator, are Wannier states [115]. Since the eigenstates of $C\hat{X}C$ fulfill $\langle w_{j\nu}|\, x\, |w_{0\mu}\rangle = 0$ for $j \neq 0$, $\tilde{\Omega}$ vanishes and they are maximally localized. Consider now the average position of the Wannier states, also known as the Wannier centers,

$$
\begin{aligned}
\langle w_{0\mu}|\, x\, |w_{0\mu}\rangle &= \int_0^L \frac{dx}{L} \int_0^{2\pi} \frac{dk}{2\pi} \int_0^{2\pi} \frac{dp}{2\pi} \langle u_{k\mu}|\, e^{-i\beta_\mu(k)} e^{-ikx} x e^{ipx} e^{i\beta_\mu(p)} |u_{p\mu}\rangle \\
&= \int_0^L \frac{dx}{L} \int_0^{2\pi} \frac{dk}{2\pi} \int_0^{2\pi} \frac{dp}{2\pi} \langle u_{k\mu}|\, e^{-i\beta_\mu(k)} e^{-ikx} \left(-i\partial_p e^{ipx}\right) e^{i\beta_\mu(p)} |u_{p\mu}\rangle \\
&= \int_0^L \frac{dx}{L} \int_0^{2\pi} \frac{dk}{2\pi} \langle u_{k\mu}|\, e^{-i\beta_\mu(k)} e^{-ikx} e^{ipx} e^{i\beta_\mu(p)} |u_{p\mu}\rangle \Big|_{p=0}^{p=2\pi} \\
&\quad - \int_0^L \frac{dx}{L} \int_0^{2\pi} \frac{dk}{2\pi} \int_0^{2\pi} \frac{dp}{2\pi} \langle u_{k\mu}|\, e^{-i\beta_\mu(k)} e^{-ikx} e^{ipx} \left(-i\partial_p e^{i\beta_\mu(p)}\right) |u_{p\mu}\rangle \\
&\quad - \int_0^L \frac{dx}{L} \int_0^{2\pi} \frac{dk}{2\pi} \int_0^{2\pi} \frac{dp}{2\pi} \langle u_{k\mu}|\, e^{-i\beta_\mu(k)} e^{-ikx} e^{ipx} e^{i\beta_\mu(p)} \left(-i\partial_p |u_{p\mu}\rangle\right).
\end{aligned}
\tag{2.77}
$$

The first term vanishes because the integrand is periodic in p. The second one, after integrating x and k gives

$$
\begin{aligned}
&- \int_0^{2\pi} \frac{dp}{2\pi} \langle u_{p\mu}|\, e^{-i\beta_\mu(p)} \left(-i\partial_p e^{i\beta_\mu(p)}\right) |u_{p\mu}\rangle \\
&= - \int_0^{2\pi} \frac{dp}{2\pi} \partial_p \beta_\mu(p) \\
&= 0,
\end{aligned}
\tag{2.78}
$$

which also vanishes since $\beta_\mu(p)$ is also periodic. Finally the Wannier center gives

$$
\langle w^{0\mu}|\, x\, |w^{0\mu}\rangle = \int_0^{2\pi} \frac{dk}{2\pi} \langle u_{k\mu}|\, i\partial_k |u_{k\mu}\rangle.
\tag{2.79}
$$

which we can identify with the bulk polarization associated with the band μ, see Eq. (2.33). Note that the result is independent of the gauge choice of $\beta_\mu(k)$. In the context of Wannier states the bulk polarization recovers its original interpretation if one thinks of the Wannier states as describing point particles situated at the Wannier center.

Since all Wannier states are related by translation of one lattice site, the Wannier centers $\langle x \rangle_{0\mu}$ and $\langle x \rangle_{0\tilde{\mu}} = \langle x \rangle_{0\mu} + n$, with n being an integer, describe two indistinguishable states. This is related to the fact, mentioned above, that the bulk polarization can be only determined modulo 1. However, if we can follow the adiabatic evolution between the two states, we would then be able to differentiate between a case with $\Delta \mathcal{P}^{\text{Bloch}} = 0$, where the Wannier states would come back to the same point, to a case with $\Delta \mathcal{P}^{\text{Bloch}} = n$, where the Wannier states would shift n lattice sites. For a closed path, this is precisely the quantized charge transport discussed at the end of last section in relation to the Chern number.

2.4 Entanglement spectrum

2.4.1 Entanglement and topology

Quantum entanglement has played an important role in the characterization of topological phases, in particular describing *topological order* [29], in systems like the fractional quantum Hall liquid [6, 116–118] or quantum spin liquids [119, 120]. These are strongly-correlated systems which are described in the low-energy and long-distance limit by an effective *topological quantum field theory* (TQFT). These phases cannot be reproduced in non-interacting systems, as interactions play an essential role in topological order. Like SPT phases, topologically ordered phases have features which are very robust against perturbations and do not depend on details of the system. Topologically ordered phases, however, are more fundamental than SPT phases, as they do not require symmetries to protect the phase. The first measure of entanglement used to characterize these phases was the entanglement entropy [30, 31, 121], which we introduce now.

The Hilbert space of a system, $\mathcal{H}$, can be partitioned into two different subspaces, $\mathcal{H}_A$ and $\mathcal{H}_B$. The two most common are spatial partitions [31], which we consider in this chapter, and particle-number partitions [121]. The ground state of the system can then be decomposed, using a Schmidt decomposition, as

$$|\Psi_0\rangle = \sum_i c_i \, |\psi_i\rangle_A \otimes |\psi_i\rangle_B \,, \tag{2.80}$$

where $|\psi_i\rangle_{A/B}$ form a basis of the corresponding Hilbert subspace. The coefficients c_i have information on the entanglement of the ground state between the two subspaces. The reduced density matrix of the system can be expressed as

$$\rho_A = \sum_i c_i^2 \, |\psi_i\rangle_A \, \langle \psi_i|_A \,, \tag{2.81}$$

and the entanglement entropy is then defined as the von Neumann entropy of the reduced density matrix,

$$S = -\operatorname{Tr}[\rho_A \log \rho_A]$$
$$= \sum_i c_i^2 \log[c_i^2]. \tag{2.82}$$

The coefficients c_i^2 are also eigenvalues of ρ_B, so the entanglement entropy can be computed from the reduced density matrix of either block. It was found [30, 31] that the entanglement entropy for the ground state of a gapped 2D system has the general form

$$S = \alpha L - \gamma + O(1/L) + ..., \tag{2.83}$$

where L is the size of the boundary of the subsystem and γ is the so-called *topological entanglement entropy*, as $\gamma \neq 0$ implies non-trivial topological order. This quantity is related to the total quantum dimension of the corresponding topological quantum field theory (TQFT) describing the phase, $\gamma = \log \mathcal{D}$, which is a measure of topological order. However, different TQFTs can have the same total quantum dimension and therefore the topological entanglement entropy is not, in general, sufficient to fully characterize the topology of the system.

In general, the reduced density matrix can be expressed as

$$\rho_A = e^{-\hat{\mathcal{H}}_E}, \tag{2.84}$$

where $\hat{\mathcal{H}}_E$ is known as the *entanglement Hamiltonian*, and its spectrum is known as the *entanglement spectrum*, which is equivalent to the spectrum of the reduced density matrix. The entanglement entropy is therefore equivalent to the thermodynamic entropy of the system described by the entanglement Hamiltonian at temperature $T = 1/k_B$. Li and Haldane proposed to use the entanglement spectrum [32] to characterize topologically ordered states, as it can provide much more information than the topological entanglement entropy. This was shown for Kitaev spin liquids [122] as well as for fractional quantum Hall [33]. For certain systems the low-lying spectrum of the entanglement Hamiltonian was found to be a fingerprint of the conformal field theory (CFT) that characterizes the topological order [32, 123].

The entanglement spectrum also proved to be a valuable tool in the study of non-interacting topological insulator and superconductor phases, where the topological entanglement entropy vanishes. In these systems the entanglement spectrum was shown to provide information about the edge spectrum. In particular it is equivalent to the spectrum of the flat-band Hamiltonian of the system with open boundaries. This was shown both for gapped systems [124] as well as gapless

systems [98] in higher dimensions. Even for non-interacting systems the reduced density matrix, and the entanglement spectrum, is difficult to compute. However, as noted by Peschel [36], for non-interacting systems the reduced density matrix can formally be expressed as

$$\rho_A = \mathcal{N}e^{-\hat{\mathcal{H}}_A}, \tag{2.85}$$

where $\mathcal{N}$ is a normalization and $\hat{\mathcal{H}}_A$ is now is a quadratic Hamiltonian, i.e. it describes free fermions. The entanglement spectrum can therefore be obtained from single-particle quantities, making it much easier to compute, see next section for more details.

As mentioned above the entanglement spectrum is a valuable tool in the study of topological order, but it is unclear what other information might be encoded in it beyond signatures of edge states, or how to extract it. This is also an open question for non-interacting systems, which are much easier to deal with. Our motivation in this part of the thesis is to study the entanglement spectrum of non-interacting systems as a stepping stone towards improving our understanding of the entanglement spectrum of strongly correlated systems.

2.4.2 Correlation matrix spectrum

In the case of non-interacting systems, such as the ones we focus on in this thesis, calculating the ES can be greatly simplified by using the correlation matrix, as shown by Peschel [36]. The entanglement Hamiltonian can be written as

$$\hat{\mathcal{H}}_A = \sum_{ij \in A} c_i^\dagger H_{A,ij} c_j, \tag{2.86}$$

where i, j can be any combination of numbers labelling the fermions in subsystem A. The entanglement Hamiltonian can be diagonalized as

$$\hat{\mathcal{H}}_A = \sum_\mu \varepsilon_\mu \gamma_\mu^\dagger \gamma_\mu, \tag{2.87}$$

where the new fermions are defined by $c_i = \sum_\mu \psi_\mu^i \gamma_\mu$, with $(U)_{\mu i} = \psi_i^\mu$ being the matrix that diagonalizes the single-particle entanglement Hamiltonian. In the following we will denote the spectrum of the single-particle entanglement Hamiltonian H_A, as *single-particle entanglement spectrum*.

We are now interested in computing the correlation matrix, $C_{ij} = \left\langle c_i^\dagger c_j \right\rangle$. In order to do so, let us first consider the expectation value

$$\begin{aligned} \left\langle \gamma_\mu^\dagger \gamma_\nu \right\rangle &= \text{Tr}[\rho_A \gamma_\mu^\dagger \gamma_\nu] \\ &= \mathcal{N}\text{Tr}[e^{-\sum_\lambda \varepsilon_\lambda \gamma_\lambda^\dagger \gamma_\lambda} \gamma_\mu^\dagger \gamma_\nu]. \end{aligned} \tag{2.88}$$

Notice first that

$$e^{-\sum_\lambda \varepsilon_\lambda \gamma_\lambda^\dagger \gamma_\lambda} \gamma_\mu^\dagger |n_\mu = 0\rangle = \gamma_\mu^\dagger e^{-\varepsilon_\mu} e^{-\sum_\lambda \varepsilon_\lambda \gamma_\lambda^\dagger \gamma_\lambda} |n_\mu = 0\rangle$$

$$e^{-\sum_\lambda \varepsilon_\lambda \gamma_\lambda^\dagger \gamma_\lambda} \gamma_\mu^\dagger |n_\mu = 1\rangle = \gamma_\mu^\dagger e^{-\varepsilon_\mu} e^{-\sum_\lambda \varepsilon_\lambda \gamma_\lambda^\dagger \gamma_\lambda} |n_\mu = 1\rangle = 0. \qquad (2.89)$$

Using this we can rewrite the expectation value as

$$\begin{aligned}
\left\langle \gamma_\mu^\dagger \gamma_\nu \right\rangle &= e^{-\varepsilon_\mu} \mathcal{N} \text{Tr}[\gamma_\mu^\dagger e^{-\sum_\lambda \varepsilon_\lambda \gamma_\lambda^\dagger \gamma_\lambda} \gamma_\nu] \\
&= e^{-\varepsilon_\mu} \left\langle \gamma_\nu \gamma_\mu^\dagger \right\rangle \\
&= e^{-\varepsilon_\mu} (\delta_{\mu\nu} - \left\langle \gamma_\mu^\dagger \gamma_\nu \right\rangle),
\end{aligned} \qquad (2.90)$$

and therefore

$$\left\langle \gamma_\mu^\dagger \gamma_\nu \right\rangle = \frac{1}{1 + e^{\varepsilon_\mu}} \delta_{\mu\nu}. \qquad (2.91)$$

We can now compute the elements of the subsystem correlation matrix as

$$\begin{aligned}
C_{A,ij} &= \left\langle c_i^\dagger c_j \right\rangle \\
&= \sum_{\mu\nu} \left\langle (\gamma_\mu^\dagger \psi_\mu^{*\,i})(\psi_\nu^j \gamma_\nu) \right\rangle \\
&= \sum_\mu \psi_\mu^{*\,i} \psi_\mu^j \frac{1}{1 + e^{\varepsilon_\mu}},
\end{aligned} \qquad (2.92)$$

where $i, j \in A$. The eigenvalues of the subsystem correlation matrix, which we will denote by ξ_μ, are related to the single-particle eigenvalues of the entanglement Hamiltonian as

$$\begin{aligned}
\xi_\mu &= (1 + e^{-\varepsilon_\mu})^{-1} \\
\varepsilon_\mu &= \log[(1 - \xi_\mu)/\xi_\mu],
\end{aligned} \qquad (2.93)$$

with the eigenstates being equal. The full correlation matrix is nothing else than the projector onto the occupied bands, and therefore for a gapped system at zero temperature it has eigenvalues 0 and 1. The eigenvalues of the subsystem correlation matrix, however, may lay anywhere in between, $\xi_\mu \in [0, 1]$. The spectrum of the subsystem correlation matrix is denoted, following reference [39], as the *entanglement occupancy spectrum* (EOS).

Once the relation between the EOS and the single-particle ES has been established, it is also easy to relate the ES to the EOS [125]. Using the diagonal form

of the entanglement Hamiltonian the reduced density matrix can be obtained as

$$\rho_A = \prod_\mu \frac{e^{-\varepsilon_\mu \gamma_\mu^\dagger \gamma_\mu}}{1 + e^{-\varepsilon_\mu}}. \tag{2.94}$$

The eigenstates of the reduced density operator are then obtained by occupying different numbers of the single-particle eigenstates of C_A, according to a set of occupation numbers $\{n_i\}$. In terms of the EOS, the eigenvalues in the ES are then given by

$$\lambda[\{n_i\}] = \prod_{\mu \in occ} \xi_\mu \prod_{\mu \in emp} (1 - \xi_\mu)$$

$$= \prod_\mu (1 - \xi_\mu) \left(\frac{\xi_\mu}{1 - \xi_\mu} \right)^{n_i^\mu}. \tag{2.95}$$

Since the information of the ES is already contained in the EOS, and it is considerably easier to work with the latter, we will focus on the EOS in this thesis.

2.4.3 Properties of the Entanglement Occupancy Spectrum

In the introduction of this chapter we mentioned that the ES has information about the edge-spectrum of the corresponding system with open boundaries [32, 98, 124]. For a gapped system at zero temperature the correlation matrix can also be expressed in terms of the flat-band Hamiltonian, $Q = H \cdot (H^{-2})^{1/2}$, as

$$C = \frac{1}{2}(I - Q). \tag{2.96}$$

A Hamiltonian invariant under, for example, a local chiral symmetry S, $SHS^{-1} = -H$, will result in

$$SCS^{-1} = \frac{1}{2}(I - SHS^{-1} \cdot [(SHS^{-1})^2]^{1/2}).$$

$$= \frac{1}{2}(I + H \cdot (H^2)^{1/2})$$

$$= I - C. \tag{2.97}$$

The same applies to the subsystem correlation matrix, $SC_A S^{-1} = I_A - C_A$. Consider an eigenstate $|\psi\rangle$ of C_A that is also an eigenstate of the symmetry $S |\psi\rangle = \pm |\psi\rangle$. Applying the chiral symmetry on C_A and acting on the eigenstate with the transformed matrix gives

$$SC_A S |\psi\rangle = (I_A - C_A) |\psi\rangle$$

$$= (1 - \xi) |\psi\rangle. \tag{2.98}$$

On the other hand, using that the eigenstate is also an eigenstate of the symmetry, we have

$$
\begin{aligned}
SC_A S \left| \psi \right\rangle &= \pm \, SC_A \left| \psi \right\rangle \\
&= \pm \, \xi S \left| \psi \right\rangle \\
&= \xi \left| \psi \right\rangle .
\end{aligned}
\tag{2.99}
$$

The symmetric eigenstate must have a corresponding eigenvalue $\xi = 1/2$. These are the *virtual topological edge states*. A similar consideration can be made for other symmetries, such as particle-hole symmetry.

In Fig. 2.5 we show the EOS and the surface spectrum for the dashed line in the phase diagram in Fig. 2.3 ($t_2 = -2t_1, \kappa = \kappa' = 0$). In Fig. 2.5(a) and (b) we show the result for a large system ($L = 200$). As we saw before, the surface spectrum presents a number of zero-energy states per edge equal to the winding number of the system, and gapless points where the topological transitions happen. These zero-energy topological edge states are reflected in the EOS as $1/2$ virtual topological edge states. The transition points are marked by a discontinuity where the edge states leave $\xi = 1/2$ and meet with the bulk. In Fig. 2.5(c) and (d) we look at the same plots for a very small system ($L = 12$), where the situation is very different. In the surface spectrum there is a finite size effect where the edge states hybridize and split from zero energy. As a result, it is not so obvious looking at the surface spectrum in which topological phase the system is in or even where the transitions are. In the EOS, however, the finite size effect is generically weaker, given that it is computed for PBC. Most remarkably, in the $\nu = 1$ phase there is no hybridization of the $1/2$ states even though they sit on top of each other. This behaviour of the EOS has been observed for certain systems [126]. This is no longer true for the $\nu = 2$ phase but the gap between the virtual topological edge modes and the bulk is still large. Furthermore, the transition points can still be easily identified by discontinuities in the EOS. The properties of the edge are therefore often easier to interpret using the EOS rather than the surface energy spectrum.

It is interesting to note that for the EOS shown here all states are doubly degenerate. This is in fact a consequence of translational invariance. Consider the full correlation function expressed as

$$
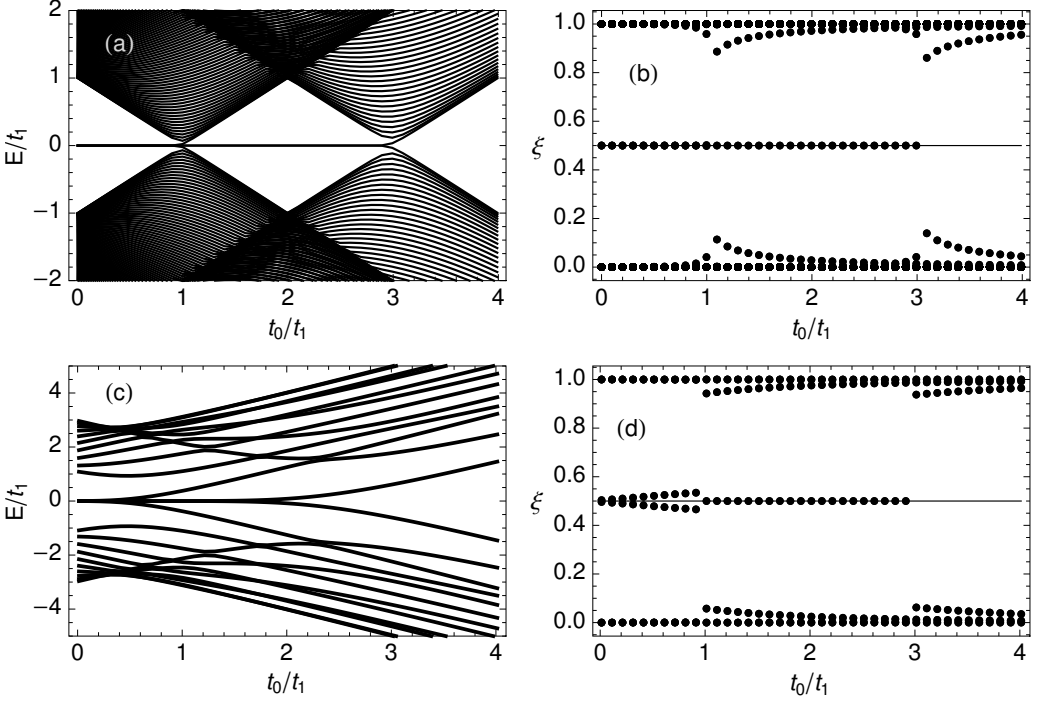C = \begin{pmatrix} C_A & C_{AB} \\ C_{AB}^\dagger & C_B \end{pmatrix}.
\tag{2.100}
$$

Figure 2.5: Edge spectrum and EOS along the dashed path (i.e. $t_2 = -2t_1$) of Fig. 2.3 for parameters $\kappa = \kappa' = 0$. (a) and (b) are computed for $L = 200$ sites. (c) and (d) are computed for a small system of $L = 12$ sites. In the energy spectrum of the small system it is difficult to tell where the phase transition happens due to a finite size effect. This finite size effect is much smaller in the EOS where, even for a small system, discontinuities in the spectrum signal phase transitions.

Using the projector property, $C^2 = C$, we obtain the following identities

$$
\begin{aligned}
C_A(1 - C_A) &= C_{AB}C_{AB}^\dagger \\
C_B(1 - C_B) &= C_{AB}^\dagger C_{AB} \\
C_A C_{AB} + C_{AB}C_B &= C_{AB} \\
C_{AB}^\dagger C_A + C_B C_{AB}^\dagger &= C_{AB}^\dagger.
\end{aligned} \tag{2.101}
$$

If $|\psi\rangle$ is an eigenstate of C_A with eigenvalue ξ, we have

$$
\begin{aligned}
C_B(C_{AB}^\dagger |\psi\rangle) &= (C_{AB}^\dagger - C_{AB}^\dagger C_A) |\psi\rangle \\
&= (1 - \xi)(C_{AB}^\dagger |\psi\rangle),
\end{aligned} \tag{2.102}
$$

i.e. $C_{AB}^\dagger \ket{\psi}$ is an eigenstate of C_B with eigenvalue $1 - \xi$. This in turn implies that the spectra of C_A and C_B are symmetric with respect of each other. If the system furthermore posses translational invariance, such that $C_B = C_A$, we have

$$C_A(C_{AB}^\dagger \ket{\psi}) = (1 - \xi)(C_{AB}^\dagger \ket{\psi}), \qquad (2.103)$$

and the EOS is itself symmetric. This implies that if the ES has an eigenvalue ε, $-\varepsilon$ must also be an eigenvalue of the ES. This in combination with an additional symmetry such as chiral symmetry makes the EOS two-fold degenerate.

As it is implied, the $1/2$ virtual topological edge states localize on the virtual edges, but there is a more general relation between the eigenvalues of the EOS and localization. It was found by Peschel that all low-lying states in the ES are localized at the boundaries [37] for large enough systems such that the two virtual cuts are independent of each other. In Fig. 2.6(a) and (b) we show the first few low-lying eigenstates in the surface spectrum and EOS, respectively, in the $\nu = 1$ phase. In the surface spectrum there are only two states that localize on the boundaries of the system while the rest are bulk states. In the EOS, however, all low-lying states localize in the virtual edges.

In Fig. 2.6.(c) we show the average position of all the eigenstates of the EOS, $\langle x \rangle_\mu = \langle \psi_\mu | \hat{x} | \psi_\mu \rangle$, ordered by their eigenvalue. We find, apparently, two different sets of eigenstates. We refer as *bulk states* those exponentially close to $\xi = 0, 1$ and as *edge states* the states away from $\xi = 0, 1$ that localize near the virtual edges. Note that typically the closer an eigenstate is to $\xi = 1/2$ the more localized it is on the virtual edge, with the virtual topological edge state being the most localized on the edge. The reason the bulk states do not follow the trend of the edge states is purely due to numerical reasons since they are all almost degenerate at $\xi \approx 0, 1$. Note that, since the bulk states are, to a good approximation, also eigenstates of C they can be expressed as Wannier states [115], which are maximally localized. This makes the distinction between bulk and edge states somewhat artificial, but we will keep the nomenclature for practical purposes. Sometimes the low-lying states around $\xi = 1/2$ are also found in the literature referred to as 'midgap states'.

2.4.4 Extracting the bulk polarization from the entanglement occupancy spectrum

In paper I we study how the bulk polarization $\tilde{\mathcal{P}}$, defined in Eq (2.57), is encoded in the EOS and how can it be extracted. First we study the case of systems with an equispaced ES, which is a typical feature of integrable systems [35]. Equispaced means that the entanglement energies associated to each virtual edge are given, in the thermodynamic limit, by $\varepsilon_{n\alpha} = \varepsilon_\alpha + n\delta_\alpha$, where $\alpha = L, R$ labels the two edges
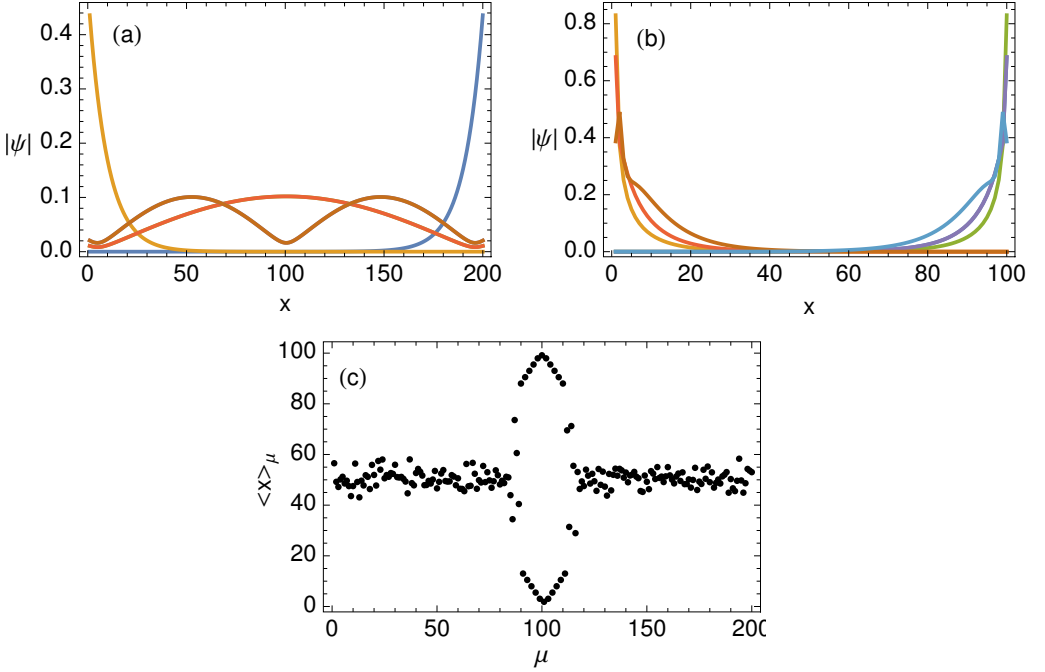
Figure 2.6: (a) and (b) Low-lying eigenstates of the Hamiltonian with open boundary conditions and the EOS, respectively. Computed for $L = 200$ at $t_0 = 0.9t_1, t_2 = 0$. (c) Average position of the eigenstates of the EOS (obtained for the same parameters), $\langle x \rangle_\mu = \langle \psi_\mu | \hat{x} | \psi_\mu \rangle$, ordered by their eigenvalue. Generically the closer the eigenvalue is to $1/2$, the more localized to the edge a state is. The band around $\langle x \rangle_\mu = 50$ corresponds to near-degenerate bulk states at $\xi = 0, 1$.

of region A and n is an integer labelling all states. In this type of systems we found that if we order the eigenvalues of the EOS by their value and we sum up every other one,

$$\chi = \sum_j \xi_{2j-1} \bmod 1, \tag{2.104}$$

we could obtain the bulk polarization $\tilde{\mathcal{P}}$ in the thermodynamic limit up to a sign,

$$\lim_{L \to \infty} \left| \tilde{\mathcal{P}} \right| = \lim_{L \to \infty} \chi \bmod 1. \tag{2.105}$$

This means that the bulk polarization could be $\tilde{\mathcal{P}} = \chi$ or $\tilde{\mathcal{P}} = 1 - \chi$. This expression explains previous observations found in the literature about similarities between the Zak phase and the edge states in the EOS [38, 39]. The two become identical when there is only one pair of midgap states, away from $\xi = 0, 1$ [40].

In the special case of chiral symmetric systems, the relation between the Zak phase and the virtual topological states becomes especially simple. For each eigenvalue ξ included in χ there is another eigenvalue $1 - \xi$ in the sum and therefore their contribution vanishes when taken modulo 1. The only eigenvalues whose contribution do not vanish are the ones from the virtual topological edge states, $\xi = 1/2$. Therefore $\tilde{\mathcal{P}} = 0$ for phases with an even number of virtual topological edge states while $\tilde{\mathcal{P}} = 1/2$ corresponds to phases with an odd number of them. This is a well-known consequence of the bulk-boundary correspondence which is shown here in a new way.

For general non-interacting gapped system in 1D, the formula in Eq. (2.104) needs to be adapted. Instead of summing up every other eigenvalue, we sum up all eigenvalues related to the left virtual edge,

$$\chi = \sum_{j \in \mathcal{L}} \xi_j \bmod 1. \tag{2.106}$$

One can obtain $\tilde{\mathcal{P}}$ in the thermodynamic limit as

$$\lim_{L \to \infty} \tilde{\mathcal{P}} = \lim_{L \to \infty} \chi \bmod 1. \tag{2.107}$$

In practice, see the discussion at the end of section 2.4.3, we define the subspace $\mathcal{L}$ as the one including all eigenstates with $\langle x \rangle < L/4$, where $L/4$ is the center of region A. How exactly we choose the eigenvalues included in the sum is not important as long as we include all the edge states from the left virtual edge that are far from $\xi = 0, 1$, and none of the ones from the right virtual edge.

The expression above reduces to Eq.(2.105) for systems with an equispaced ES, and the sign ambiguity comes from summing either over the left virtual edge states or over the right ones. This result is a consequence of a known correspondence between the ES and the bulk polarization [127] which is now greatly simplified in terms of the EOS. In paper I we also show numerical results comparing our method with the polarization obtained using Resta's expression (see Eq.(2.40)), using the long-range SSH model both in the clean limit and in presence of disorder.

2.4.5 Alternative bulk polarization and Chern numbers from the entanglement occupancy spectrum

In Eq. (2.106) we have to take the modulo 1 because there is an ambiguity in how many $\xi = 1$ bulk modes are included into the sum. If we found a way of treating the bulk modes in a consistent way we could construct an equivalent bulk polarization defined in $\mathbb{R}$. By opening the system at the bond between $j = L/2$ and $j = L/2 + 1$

all eigenvalues in the EOS that are not related to the left virtual cut are pushed to $\xi = 0, 1$. We then define the alternative bulk polarization $\tilde{\mathcal{P}}_o$ as the one obtained when we introduce a flux as

$$\left| \tilde{\Psi}_o^\Phi \right\rangle = e^{-i\Phi \hat{N}_A} \left| \tilde{\Psi}_o^0 \right\rangle \tag{2.108}$$

to the ground state of the open chain, $\left| \tilde{\Psi}_o^0 \right\rangle$. Note that Φ is not actually a magnetic flux, as the chain is open, but just a parameter. $\tilde{\mathcal{P}}_o$ is therefore not the actual polarization of the open chain. This alternative bulk polarization can be obtained simply as

$$\tilde{\mathcal{P}}_o = \text{Tr}[C_{A,o}], \tag{2.109}$$

where $C_{A,o}$ is the subsystem correlation matrix for the open chain. Comparing with Eq.(2.107) we see that $\tilde{\mathcal{P}}_o$ includes all the left edge eigenvalues of the EOS and as long as the Hamiltonian of the open chain remains gapped, i.e. no states crossing the Fermi energy, the bulk modes give a continuous contribution to $\tilde{\mathcal{P}}_o$. This means that for any two points in parameter space connected by a gapped path, C_λ, the total change in the bulk polarization over such a path can be obtained as

$$\Delta \tilde{\mathcal{P}}_{C_\lambda} = \tilde{\mathcal{P}}_o(\lambda_f) - \tilde{\mathcal{P}}_o(\lambda_i), \quad \Delta \tilde{\mathcal{P}}_{C_\lambda} \in \mathbb{R}, \tag{2.110}$$

where this change is defined in $\mathbb{R}$, unlike the one introduced in Eq. (2.31).

There is, however, one caveat to using $\tilde{\mathcal{P}}_o$. For topological phases there will be zero-energy modes in the open chain and its Hamiltonian is therefore not gapped. The ground state of the open chain is degenerate and therefore $\tilde{\mathcal{P}}_o$ is not well defined. We can, however, break the symmetries, by using $\kappa \neq 0$ in the model (see Eq 2.8), and study the bulk polarization in the parameter space (t_0, κ), where t_0 drives the phase transition. We find that $\tilde{\mathcal{P}}_o$ presents discontinuities at the symmetric limit that signal the presence of topological edge states. This was observed previously in $\text{Tr}[C_{A,o}]$ [125].

As mentioned in section 2.3.4 the change in the bulk polarization over a loop is equal to the correspondent Chern number. In our specific case, the change in the bulk polarization over a loop in (t_0, κ) parametrized by θ gives the Chern number over the torus defined by (θ, Φ), where Φ is the parameter introduced in Eq. (2.108). Using $\tilde{\mathcal{P}}$, it is given by

$$C = \int_0^{2\pi} d\theta \, \partial_\theta \tilde{\mathcal{P}}(\theta). \tag{2.111}$$

However, since $\tilde{\mathcal{P}}$ is defined modulo 1 one has to be careful when computing the derivative, as the jumps need to be properly accounted for. If we use $\tilde{\mathcal{P}}_o$,

$$C = \int_0^{2\pi} d\theta \, \partial_\theta \tilde{\mathcal{P}}_o(\theta), \tag{2.112}$$

the only contribution to the integral comes from the discontinuities, which only happen at the symmetric limit $\kappa = 0$. Consider a loop that crosses $\kappa = 0$ at two points $(t_0, 0)$ and $(t'_0, 0)$. If we place t'_0 somewhere in the trivial phase there will be no discontinuities at this point, and the Chern number of this loop can then be obtained as

$$C = \tilde{\mathcal{P}}_o(t_0, \kappa = 0^+) - \tilde{\mathcal{P}}_o(t_0, \kappa = 0^-), \tag{2.113}$$

see Fig.6 in paper I.

Next we focus on 2D systems and study the bulk polarization for an inversion symmetric Chern insulator described by the Hamiltonian

$$H = \sum_{i\alpha, j\beta} \sum_k c_{i\alpha}^\dagger(k) H_{i\alpha, j\beta}(k) c_{j\beta}(k),$$

$$H_{i\alpha, j\beta}(k) = \frac{1}{2}(i\sigma_x - \sigma_z)\delta_{i, j+1} + \frac{1}{2}(-i\sigma_x - \sigma_z)\delta_{i, j-1}$$
$$+ (\sin(k)\sigma_y + [2 - m - \cos(k)]\sigma_z)\delta_{ij}. \tag{2.114}$$

Considering the torus defined by the two momenta, we can make a virtual cut along one of the directions and obtain two cylinders. The momentum of the periodic direction can be regarded as a parameter and the system can be treated effectively as 1D for each momentum k, such that the discussion above also applies. $\tilde{\mathcal{P}}_o(k)$ has discontinuities when the gapless modes cross the Fermi energy, which in the model used can only happen at $k = 0, \pi$. We can then use this to compute the Chern number of the occupied bands as

$$C = [\tilde{\mathcal{P}}_o(k = 0^-) - \tilde{\mathcal{P}}_o(k = -\pi^+)] + [\tilde{\mathcal{P}}_o(k = \pi^-) - \tilde{\mathcal{P}}_o(k = 0^+)]. \tag{2.115}$$

In the context of 2D Chern insulators it was shown that the presence of gapless modes was encoded in the discontinuities of $\text{Tr}[C_{A,o}]$ [125]. The sum of the changes in the trace at every discontinuity was referred to as the *trace index*, which was shown to be equal to the Chern number by relating it to the Hall current. Our results show this connection in another way by framing $\text{Tr}[C_{A,o}]$ as a geometric quantity.

2.4.6   Wannier states and the entanglement occupancy spectrum

In Section 2.4.4 we discussed a relation between the EOS and the bulk polarization. The latter is equivalent to the Wannier center, as discussed in Section 2.3.5. However, the relation between the entanglement spectrum and Wannier states is not restricted to that quantity. It has been pointed out in the literature [38, 39, 128] that the subsystem correlation matrix, $C_A = R_A P R_A$, has the same spectrum

as PR_AP, where P is the occupied band projector and R_A is the projector onto subsystem A. This is due to the fact that both P and R_A are projectors. The form of the operator PR_AP has a resemblance to PXP, whose eigenvectors are the Wannier states and eigenvalues are the Wannier spectrum. By interpolating between X and R_A it has been shown that the EOS and the Wannier spectrum share some properties, like the spectral flow. It has also been used to estimate the spacing between entanglement eigenvalues in terms of the Wannier center and localization properties of the Wannier states [128]. In this section we give a approximate interpretation of the EOS in terms of Wannier states. The aim is to give some qualitative understanding of the EOS rather than rigorous relations.

Since they are constructed from the occupied band, Wannier states are eigenstates of the correlation matrix,

$$C \ket{w_j} = \ket{w_j}. \tag{2.116}$$

This implies that Wannier states that fully localize in subsystem A will also be eigenstates of C_A, with eigenvalue 1. A similar argument can be made with the empty band Wannier states, which will result in a 0 eigenvalue. These states correspond to the bulk of the EOS. Wannier states that have weight in both A and B, will no longer be exact eigenstates of C_A, and will contribute to the part of the spectrum with $0 < \xi < 1$.

We consider an ansatz based on truncated Wannier states to approximate the eigenvectors of C_A. A Wannier state can be expressed in terms of subsystem A and B as

$$\ket{w_j} = \begin{pmatrix} \ket{w_{jA}} \\ \ket{w_{jB}} \end{pmatrix}. \tag{2.117}$$

The subsystem correlation matrix is then given by

$$C_A = \sum_j \ket{w_{jA}} \bra{w_{jA}}. \tag{2.118}$$

Acting now with $\ket{w_{jA}}$ we have

$$C_A \ket{w_{jA}} = \braket{w_{jA}|w_{jA}} \ket{w_{jA}} + \sum_{l \neq j} \braket{w_{lA}|w_{jA}} \ket{w_{lA}}. \tag{2.119}$$

This is an approximate eigenvalue equation, $Ax = \lambda_x x + r$. From the Bauer-Fike theorem, C_A has an eigenvalue λ such that

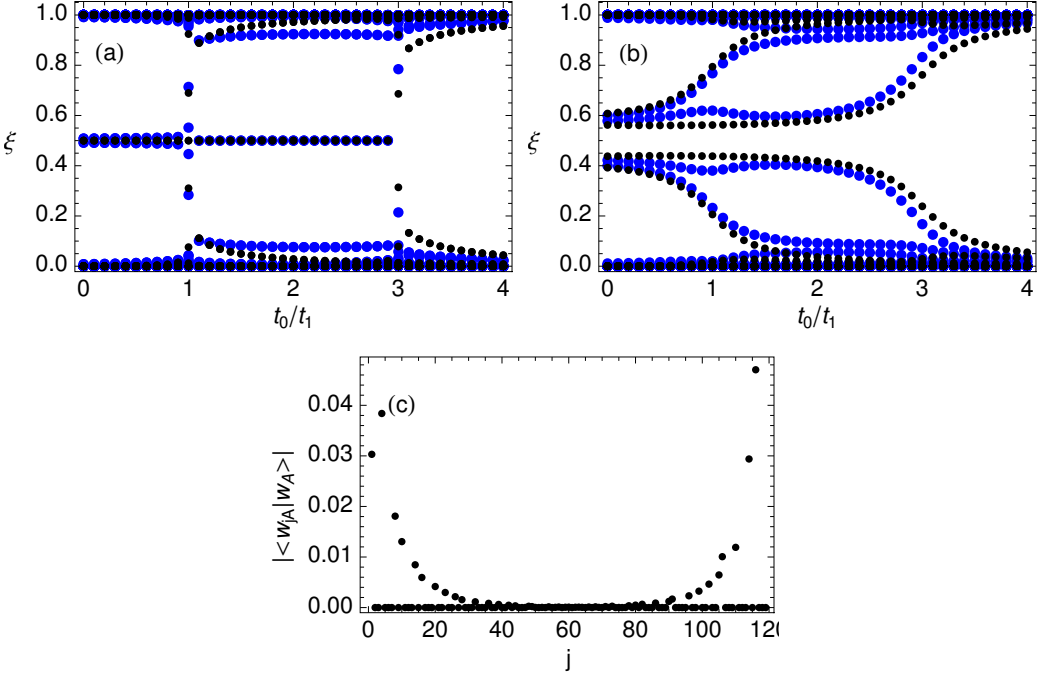$$|\lambda - \lambda_x| \leq \frac{\|r\|}{\|x\|}. \tag{2.120}$$

Figure 2.7: (a) and (b) EOS (black dots) and approximation in Eq.(2.121) (blue dots) for the model in Eq.(2.8) with parameters $t_2 = -2t_1$ and system size of $L = 120$. For the topological case in (a), with $\kappa = 0$ and the trivial case (b) with $\kappa = 0.3t_1$. In (c) we show the overlap between the truncated Wannier state $|w_A\rangle$ closest to $1/2$ and the rest of Wannier states. Even for the truncated case the overlaps are small, which leads to a small error in the approximation, see below Eq.(2.121).

The eigenvalues of C_A are then approximated by

$$\xi_j = \langle w_{jA}|w_{jA}\rangle, \tag{2.121}$$

and the error is estimated by

$$\frac{\|r\|}{\|x\|} \leq \sum_{l \neq j} |\langle w_{lA}|w_{jA}\rangle| \times \frac{\||w_{lA}\rangle\|}{\||w_{jA}\rangle\|}. \tag{2.122}$$

The overlap between different Wannier states vanishes in the full system, $\langle w_l|w_j\rangle = \delta_{jl}$. We observe numerically that this overlap is small even when the Wannier states are truncated, see Fig.2.7.(c). To minimize the error further we consider the Wannier states with highest weight on subsystem A. A similar argument can be done using the empty band Wannier states, however the corresponding eigenvalues

can be obtained by using the chiral symmetry of the EOS. There are two sanity checks we can do to see that the approximation is not bad. A Wannier state that fully localizes in subsystem A will have $\xi_j = \langle w_{jA}|w_{jA}\rangle \approx 1$. Secondly, for a system with chiral or inversion symmetry, the Wannier center is located at a bond, therefore there must be one Wannier state such that $\xi_j = \langle w_{jA}|w_{jA}\rangle = 1/2$, corresponding to a topological virtual edge state of the EOS. In Fig.2.7.(a) and (b) we compare the exact EOS (in black) with the approximate values obtained using Eq. (2.121) (in blue), for (a) a topological and (b) non-topological case. The approximation reproduces the EOS qualitatively.

Another interesting thing to note is that this approximation reproduces the result from paper I, discussed in Section 2.4.4. We want to consider the eigenvalues related to the right boundary of A. This implies that the Wannier states we must use in the approximation are those that localize near the right boundary of A. Since the Wannier states are related by a one-site translation, the eigenvalues related to the right boundary of A can be obtained as the cumulative weights of a Wannier state. These can be obtained as

$$\xi_\mu = \sum_{x=1}^{\mu} w^2(x). \tag{2.123}$$

The resulting spectrum is the same regardless of the choice of the Wannier state $|w\rangle$ as long as it has not been truncated by the left boundary. Summing all the right eigenvalues we have

$$\sum_\mu \xi_\mu = \sum_{\mu=1}^{L}\sum_{x=1}^{\mu} w^2(x)$$
$$= \sum_{x \leq \mu} w^2(x). \tag{2.124}$$

The latter double sum can be rewritten into

$$\sum_\mu \xi_\mu = \sum_{x=1}^{L}\sum_{\mu=x}^{L} w^2(x)$$
$$= \sum_{x=1}^{L}(L+1-x)w^2(x), \tag{2.125}$$

Noting than the last term is minus the Wannier center, which is equal to the bulk polarization, we have

$$\sum_\mu \xi_\mu = -\mathcal{P}^{\text{Bloch}} + (L+1), \tag{2.126}$$

and we recover the result from paper I, discussed in Section 2.4.4.

Chapter 3

Topology in critical systems

In the last chapter we discussed the classification of topological insulators and superconductors, see Section 2.2, where one key assumption is the existence of a bulk gap. At the critical point between two different topological phases, where there is no bulk gap, the topological invariants introduced for gapped systems are not well-defined, as they have to change between different integer values. Furthermore, when considering topological systems with open boundary conditions (OBC), it was thought that at the phase transition all edge modes hybridize with the bulk, as the correlation length diverges. Recently this question was revisited [45–49] and it was shown that critical systems can indeed host topological zero-energy edge modes. However, it seems that one needs to introduce new topological invariants to characterize the topological modes.

Let us consider as an example the winding number defined for two-band gapped systems with chiral symmetry, defined in Eq. (2.64). There are several expressions used in the literature that are equivalent to each other when a gap is present, e.g.

$$
\begin{aligned}
\nu &= \frac{1}{2\pi} \oint dk \, \partial_k \, \mathrm{Im} \log[h_x(k) - ih_y(k)] \\
&= \frac{1}{2\pi} \oint dk \, \frac{(\partial_k h_x(k))h_y(k) - h_x(k)\partial_k h_y(k)}{h_x(k)^2 + h_y(k)^2}.
\end{aligned} \tag{3.1}
$$

When computing this winding number at a critical point, at the momenta where the bands cross each other ($h_x(k_c) = h_y(k_c) = 0$), the two expressions are not necessarily identical any longer. The first expression is not well defined while the second one can be well defined in some specific cases, but not in general. To gain more intuition, we can rewrite the winding number into an expression that depends explicitly on the eigenstates [110, 111] ,

$$
\nu = \frac{2i}{\pi} \oint dk \, \mathrm{Tr}[P_B P_{\mathrm{occ}}(k) P_A \partial_k P_{\mathrm{occ}}], \tag{3.2}
$$

where $P_{A/B} = (I \pm S)/2$ are the projectors onto the two sublattices defined by the chiral symmetry S, and $P_{\mathrm{occ}}(k)$ is the projector onto the occupied band. Since the system is gapless, the occupied band is not uniquely defined. Furthermore, in some critical points, the bands cross each other at some momenta k_c. Since there is a crossing, the occupied band is continuous at this point, but not differentiable, which makes the winding number ill-defined.

Since the topic only started to attract attention recently, the description of topological phases in gapless systems is far from being complete. In this chapter we will give an overview of the different ways that have been proposed for regularizing the topological invariants at critical points, and discuss their advantages and shortcomings. We will also discuss the regularization procedure we proposed in paper III.

3.1 Existence of topological edge modes

Before jumping into the discussion about topological invariants, it is a good exercise to show that an interphase between a critical and a gapped phase can host a state exponentially localized at the boundary. Consider again the Bloch Hamiltonian of the extended SSH chain (see Eq. (2.10)),

$$
H(k) = \begin{pmatrix} 0 & t_0 + t_1 e^{ik} + t_2 e^{2ik} \\ t_0 + t_1 e^{-ik} + t_2 e^{-2ik} & 0 \end{pmatrix}
$$
$$
= \begin{pmatrix} 0 & f(k) \\ f(k)^* & 0 \end{pmatrix}. \tag{3.3}
$$

The model has a gapless point at $k = 0$ for $t_0 + t_1 + t_2 = 0$. Near this point we can expand into

$$
f(k) = (t_0 + t_1 + t_2) + ik(t_1 + 2t_2) - k^2(t_1/2 + 2t_2), \tag{3.4}
$$

where we ignore higher order terms. We consider first the case $t_2 = 0$, which corresponds to the usual SSH chain. We can then transform the Hamiltonian into real space by making the substitution $ik \to \partial_x$,

$$
H(x) = \begin{pmatrix} 0 & (t_0 + t_1) + t_1 \partial_x \\ (t_0 + t_1) + t_1 \partial_x^\dagger & 0 \end{pmatrix}. \tag{3.5}
$$

In this Hamiltonian we can identify the mass term $m = t_0 + t_1$, which now we promote to a position dependent parameter $m(x)$. We use the ansatz $\Psi(x) =$

$(0, \psi(x))$, so that

$$H(x)\Psi(x) = \begin{pmatrix} \partial_x \psi(x) + m(x)\psi(x) \\ 0 \end{pmatrix}$$

$$= 0, \tag{3.6}$$

which is fulfilled by

$$\psi(x) = N e^{-\int_0^x dy\, m(y)}. \tag{3.7}$$

Before considering critical points, we examine first an interphase between two gapped phases with

$$m(x) = \begin{cases} +|m_0| & x > 0. \\ -|m_0| & x < 0. \end{cases}, \quad \psi(x) = \begin{cases} N e^{-|m_0|x} & x > 0 \\ N e^{|m_0|x} & x < 0, \end{cases} \tag{3.8}$$

which indeed describes a state localized at the interphase where the mass term changes sign, as depicted in Fig.3.1.(a). This effect is commonly known as *mass inversion* [129] and it is at the source of the bulk-boundary correspondence in gapped systems.

We can consider now an interphase between the critical phase of the SSH chain and one of the gapped phases [46], depicted in Fig. 3.1.(b),

$$m = \begin{cases} +|m_0| & x > 0. \\ 0 & x < 0. \end{cases}, \quad \psi(x) = \begin{cases} N e^{-|m_0|x} & x > 0 \\ N & x < 0. \end{cases} \tag{3.9}$$

This solution corresponds to an extended state in the critical phase that decays into the gapped phase, but no localized topological states are found in this case. Next, consider again the Hamiltonian obtained by expanding around the gapless point, Eq. (3.4). We set $-(t_1/2 + 2t_2) = 1$ and identify again $m = (t_0 + t_1 + t_2)$ as a mass term, and $\kappa = -t_1 - 2t_2$ as a kinetic term. We can now express the Hamiltonian in position space as

$$H(x) = \begin{pmatrix} 0 & m - \kappa \partial_x - \partial_x^2 \\ m - \kappa \partial_x^\dagger - \partial_x^{\dagger 2} & 0 \end{pmatrix}. \tag{3.10}$$

We, again, promote the mass and kinetic term to position dependent quantities, and use the same ansatz as before, obtaining

$$H(x)\Psi(x) = \begin{pmatrix} m(x)\psi(x) - \kappa(x)\partial_x \psi(x) - \partial_x^2 \psi(x) \\ 0 \end{pmatrix}$$

$$= 0, \tag{3.11}$$

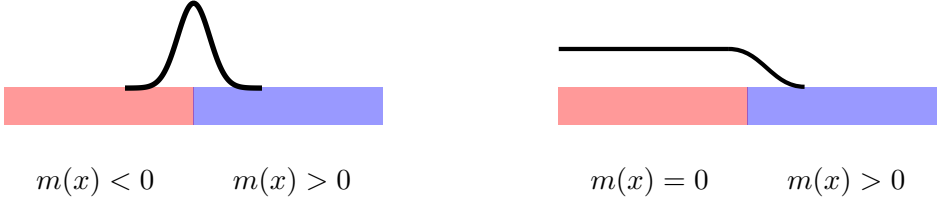$$m(x) < 0 \qquad m(x) > 0 \qquad\qquad m(x) = 0 \qquad m(x) > 0$$

Figure 3.1: Diagram of the interphase between two phases (red and blue) with the correspondent mass term that characterizes each phase. Zero energy solutions are shown in black. (a) Interphase between trivial and non-trivial gapped phase. (b) Interphase between trivial gapless and gapped phases.

Consider now an interphase between a gapless phase and a gapped phase, depicted in Fig.3.2, where the kinetic term changes sign,

$$m(x) = \begin{cases} +|m_0| & x > 0. \\ 0 & x < 0. \end{cases}, \quad \kappa(x) = \begin{cases} +|\kappa_0| & x > 0 \\ -|\kappa_0| & x < 0. \end{cases} \tag{3.12}$$

We can now look at a piece-wise solution. In the left, $x < 0$, we have

$$\begin{aligned} 0 =& \partial_x^2 \psi(x) - |\kappa_0| \partial_x \psi(x) \\ =& \partial_x (\partial_x \psi(x) - |\kappa_0| \psi(x)), \end{aligned} \tag{3.13}$$

for which there are two types of solutions. $\psi(x)$ can be a constant as in the case above with $t_2 = 0$, which corresponds to a gapless extended state. However, now we have an additional solution where

$$\partial_x \psi(x) - |\kappa_0| \psi(x) = 0, \tag{3.14}$$

which is fulfilled by an exponentially decaying state

$$\psi(x) = N e^{|\kappa_0| x} \quad x < 0. \tag{3.15}$$

Consider now the right side of the interphase, $x > 0$, we have

$$|m_0| \psi(x) - |\kappa_0| \partial_x \psi(x) - \partial_x^2 \psi(x) = 0, \tag{3.16}$$

which is solved by

$$\psi(x) = N \exp\left\{ -|\kappa_0| x \left(1 \pm \sqrt{1 + 4|m_0|/|\kappa_0|^2} \right) /2 \right\} \quad x > 0, \tag{3.17}$$

where both zero-energy solutions decay exponentially in the gapped phase. Thus, one of the solutions describes a state that is localized at the boundary, despite the lack of a bulk gap on the left side of the boundary [46]. This seems to indicate that, just as for gapped phases, there are critical points that have non-trivial topological phases that host zero-energy edge modes, and trivial critical points that do not.
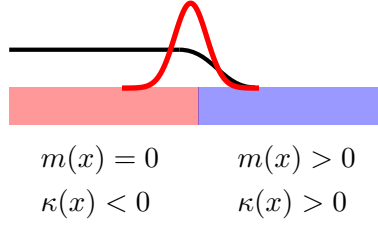
Figure 3.2: Diagram of the interphase between a non-trivial gapless phase (red) and a trivial gapped phase (blue). Two zero energy solutions are found, an extended state (black) and a topological boundary mode (red).
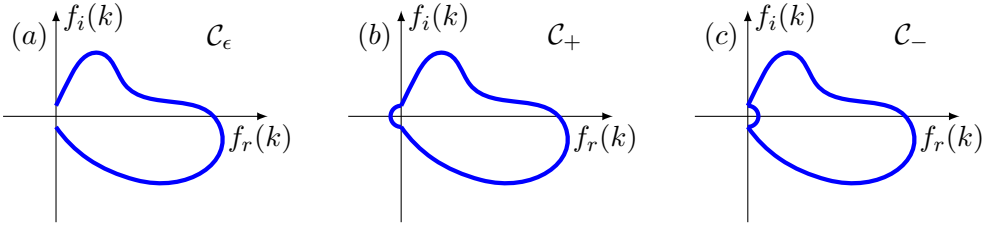
Figure 3.3: Representation of the different paths considered in the integrals of (a) ν_ϵ, (b) ν_+ and (c) ν_-, where $f_r(k), f_i(k)$ stand for the real and imaginary parts of $f(k)$, respectively. For a simple case with only a single zero.

3.2 Half-integer topological invariants

The simplest way one can regularize the winding number in Eq. (2.64) is by removing the problematic points from the integral [46],

$$\nu_\epsilon = \int_{|k-k_c|>\epsilon} \frac{dk}{2\pi} \, \partial_k \operatorname{Im} \log[h_x(k) - ih_y(k)] \tag{3.18}$$

for any number of crossing points, k_c. Consider the function $f(k) = h_x(k) - ih_y(k)$ in the complex plane. The integrating path, which we also denote by $\mathcal{C}_\epsilon$, is sketched in Fig. 3.3.(a) for a simple example with a single zero. We introduce now a small perturbation that gaps the system, i.e. moves $f(k)$ away from the zero. This can be done in two ways, paths $\mathcal{C}_+$ and $\mathcal{C}_-$ as shown in Fig. 3.3.(b) and (c), and the resulting winding numbers ν_+ and ν_- correspond to the winding numbers of the two adjacent gapped phases.

It is now interesting to consider path $\mathcal{C}_+ - \mathcal{C}_\epsilon$. In this path the function $f(k)$ has

a constant norm, $f(k) = \rho_0 e^{i\phi(k)}$, and the integral can be approximated as

$$
\begin{aligned}
\lim_{\epsilon \to 0} \nu_+ - \nu_\epsilon &= \lim_{\epsilon \to 0} \int_{\mathcal{C}_+ - \mathcal{C}_\epsilon} \frac{dk}{2\pi} \, \partial_k \operatorname{Im} \log\left(\rho_0 e^{i\phi(k)}\right) \\
&= \int_{3\pi/2}^{\pi/2} \frac{d\phi}{2\pi} \, \partial_\phi \operatorname{Im} \log\left(\rho_0 e^{i\phi}\right) \\
&= -\frac{1}{2}.
\end{aligned}
\tag{3.19}
$$

Similarly, for the path $\mathcal{C}_- - \mathcal{C}_\epsilon$ one obtains

$$
\lim_{\epsilon \to 0} \nu_- - \nu_\epsilon = \frac{1}{2}.
\tag{3.20}
$$

Combining both we obtain that

$$
\lim_{\epsilon \to 0} \nu_\epsilon = \frac{\nu_+ + \nu_-}{2}.
\tag{3.21}
$$

This implies that the regularized winding number ν_ϵ, in the infinitesimal limit, is the average of the winding numbers of the gapped phases that surround the gapless point [46]. It can take half-integer values whenever the transition changes the winding number of the gapped phases by an odd integer. This argument can be generalized to other examples with higher winding or a higher number of zeros with the same result.

This regularization procedure is not unique to the winding number. It can be generalized to any topological invariant defined in momentum space, as long as the system only has isolated gapless points. In particular, this regularization was also applied to the Chern number [46], resulting in a Chern number at the critical point that is also the average of the Chern numbers of the adjacent gapped phases. Even though this winding number is quantized and it serves to distinguish certain topological phases, it has no direct connection to edge modes, as different critical points (between phases with $\nu = 0$ and 3, or between phases with $\nu = 1$ and 2) can have the same winding number ($\nu = 3/2$) but different number of edge modes. This will be explored in the next section.

There is evidence in the literature that seems to indicate a connection to transport phenomena. In gapped systems there is a direct relation between the existence of edge modes and quantized transport. This is more clear in the case of Chern insulators, where each gapless topological edge modes contributes a quantum of conductance, while the bulk is gapped and insulating. In the case for critical system this one-to-one correspondence is no longer present. In the case of quantum Hall it has been known for a long time that at criticality the system has

an unstable fixed point resulting in a quantized conductance that can also take half-integers [130–134] and seems to coincide with this regularized Chern number. Recently, synthetic Hall phases have been engineered by using periodic drives [135], resulting in a half-integer energy current at the transition between two topological phases. Furthermore, charge pumping in a Thouless pump setup going through the critical point has also been recently investigated [136], which also results in a half-integer charge pumping.

3.3 Integer winding number

An alternative formulation of the winding number with a direct connection to edge modes has also been proposed. Consider again the function $f(k)$, defined in Eq. (3.3), that characterizes a chiral-symmetric two-band Hamiltonian. It can be expressed as

$$f(k) = \sum_{n=-M}^{M} t_n e^{ikn}, \tag{3.22}$$

where t_n are all the hoppings present and M is a cutoff to the range of the hoppings, since we assume the Hamiltonian must be local. Consider the analytical continuation of the function into the complex plane,

$$f(z) = \sum_{n=-M}^{M} t_n z^n, \tag{3.23}$$

with $z = e^{ik}$ being now a general complex number. The winding number can now be expressed as

$$\begin{aligned} \nu &= \frac{1}{2\pi} \operatorname{Im} \oint_{|z|=1} dz \, \partial_z \log(f(z)) \\ &= \frac{1}{2\pi} \operatorname{Im} \oint_{|z|=1} dz \, \frac{f(z)'}{f(z)}, \end{aligned} \tag{3.24}$$

where the integral is performed over the unit circle, $|z| = 1$, equivalent to the Brillouin zone. For gapped systems, where $f(z)$ has no zeros in the unit circle, using the residue theorem the integral results in

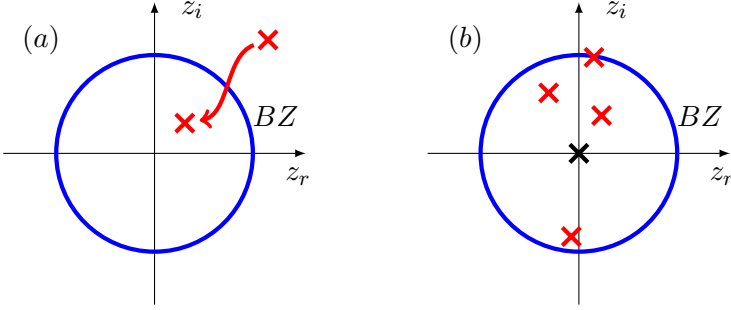$$\oint_{|z|=1} dz \, \frac{f(z)'}{f(z)} = 2\pi i(Z - P), \tag{3.25}$$

Figure 3.4: Zeros (red crosses) and poles (black crosses) of the function $f(z)$ in the complex plane, where z_r and z_i correspond to the real and imaginary pars of z, respectively. The Brillouin zone corresponds to the unit circle, shown as a blue line. (a) Example of a transition between phases with winding number $\nu = 0$ to $\nu = 1$, where one zero of $f(z)$ moves inside the unit circle. (b) Example of a gapless phase, with a zero on the unit circle. With additional three zeros and one pole inside the unit circle, which give it a winding number of $\nu = 2$.

where Z and P are the zeros and poles inside the closed integration curve. This equivalence is not valid in the gapless case because the integrand diverges along the path, however one can still define a winding number as

$$\nu = Z - P, \tag{3.26}$$

where Z and P are still the zeros and poles *strictly* inside the unit circle [45, 49], excluding the zeros on the unit circle that make the system gapless.

As opposed to the half-integer invariants introduced last section, this invariant has a direct relation to topological edge modes [45, 49], which we will show now for a simple system with no poles inside the unit circle. This implies that the Hamiltonian is defined by the function

$$f(k) = \sum_{n=0}^{M} t_n e^{ikn}. \tag{3.27}$$

Consider the Hamiltonian of a semi-infinite chain with chiral symmetry and a boundary on the left,

$$H = \sum_{n \geq 0} \sum_{j \geq 1} t_n \ket{j, A} \bra{j + n, B} + h.c. \tag{3.28}$$

and the ansatz

$$\ket{\psi_\mu} = \sum_{j \geq 1} b_{\mu,j} \ket{j, B}. \tag{3.29}$$

For the ansatz to be a zero energy eigenstate, we have

$$
\begin{aligned}
H \left| \psi_\mu \right\rangle &= \sum_{n \geq 0} \sum_{j,l \geq 1} t_n b_{\mu,l} \left| j, A \right\rangle \left\langle j+n, B | l, B \right\rangle \\
&= \sum_{n \geq 0} \sum_{j \geq 1} t_n b_{\mu,j+n} \left| j, A \right\rangle \\
&= 0.
\end{aligned}
\tag{3.30}
$$

This lead to,

$$
\sum_{n \geq 0} t_n b_{\mu,j+n} = 0.
\tag{3.31}
$$

Consider now $b_{\mu,j} = z_\mu^{j-1}$,

$$
\begin{aligned}
\sum_{n \geq 0} t_n z_\mu^{n+j-1} &= z_\mu^{j-1} \left(\sum_{n \geq 0} t_n z_\mu^n \right) \\
&= z_\mu^{j-1} f(z_\mu).
\end{aligned}
\tag{3.32}
$$

If z_μ is the zero of function $f(z_\mu) = 0$, the equation above vanishes for all j, and the state given by

$$
\left| \psi_\mu \right\rangle = \sum_{j \geq 1} z_\mu^{j-1} \left| j, B \right\rangle,
\tag{3.33}
$$

is indeed a zero-energy state. We can now compute the norm of the state,

$$
\begin{aligned}
\left\langle \psi_\mu | \psi_\mu \right\rangle &= \sum_{j \geq 1} \left(|z_\mu|^2 \right)^{j-1} \\
&= \frac{1}{1 - |z_\mu|^2}.
\end{aligned}
\tag{3.34}
$$

As long as $|z_\mu| < 1$, the sum converges and the state is normalizable. Furthermore, the weight of the state at each site decays for larger positions, it corresponds to states exponentially localized at the boundary. The case $|z_\mu| = 1$ corresponds to a gapless mode constant in space and the solutions with $|z_\mu| > 1$ are not normalizable and therefore unphysical. Therefore, each zero of the function $f(z)$ inside the unit circle corresponds to a pair (for full OBC) of topological zero-energy edge states, and the integer winding number in Eq. (3.26) corresponds to the total number of pairs of zero-energy edge states. This is always true, independently of the existence
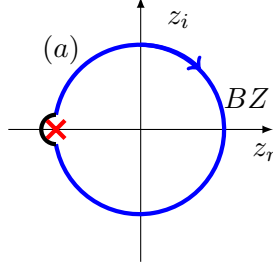
Figure 3.5: Path considered to show the relation between the half-integer and integer winding numbers. In blue it is shown the path over the unit circle excluding the environment of the zeros present on the unit circle, shown in red. In black we consider an additional path such that both form a closed loop that encircles all zeros on the unit circle.

or not of other gapless bulk states. Since these states are localized at the boundary, considering instead a chain with full OBC is expected have very little effect on them.

We can also consider the half-integer winding number in this picture in order to explore its relation to the edge modes. In a similar way to how we obtained the quantization to half-integers in Eq. (3.21) we consider a path, now in the complex plane of z that includes the zeros at the unit circle. We know that the resulting winding number is $Z + Z_{BZ}$ where Z is the number of zeros strictly inside the unit circle and Z_{BZ} is the number of zeros on the unit circle. We can now compute the difference between this closed path and the open path in the Brillouin zone excluding an infinitesimal surrounding of the zeros, the resulting path is depicted in Fig. 3.5 in black. Near the zero the function $f(z)$ can be approximated by $f(z) = f_\mu (z - z_\mu)^n_\mu$, where n is the multiplicity of the zero. Performing the integral over this path gives

$$\int_{\mathcal{C}} dz \, \frac{f(z)'}{f(z)} = \int_{\mathcal{C}_\mu} dz \, n_\mu \frac{1}{z - z_\mu}$$
$$= \frac{n_\mu}{2},$$
(3.35)

for each zero. In total $\sum_\mu n_\mu = Z_{BZ}$. Finally, the half-integer winding number can also be expressed as

$$\nu = Z + Z_{BZ} - \frac{Z_{BZ}}{2}$$
$$= Z + \frac{Z_{BZ}}{2}.$$
(3.36)

3.4 Topological invariants at finite low temperature

So far we have discussed two examples of topological invariants from gapped systems being generalized to critical systems. However, these examples have some shortcomings. The integer winding number correctly describes the edge modes but there has not been any similar generalizations for other topological invariants, like a Chern number. The method for obtaining the half-integer invariants, on the other hand, is not directly related to edge modes but it is easily generalizable to other invariants. In both cases the topological invariants proposed rely heavily on the momentum space formulation, and are therefore only valid for translationally invariant systems. Furthermore, they require careful attention to the crossings. Last, but not least, the invariants for the critical systems are distinct from those of the gapped systems.

In view of these two shortcomings, we propose in paper III a method for generalizing gapped topological invariants to critical systems that can be computed in momentum or position space and treats gapped and gapless systems on the same footing. This method relies on using a finite low temperature to deal with the degeneracy and the discontinuity of the ground state for critical systems (see below Eq.(3.2) for a discussion on both issues).

We distinguish between two types of invariants. First, we express invariants for gapped systems in terms of projectors onto an occupied subspace. We then promote the projectors correlation functions at finite temperature,

$$P_{occ} = \sum_{\mu \in occ} |\psi_\mu\rangle \langle\psi_\mu| \quad \rightarrow \quad C = \sum_\mu n_f(E_\mu) |\psi_\mu\rangle \langle\psi_\mu|. \tag{3.37}$$

where n_f is the Fermi distribution. Even when computed in momentum space, the correlation function $C(k)$ is always continuous and differentiable, unlike $P_{occ}(k)$. We illustrate this procedure with the winding number, which can be computed in position space [110, 111] as

$$\nu = -4\mathcal{T}\{P_B P_{occ} P_A [X, P_{occ}]\}, \tag{3.38}$$

where $\mathcal{T}$ is the bulk trace per volume. This is the generalization of Eq. (3.2) to position space. We then define a winding number at finite temperature as

$$\tilde{\nu} = -4\mathcal{T}\{P_B C P_A [X, C]\}, \tag{3.39}$$

and extract its $T \rightarrow 0$ limit. This winding number, computed for translationally invariant systems, gives the same result as the winding number obtained by excluding the gapless points (see Eq. (3.18)).
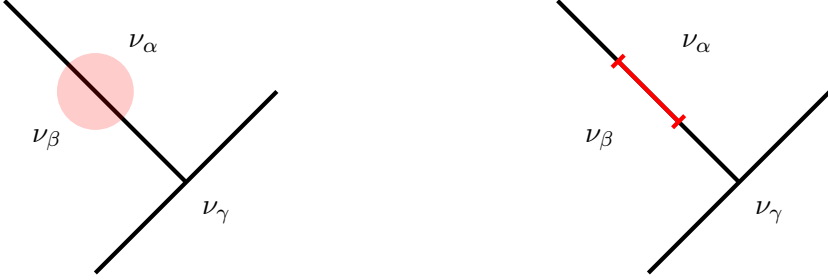
Figure 3.6: Sketch of a phase diagram with critical lines (black) between three topological phases characterized by winding numbers ν_α, ν_β and ν_γ. At a critical point, (a) Random disorder allows parameters within the red circle and thus places the system locally into different gapped phases. (b) A disordering perturbation forces the system locally to have gapless excitations (local parameters are fixed to lie on the red line), albeit being globally uncorrelated.

The second type of invariants considered are topological invariants given by expectation values, which can then be computed at finite temperatures. This is exemplified by the polarization, which at finite temperature can be obtained [137] as

$$
\begin{aligned}
\mathcal{P} &= \frac{1}{L} \left\langle \hat{X} \right\rangle_T \\
&= \frac{1}{2\pi} \operatorname{Im} \ln \det \left[I - C + C e^{-i \frac{2\pi}{L} \hat{x}} \right],
\end{aligned}
\tag{3.40}
$$

where the average of the many-body position operator was defined in Eq. (2.34) . One might expect this polarization to reproduce the result for the winding number, being quantized to $1/4$ and $3/4$. However, the polarization is still quantized to $0, 1/2$ for gapless systems. An analysis of the model system suggests that this polarization reproduces the parity of the number of edge modes, just as for gapped systems. A disadvantage of this method is that it is only well defined for finite systems, as the polarization is given by the phase of a number that tends to zero in the thermodynamic limit. Furthermore, while for gapped systems the information of the polarization is contained in the winding number, this is no longer the case for critical systems. Instead, the two topological invariants provide complementary information about the system.

The formulations introduced here provide two main advantages. They treat gapped and gapless phases on the same footing, and they do not rely on momentum calculations. The former allows us to study the behavior of topological invariants when going through a phase transition. The latter allows us to study the effect of disorder on the topological invariants. We studied two types of disorder,

depicted in Fig.3.6. For random disorder, shown in Fig.3.6.(a), the local parameters can take any value within the red circle. Thus it puts the system locally into either of the gapped phases that surround the critical point. The disorder averaged invariants therefore results in the average of the two gapped phases, but the value for each disorder configuration varies substantially. We then considered a disordering perturbation that keeps the system locally on the same critical line, e.g., the red line sketched in Fig.3.6.(b), while being globally uncorrelated. We were able to show that the invariants are robust to the disordering perturbation, even for individual disorder configurations, up to a point where the perturbation is strong enough to probe neighbouring multi-critical points.

3.4.1 Entanglement in critical systems

Like the surface spectrum, the EOS of a critical system at finite temperature hosts virtual topological edge states. In Fig.3.7.(a) and (b) we show the EOS computed for the trivial and non-trivial critical points of the long-range SSH model, with the non-trivial critical point showing two exact $1/2$ eigenvalues. Looking at the eigenstates, in Fig.3.7.(c) and (d), we confirm that the eigenstates with $\xi = 1/2$ are exponentially localized at the edges.

In Section 2.4.6 we discussed how the eigenstates of C_A can be approximated by Wannier states, which are localized. At finite temperature this is no longer the case, since it required C to be a projector. We plot in Fig.3.7.(c) and (d) a few of the eigenstates closest to $\xi = 1/2$, which are all extended states with the exception of the virtual topological edge modes described above. Thus, the EOS, when computed for a critical system at finite temperature, still correctly reproduces the topological edge states of the corresponding open system.

Since the eigenstates of C_A for gapped systems at zero temperature were found to localized at the boundaries, the two boundaries could be treated as independent of each other in the thermodynamic limit. This allowed us to relate the EOS to the polarization in paper I, as discussed in Section2.4.4. This property of the EOS is lost for critical systems at finite temperature, and the relation in Eq. (2.106) cannot be generalized to this case in a straightforward way. Nonetheless, since for critical systems the EOS also has the same topological modes as the surface spectrum, the polarization still characterizes the parity of the number of virtual topological edge modes in the EOS.

Entanglement can also be used to characterize critical points. The entanglement entropy, defined in Eq. (2.82), is known to have a universal scaling for 1D systems
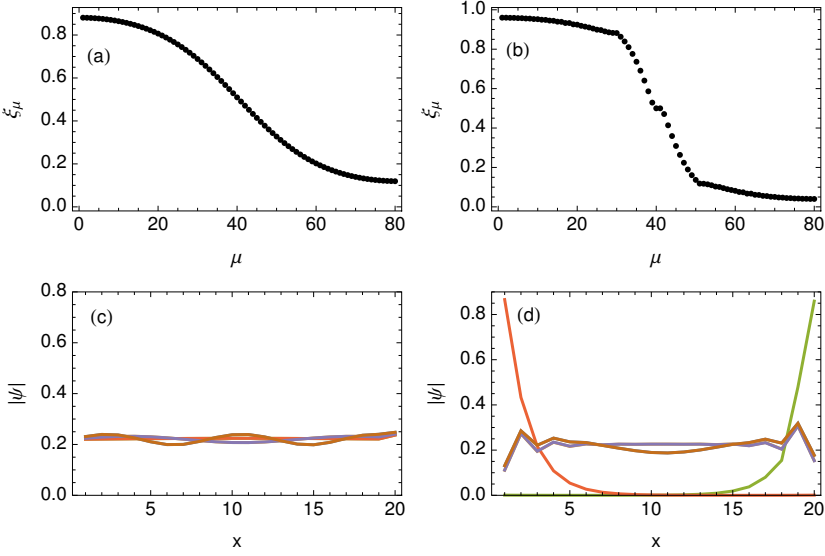
Figure 3.7: (a) and (b) show the EOS computed at finite temperature, $\beta = t_1$, for the trivial critical point ($t_1 = t_0, t_2 = 0$) and the non-trivial point ($t_1 = t_0, t_2 = -2t_1$), showing that the non-trivial point hosts two $1/2$ virtual topological edge modes. (c) and (d) show the lowest lying eigenstates (closest to $\xi = 1/2$) for the trivial and non-trivial points, respectively. As opposed that the gapped case, where all eigenstates of C_A are found to be localized, in the critical case only the topological virtual edge states are found to be localized.

at critical points [138–140]. It is given by

$$S_A = \frac{c}{3} \log \left[\frac{L_A}{L} \right], \tag{3.41}$$

where L is the total length of the system, L_A the length of the subsystem considered and c is a quantity that characterizes the critical point known as the *central charge*. In paper III we also used the central charge to study the effect of disorder on the critical point of the SSH ($t_2 = 0, t_1 = t_0$), which has $c = 1$ without any disorder. When random disorder is introduced, as disorder strength is increased the central charge flows to $c = \log[2]$, characterizing a well known infinite-randomness fixed point [141]. The situation when we apply the disordering perturbation shown in Fig.3.6.(b), however, is quite different. The central charge is shown to be robust for weak disorder up to a point where the disorder probes a nearby multi-critical point, where the central charge jumps. This result suggests that the critical point is indeed robust against the disordering perturbation.

Chapter 4

Non-Hermitian Topological phases

In this chapter we extend the study of symmetry protected topological phases to systems described by Hamiltonians that are no longer Hermitian, $H \neq H^\dagger$. The Hermiticity of the Hamiltonian is a fundamental assumption in the physics of isolated quantum systems that ensures unitary evolution. However, in open systems interacting with an environment, effective Hamiltonians describing processes such as dissipation, gain or finite-lifetime quasiparticles, are in general not Hermitian [54–61]. This requires us to rethink quantum mechanics, where Hermiticity is a fundamental assumption, and it opens up the possibility for new physics to appear, even if just in an effective description. There are mainly three points where non-Hermiticity breaks down the usual interpretation of quantum mechanics. The first consequence one notices is that eigenenergies are in general no longer real, they have an imaginary part that accounts for dissipation and gain in the system. This, however, is not always the case for non-Hermitian systems as there are certain symmetries, e.g., $\mathcal{PT}$ symmetry, that can ensure that the spectrum is real [142–144]. Another fundamental difference with the Hermitian case is that left and right eigenvectors are no longer related by conjugation, they are now independent. This results in an arbitrariness when computing expectation values, where different choices can be relevant in different contexts. Finally, there exists sets of parameters, coined *exceptional points*, where the Hamiltonian is no longer diagonalizable [65, 68, 145]. At these points different eigenstates coalesce into the same one, such that the set of eigenstates no longer spans the whole Hilbert space. The physics of exceptional points has attracted a lot of attention recently [146–148], but it is something that goes beyond the scope of this thesis.

In the past years the focus on non-Hermitian systems has shifted, from it being a mere practical effective description, to a more theoretical analysis where novel phe-

nomena can be found. This is the case for topological phases, where the existence of new symmetries results in numerous new topological classes being required for a complete description [51–53, 149] . Most importantly, the bulk-boundary correspondence principle, an important result for topological gapped Hermitian systems is found to be broken for certain non-Hermitian systems due to the skin effect, see Section 4.2.3 for a more detailed discussion.

In this chapter we describe the biorthogonal quantum mechanics used to treat non-Hermitian systems in Section 4.1. In Section 4.2 we give a brief overview of the topological classification in non-Hermitian systems, with a focus on more practical aspects required to understand the accompanied papers. In Section 4.3 we describe how the polarization and the entanglement spectrum, topological signatures used in the previous chapters, are affected by the non-Hermiticity. Finally we summarize in Section 4.4 how some features of a class of non-Hermitian systems are inherited from related gapless Hermitian systems, rather than being intrinsically non-Hermitian.

4.1 Biorthogonal quantum mechanics

The methods of quantum mechanics were developed with the assumption that the Hamiltonian is Hermitian. When this is no longer the case these methods need to be adapted to obtain a coherent description. There are several approaches, considering quasi-Hermitian Hamiltonians [150, 151] or systems with $\mathcal{PT}$ symmetry [152, 153]. In this chapter we describe another approach which has gained attention in recent years, known as *Biorthogonal quantum mechanics* [154, 155].

A general non-Hermitian matrix, in this case the Hamiltonian, has left and right eigenvectors

$$H \left| \psi_\mu^R \right\rangle = E_\mu \left| \psi_\mu^R \right\rangle, \quad \left\langle \psi_\mu^L \right| H = \left\langle \psi_\mu^L \right| \bar{E}_\mu, \tag{4.1}$$

where the eiengenergies $E_\mu, \bar{E}_\mu$ are, in general, complex. We start with the assumption that the two sets of energies are independent of each other. There are three normalization conditions one could consider depending on if we take both states to be left, right, or a combination of both. Consider first the case with *right-right*, one has

$$\left\langle \psi_\mu^R \right| (H - H^\dagger) \left| \psi_\nu^R \right\rangle = (E_\nu - E_\mu^*) \left\langle \psi_\mu^R | \psi_\nu^R \right\rangle. \tag{4.2}$$

Considering a system with no degeneracies for simplicity, $\left\langle \psi_\mu^R | \psi_\nu^R \right\rangle$ is in general finite, since the left hand side of Eq. (4.2) does not vanish in general for non-Hermitian systems. The eigenstates therefore can be chosen to have unit norm but

the set of right (or left) eigenstates cannot be chosen to be orthogonal. However, considering the *left-right*, we have

$$\left\langle \psi_\mu^L \right| H \left| \psi_\nu^R \right\rangle = E_\nu \left\langle \psi_\mu^L | \psi_\nu^R \right\rangle = \bar{E}_\mu \left\langle \psi_\mu^L | \psi_\nu^R \right\rangle. \tag{4.3}$$

There are only two types of solutions to the later equation. If $E_\nu \neq \bar{E}_\mu$, necessarily we have that $\left\langle \psi_\mu^L | \psi_\nu^R \right\rangle = 0$, the two states are orthogonal to each other. Alternatively, if $E_\nu = \bar{E}_\mu$, then $\left\langle \psi_\mu^L | \psi_\nu^R \right\rangle$ can be finite. In this thesis we assume always that the system is not at a exceptional point. Given this assumption, each set of states, left and right, is linearly independent and spans the whole Hilbert space. Therefore we cannot have that $\left\langle \psi_\mu^L | \psi_\nu^R \right\rangle = 0$ for all μ, ν, necessarily there is one state for which $\bar{E}_\mu = E_\mu$. Even though one could assume that the left and right eigenspectrums are independent of each other, the eigenstates of the Hamiltonian actually come in pairs of left and right eigenstates with the same energy. One can therefore impose the biorthogonal normalization condition that

$$\left\langle \psi_\mu^L | \psi_\nu^R \right\rangle = \delta_{\mu\nu}. \tag{4.4}$$

In the Hermitian case, where $\left| \psi_\mu^L \right\rangle = \left| \psi_\mu^R \right\rangle$, the normalization condition fixes the eigenstates up to a phase. For non-Hermitian systems, however, the biorthogonal normalization condition can only fix the left and right eigenstates up to a complex constant. One can always define new states $\left| \phi_\mu^R \right\rangle = c_\mu \left| \psi_\mu^R \right\rangle$ and $\left| \phi_\mu^L \right\rangle = c_\mu^{-1} \left| \psi_\mu^L \right\rangle$ which are also eigenstates and fulfill the biorthogonal normalization above.

Numerical diagonalization procedure: In the Hermitian case, there are simple numerical methods for imposing orthonormalization on a set of vectors that can be applied to the eigenstates of the Hamiltonian. For non-Hermitian systems, however, the biorthogonalization procedure is more involved and needs to be imposed manually.

Consider a Hamiltonian H. One can easily obtain the right and left eigenvectors numerically,

$$HU_R = U_R E \quad U_L H = E U_L, \tag{4.5}$$

where E is a diagonal matrix and U_L, U_R are matrices with the left and right eigenstates. However, these are not properly normalized. In the following we describe an efficient way to obtain the biorthonormal basis. We define the overlap matrix as

$$Y = U_L U_R, \tag{4.6}$$

and perform an LU decomposition,

$$PY = LU, \tag{4.7}$$

where L and U are lower and upper triangular matrices, and P is a permutation matrix which needs to be included for systems with degeneracies. We then have

$$P^{-1}LU = U_L U_R, \tag{4.8}$$

or

$$I = (L^{-1}PU_L)(U_R U^{-1}) = U'_L U'_R, \tag{4.9}$$

where the transformed matrices U'_L, U'_R are obtained by solving the linear equations

$$PLU'_L = U_L, \quad U_R = U'_R U. \tag{4.10}$$

We now show that these matrices also diagonalize the Hamiltonian. Using the eigenvalue equation for the right eigenvectors we have

$$HU'_R U = U'_R U E. \tag{4.11}$$

Now it is important to note that the overlap matrix Y is block diagonal, with the dimension of the blocks being the multiplicity of the eigenvalues. This means that in the subspace corresponding to non-degenerate eigenvalues both U and E are diagonal. And in the case where the eigenvalues are degenerate, U is no longer diagonal, but E acts as an identity. Therefore U and E always commute and we recover

$$HU'_R = U'_R E. \tag{4.12}$$

Similar arguments can be used for U'_L. Therefore, the matrices U'_L and U'_R describe left and right eigenvectors of the Hamiltonian which are biorthogonal to each other.

Projectors and expectation values: The biorthogonality condition allows us to also define biorthogonal projectors as

$$P_\mu = \left| \psi_\mu^R \right\rangle \left\langle \psi_\mu^L \right|, \tag{4.13}$$

which has all the properties of a projector. It is idempotent,

$$P_\mu^2 = \left| \psi_\mu^R \right\rangle \left\langle \psi_\mu^L | \psi_\mu^R \right\rangle \left\langle \psi_\mu^L \right| = \left| \psi_\mu^R \right\rangle 1 \left\langle \psi_\mu^L \right| = P_\mu. \tag{4.14}$$

The sum of the projectors onto all eigenstates is also the identity. Consider a general state $|\phi\rangle = \sum_\nu c_\nu \left| \psi_\nu^R \right\rangle$,

$$\sum_\mu P_\mu |\phi\rangle = \sum_{\mu\nu} P_\mu c_\nu \left| \psi_\nu^R \right\rangle = \sum_{\mu\nu} c_\nu \delta_{\mu\nu} \left| \psi_\nu^R \right\rangle = |\phi\rangle, \tag{4.15}$$

therefore $\sum_\mu P_\mu = I$. Operators, such as the Hamiltonian, can also be decomposed into a weighted sum of the projectors of the eigenstates,

$$H = \sum_\mu E_\mu \left| \psi_\mu^R \right\rangle \left\langle \psi_\mu^L \right|. \tag{4.16}$$

Regarding observables, the probabilistic interpretation of the wavefunction is lost, and so is the usual interpretation of expectation values. The most common choice for defining expectation values is the biorthogonal expectation value

$$\left\langle \hat{O} \right\rangle_\psi \equiv \left\langle \psi^L \right| \hat{O} \left| \psi^R \right\rangle, \tag{4.17}$$

because the quantities obtained this way typically behave better, i.e. more similar to their Hermitian counterpart, than when using left-left or right-right expectation values. However, there are situations when they are all equal, such as when computing geometric phases and Chern numbers [156–158].

4.2 Topological phases of non-Hermitian systems

In this section we give an basic overview on how non-Hermiticity substantially changes the classification of symmetry-protected topological phases. We will also introduce topological invariants and other quantities relevant for the models most commonly used in the field. To illustrate some of the concepts discussed here, we will employ throughout this chapter a similar model from the one introduced in Eq. (2.10), the SSH model with longer range hopping. The model is now made non-Hermitian by adding unbalance to the hoppings to the left and right directions [159], given by the Hamiltonian

$$H = \sum_{i\alpha,j\beta} c_{i\alpha}^\dagger H_{ij,\alpha\beta} c_{j\beta}, \tag{4.18}$$

where H_{ij} is

$$
\begin{aligned}
H_{ij} =& \frac{1}{2} \left[t_{0R}(\sigma_x + i\sigma_y)\delta_{i,j} + t_{0L}(\sigma_x - i\sigma_y)\delta_{i,j-1} \right] \\
&+ \frac{1}{2} \left[t_{1R}(\sigma_x + i\sigma_y)\delta_{i,j+1} + t_{1L}(\sigma_x - i\sigma_y)\delta_{i,j-1} \right] \\
&+ \frac{1}{2} \left[t_{2R}(\sigma_x + i\sigma_y)\delta_{i,j+2} + t_{2L}(\sigma_x - i\sigma_y)\delta_{i,j-2} \right].
\end{aligned} \tag{4.19}
$$

All parameters are real, and the corresponding Bloch Hamiltonian is

$$H(k) = \begin{pmatrix} 0 & t_{0R} + t_{1R}e^{ik} + t_{2R}e^{2ik} \\ t_{0L} + t_{1L}e^{-ik} + t_{2L}e^{-2ik} & 0 \end{pmatrix}.$$

There are several ways the unbalanced hopping can be introduced. In paper II we choose $t_{0R/L} = t_0 \pm \gamma, t_{1R} = t_{1L}$ and $t_{2R} = t_{2L}$, while in paper IV we choose $t_{nR/L} = e^{\pm ng}t_n$. This is done for convenience, but the two models result in the same features.

4.2.1 Symmetries, gaps and classification

In the Hermitian case the conventional classification, discussed in Section 2.2, relies on two fundamental properties of the system. The existence of a gap, and the symmetries that constrain the Hamiltonian. Let us consider first the latter. In the Hermitian case there are three 'fundamental' symmetries: Time-reversal (TRS), particle-hole (PHS) and chiral symmetry (CS),

$$TH^*(k)T^{-1} = H(-k), \quad CH^*(k)C^{-1} = -H(-k), \quad SH(k)S = -H(k), \quad (4.20)$$

where T, C and S are unitary operators, see Section 2.2. When the Hamiltonian is no longer Hermitian, additional fundamental symmetries arise which are variations of these three ones [52]. Taking time-reversal, for example, it can also be defined in terms of the transpose of the Hamiltonian,

$$TH^T(k)T^{-1} = H(-k). \quad (4.21)$$

For a Hermitian system the two symmetry equations are equivalent, but that is no longer the case for non-Hermitian matrices where $H^* \neq H^T$. Similarly for the PHS. The convention typically used in the literature [52] for these four symmetries is

$$T_{\pm}H^*(k)T_{\pm}^{-1} = \pm H(-k), \quad C_{\pm}H^T(k)C_{\pm}^{-1} = \pm H(-k), \quad (4.22)$$

where T_+ and C_- are the usual TRS and PHS symmetries, while T_- and C_+ are called PHS† and TRS†, respectively [1]. As for the extension of chiral symmetry, we have

$$\Gamma H^\dagger(k)\Gamma = -H(k), \quad SH(k)S = -H(k), \quad (4.23)$$

where Γ is the usual CS, while S is CS†, also referred to as sublattice symmetry. In non-Hermitian systems there is one additional internal symmetry called pseudo-Hermiticity, given by

$$\eta H^\dagger(k)\eta^{-1} = H(k), \quad (4.24)$$

---

[1]Note that the naming convention is not a typo. The subscript sign marks if the symmetry commutes or anticommutes con the Hamiltonian, which makes for a confusing nomenclature of the symmetries.
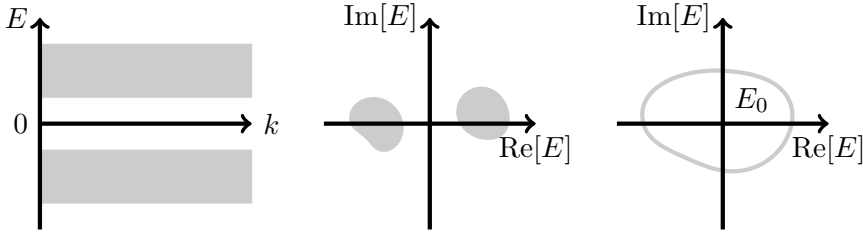
Figure 4.1: Representation of the different types of gap considered. (a) A Hermitian system has a gap whenever there is an energy region between the bands without any states. (b) Non-Hermitian systems have a line-gap between two bands whenever one can draw a line separating the two bands in the complex plane without crossing any states. (c) A non-Hermitian spectrum is point-gapped around a base point E_0 whenever the bands wind around such point.

where η is unitary and Hermitian so that it squares to the identity, $\eta^2 = I$. This symmetry is a similarity transformation relating the Hamiltonian to its Hermitian conjugate. Pseudo-Hermiticity has a similar effect to $\mathcal{PT}$ symmetry, which under certain circumstances makes the energy spectrum real. This symmetry is trivially satisfied for Hermitian systems with $\eta = I$. The model in Eq. (4.20) has TRS, $T_+ = I$ and $CS^\dagger$, $S = \sigma_z$. This places the system in class AI.

In the Hermitian case, the three fundamental symmetries result in ten different classes. The seven different symmetries in the non-Hermitian case result in a classification with 38 different classes. As opposed to the Hermitian case, there is not an intuitive way of obtaining the number of different topological classes. The problem of classifying random non-Hermitian matrices was first addressed two decades ago, known as the Bernard-LeClair symmetry classification [149] . However, it overcounted some classes and overlooked other ones. A complete classification with the 38 different classes was obtained only recently [52].

Line and point gaps: Apart from the non-unitary symmetries, the existence of a gap is fundamental in the conventional description of symmetry protected topological phases, as one aims to study the topology of isolated bands. In non-Hermitian systems, where the eigenenergies are complex, the concept of energy bands is still present, but there are different types of gaps one needs to consider, leading to additional topological classes.

Consider two bands in the complex plane. The bands are said to have a line gap (LG) whenever one can draw a line between the bands that does not cross any energy states, see Fig. 4.1.(b). Similarly to the flattening procedure for Hermitian systems, some line gapped systems can be deformed into Hermitian ones without closing the gap or breaking the symmetries [52]. These are said to have a *real* line

gap and share the same topology with the equivalent Hermitian Hamiltonian. The rest of line-gapped phases can be deformed into an anti-Hermitian Hamiltonian, and then it is said to have an *imaginary* line gap. Anti-Hermitian Hamiltonians have a topological classification equivalent to the Hermitian case. In addition to the line gap between different bands, an isolated band is said to have a point gap (PG) at some reference energy E_0 whenever the energy band encloses such reference point in the complex plane, see Fig. 4.1.(c). Note that multiple non-Hermitian bands can effectively merge into a single point-gapped band.

The topological phases of point-gapped systems are said to be inherently non-Hermitian, unlike in the line-gapped phase. The Hamiltonian in this case can be deformed into a unitary matrix, but never into a Hermitian or anti-Hermitian Hamiltonian, leading to a new classification [52]. A Hamiltonian H with a point-gap phase shares the same topological classification as the auxiliary Hermitian Hamiltonian

$$H' = \begin{pmatrix} 0 & H \\ H^\dagger & 0 \end{pmatrix}, \tag{4.25}$$

which has a new chiral symmetry $\Sigma = \sigma_z \otimes I$. However, while the bulk topology of the non-Hermitian PG phase can be found in terms of an analogue Hermitian system, the bulk-boundary correspondence of the auxiliary Hermitian system does not translate into the non-Hermitian Hamiltonian. This is due to the skin effect, which will be discussed briefly in Section 4.2.3.

4.2.2 Topological invariants

The models most prevalent in the literature of non-Hermitian topological phases in one dimensions fall in the AI class. For a system with $CS^\dagger$ that commutes with TRS (see Table VII in Ref. [52]), this class is characterized by a $\mathbb{Z}$ or $\mathbb{Z} \times \mathbb{Z}$ invariants for line gapped and point-gapped phases, respectively. The real line gapped phase can be deformed into a Hermitian one and therefore they share the same invariant, the winding number. For a two band model given by $H(k) = h_x(k)\sigma_x + h_y(k)\sigma_y$, where chiral symmetry imposes $h_z(k) = 0$, this winding number is defined in the literature as

$$\nu = \frac{1}{2\pi} \oint dk \, \frac{(\partial_k h_x(k))h_y(k) - h_x(k)\partial_k h_y(k)}{h_x(k)^2 + h_y(k)^2}, \tag{4.26}$$

just as in the Hermitian case, in Eq. (2.65). The same invariant characterizes imaginary line gapped phases.

As mentioned before, the PG phase (around a reference point E) of a non-Hermitian Hamiltonian $H(k)$ shares the same topology as the Hermitian Hamiltonian

$$H'(k) = \begin{pmatrix} 0 & H(k) - E \\ H(k)^\dagger - E & 0 \end{pmatrix}. \tag{4.27}$$

The winding number defined above can be used to characterized each block while the emergent chiral symmetry can be used to define an additional winding number [51, 63, 66, 160],

$$\nu' = \frac{1}{4\pi} \oint dk\, \partial_k \arg(\det(H(k) - E)), \tag{4.28}$$

which is equal to the winding of $\det(H(k))$ around E in the complex plane. For the two-band model introduced above, one can rewrite this winding number as

$$\nu' = \frac{1}{2\pi} \oint dk\, \partial_k \arg(h(k) - E), \tag{4.29}$$

where $h(k) = \sqrt{h_x^2(k) + h_y^2(k)}$ is the energy of one of the bands. Note that for Hermitian gapped systems the determinant is always real and E can be chosen within the gap such that the determinant always has the same sign, therefore this winding number vanishes. In the following we will consider only the case $E = 0$ and assume that $h(k) \neq 0$.

The quantity ν', sometimes also referred to as *energy vorticity*, has a clear topological origin. The winding number ν in Eq. (4.26), however, does not have an obvious topological or geometrical interpretation in the non-Hermitian case, in contrast to the Hermitian case (See Section 2.3.3). Recently, an alternative formulation of these winding numbers, with a nice geometrical interpretation, was introduced [63]. Writing the Hamiltonian as

$$H(k) = \begin{pmatrix} 0 & f_1(k) \\ f_2(k) & 0 \end{pmatrix} \tag{4.30}$$

the winding number in Eq. (4.26) can be rewritten as

$$\begin{aligned}
\nu &= \frac{1}{2\pi} \oint dk\, \frac{f_2(k)\partial_k f_1(k) - f_1(k)\partial_k f_2(k)}{2i f_1 f_2} \\
&= \frac{1}{2} \left(\frac{1}{2\pi i} \oint dk\, \frac{\partial_k f_1(k)}{f_1(k)} - \frac{1}{2\pi i} \oint dk\, \frac{\partial_k f_2(k)}{f_2(k)} \right) \\
&= \frac{1}{2} \left(\frac{1}{2\pi i} \oint dk\, \partial_k \log f_1(k) - \frac{1}{2\pi i} \oint dk\, \partial_k \log f_2(k) \right) \\
&= \frac{\nu_1 + \nu_2}{2},
\end{aligned} \tag{4.31}$$

where the new winding numbers are defined as

$$\nu_1 = \frac{1}{2\pi i} \oint dk \, \partial_k \log f_1(k)$$

$$\nu_2 = -\frac{1}{2\pi i} \oint dk \, \partial_k \log f_2(k). \tag{4.32}$$

Note the similarity with the integral in Eq. (3.25). The integrals are purely imaginary and the resulting winding numbers are real and integers by definition. The winding numbers ν_1, ν_2 were found to characterize the existence of topological gapless edge-modes in semi-infinite chains (see next section for a more detailed discussion). In the Hermitian case note that $f_2(k) = f_1(k)^*$, and therefore $\nu_1 = \nu_2$.

Consider now the second non-Hermitian winding number around $E = 0$,

$$\begin{aligned}
\nu' &= \frac{1}{4\pi i} \oint dk \, \partial_k \log \det(H(k)) \\
&= \frac{1}{4\pi i} \oint dk \, \partial_k \log f_1(k) f_2(k) \\
&= \frac{1}{4\pi i} \oint dk \, \partial_k \log f_1(k) + \frac{1}{2\pi i} \oint dk \, \partial_k \log f_2(k) \\
&= \frac{\nu_1 - \nu_2}{2},
\end{aligned} \tag{4.33}$$

which as mentioned before vanishes in the Hermitian limit, as well as for line-gapped phases.

4.2.3 Skin effect and edge modes

In this section we discuss what happens to non-Hermitian systems when OBC are imposed. As we will see below this has more relevant consequences than in the Hermitian case, and has therefore attracted a lot of attention in recent years [51, 68, 70, 72, 74]. However, this problem escapes the scope of this thesis and therefore we will only give a brief overview.

Consider one of the simplest non-Hermitian models, the Hatano-Nelson model [161–163], a chain with non-reciprocal hopping,

$$H = \sum_j (t_r c_{j+1}^\dagger c_j + t_l c_j^\dagger c_{j+1}), \tag{4.34}$$

where $t_r \neq t_l$. For PBC, the unbalanced hopping will lead to a constant current through the chain. When OBC are imposed, this current results in all charge accumulating at the boundaries. This is known as the *skin effect*, and the states

that localize at the boundaries are known as *skin states*. While for Hermitian systems the boundary conditions play a minor role, for some non-Hermitian systems even small perturbations of the boundary conditions can change the spectrum substantially [70]. There have been several proposals to take advantage of this sensitivity for quantum sensing [57, 58, 164].

A feature of Hermitian topological systems when OBC are imposed is the emergence of topological gapless edge modes. The same is true for non-Hermitian systems but there is a caveat. The bulk-boundary correspondence in Hermitian systems relates the number of topological edge modes to a topological invariant computed for PBC. However, when the skin effect is present the non-Hermitian system with PBC and OBC have very different physics, and therefore the bulk-boundary correspondence is broken. To reestablish this correspondence one needs to consider semi-infinite chains [63], which do not present skin effect, or construct topological invariants explicitly from OBC [66, 67, 69, 71].

4.3 Entanglement Spectrum and polarization

In the Hermitian case it is known that the entanglement spectrum provides the same topological information as the surface energy spectrum, as discussed in Section 2.4.1. For non-Hermitian LG systems, the entanglement spectrum is known to also provide the same topological information as the surface spectrum [75, 76], with the number of topological 1/2 modes being given by the winding number ν. For PG, however, the EOS and surface spectrum no longer give the same topological information. Since it is computed for PBC, the EOS does not suffer from the skin effect, as the surface spectrum does. The EOS of PG phases can have virtual topological 1/2 modes which are characterized by the bulk invariants. This relation however, is not as direct as for Hermitian or LG phases. For example, in the PG phase of the non-Hermitian SSH model ($\nu = 1/2, \nu' = 1/2$), no topological modes were found, and it was first believed that the EOS does not contain topological information for the PG phases [75, 76].

In paper II we revisited this question and studied the EOS of more general point-gapped phases and found that the EOS does host a number of topological 1/2 modes equal to $\min(|\nu_1|, |\nu_2|)$. In the system used in paper II, where $|\nu| \geq |\nu'|$, the number of virtual 1/2 modes are given by $|\nu| - |\nu'|$. As both winding numbers are 1/2 for the PG phase of the non-Hermitian SSH chain, the corresponding EOS does not show any topological modes. Furthermore, we studied the polarization and its relation to the EOS, generalizing our result for Hermitian systems from paper I.

The bulk polarization was only recently studied for non-Hermitian systems.

Originally, a many-body approach was used to compute it for both LG and PG phases [165], and it was found that, computed for PBC, the bulk polarization of the non-Hermitian SSH model reproduced the phase-diagram of the system with OBC. Resta's formulation was later adapted for these systems [66] and shown to reproduce the many-body result for LG phases, where the polarization behaves as in the Hermitian case, $P = \nu/2 \bmod 1$. In paper II we considered PG phases and observed that Resta's formulation, much easier to compute than the many-body calculation, also reproduces the OBC phase-diagram. It is important to note that the bulk polarization for PG phases is ill-defined in the thermodynamic limit, as $\lim_{L \to \infty} \left\langle e^{i\frac{2\pi}{L}\hat{X}} \right\rangle = 0$, similarly to the case of Hermitian critical systems (see discussion below Eq. (3.40)). Nonetheless, it is a well-defined quantity for finite systems, even if its physical interpretation is still unclear.

Furthermore, we computed for non-Hermitian systems the bulk polarization obtained from $U(1)$ flux insertion, defined for Hermitian systems in Eq. (2.57). We showed that its relation to Resta's polarization and the Wilson loop still applies. Using this form of the bulk polarization we showed that for LG phases one can express the bulk polarization in therms of the EOS (see Eq. (2.106) for a discussion in the Hermitian limit), with it being 0 when an even number of $1/2$ modes is present, and $1/2$ when the number is odd. For PG phases, however, this relation is no longer valid. This is because one important assumption used to proof the relation is that both entanglement cuts are independent of each other, which is no longer the case for PG phases.

It is also important to note that in the modern theory of polarization developed for Hermitian systems only changes in the bulk polarization carry physical meaning, were adiabaticity plays an important role. So far, the studies on bulk polarization found in the literature for non-Hermitian system are restricted to static systems, so its relation to actual physical observables is still unclear.

4.4 Point-gapped systems as generalized Hermitian gapless systems

So far we have discussed several topological features that both critical systems and non-Hermitian PG phases share. Both are described by half-integer winding numbers, such that an additional quantity is needed to characterize the virtual topological edge modes of the EOS. And in both cases the bulk polarization is quantized to $0, 1/2$, although it is ill-defined in the thermodynamic limit.

In paper IV we studied these similarities by introducing non-Hermiticity to critical systems. By introducing an imaginary shift to the momenta (equivalent to

having an imaginary flux), we showed that critical systems evolve into PG phases. We also showed that, for as long as the point-gap is open, the winding number ν of the non-Hermitian system is equal to the half-integer winding number for the critical system in Eq. (3.18), while the non-Hermitian winding number ν' is directly related to the number of gapless points of the critical system in the Hermitian limit.

Furthermore, the EOS for the models studied does not change qualitatively when the imaginary flux is introduced. This was proven for the critical point of the SSH chain, but analytical and numerical results suggest that this feature is more general. In particular, the non-Hermitian and the critical model have the same number of topological modes. This relation provides further intuition into the EOS of PG phases, since the relation between the EOS and bulk invariants for critical phases is much better understood.

4.5 Physical realizations of effective non-Hermitian systems

Non-Hermitian Hamiltonians have been used to effectively describe the process of dissipation and gain for a system interacting with an environment, most prominently in the fields of photonics [166, 167] and quantum optics [168, 169], where it is easier to implement gain and loss onto the system.

There are mainly two ways one can derive effective non-Hermitian Hamiltonians. The first one is obtained by using a Lindbland master equation approach [170]. Consider a system described by a Hermitian Hamiltonian H that interacts with an environment. The evolution of a density operator can be obtained by

$$\dot{\rho} = -i[H, \rho] + \sum_m \Gamma_m (L_m \rho L_m^\dagger - \frac{1}{2}\{L_m^\dagger L_m, \rho\}), \qquad (4.35)$$

The master equation can be rewritten as

$$\dot{\rho} = -i\left(H_{eff}\rho - \rho H_{eff}^\dagger\right) + \sum_m \Gamma_m L_m \rho L_m^\dagger, \qquad (4.36)$$

where the effective Hamiltonian is given by

$$H_{eff} = H - \frac{i}{2}\sum_m \Gamma_m L_m^\dagger L_m. \qquad (4.37)$$

The constants Γ_m are defined positive, which leads to a negative imaginary energy accounting for a finite lifetime of quasiparticles. The second term in Eq. (4.36) accounts for quantum jumps. Dropping this term, a semiclassical approximation

[170,171], one obtains that the evolution of the system is effectively given by H_{eff}, which is in general non-Hermitian. Furthermore, quantum trajectories where no quantum jumps occur are described exactly by the non-Hermitian Hamiltonian in Eq. (4.37). This can be achieved experimentally when the environment is being continuously monitored, known as *post-selection* [171, 172] .

Another situation where effective non-Hermitian Hamiltonians appear, more common in the field of solid state, is in the study of Green's functions [59,60,73,173]. Consider again a system that interacts with an environment, $H = H_0 + V$. The (retarded) Green's function is defined as

$$G^r(t) = -i \left\langle \{c^\dagger(t), c(0)\} \right\rangle \theta(t). \tag{4.38}$$

For the isolated system, the Green's function in frequency space is given by

$$g^{r\,-1}(\omega) = (\omega + i\tau)I - H_0, \tag{4.39}$$

where τ is a regularization constant that accounts for causality. The full Green's function results in

$$G^{r\,-1}(\omega) = (\omega + i\tau)I - H_0 - \Sigma(\omega), \tag{4.40}$$

where $\Sigma(\omega)$ is known as the *self-energy* and accounts for the interaction with the environment. Taking the simple case of a constant self-energy, it is easy to see that the resulting Green's function could also be obtained using the effective Hamiltonian

$$H_{eff} = H_0 + \Sigma, \tag{4.41}$$

where the self-energy is, in general, not Hermitian. In the case where the self-energy is frequency dependent one can also obtain effective Hamiltonians, for example using a low energy approximation [174]

$$H_{eff} = H_0 + \Sigma(0). \tag{4.42}$$

The perturbation resulting in dissipation can come from interacting with an environment, but also from disorder or many-body interactions. The effective non-Hermitian term can have a substantial effect in quantities related to the Green's function, such as the density of states, but it is unclear to what extent some non-Hermitian features are still relevant, e.g. the skin effect [73].

Chapter 5

Conclusion

In this dissertation we explored topological states of matter in systems beyond those described by the ten-fold way, when prerequisites used to described conventional topological insulators are removed. In particular we focus on critical systems, without an energy gap, and non-Hermitian systems. Throughout the thesis the entanglement occupancy spectrum and the polarization are used as topological signatures. In paper I, a relation between these two is revealed for Hermitian gapped systems, showing that the correlation matrix spectrum encodes information about the geometry of the eigenstates. The entanglement occupancy spectrum is also studied in paper II, where we reproduce the relation to the polarization for non-Hermitian line-gapped systems. The entanglement spectrum for point-gapped systems, previously overlooked, is shown to hold some topological information about the bulk, carrying a number of virtual topological 1/2 states related to the winding numbers. In paper III we turn to critical systems, which were recently shown to support non-trivial topology. The understanding of topology in these systems is still limited. We expand on it by proposing a method to generalize topological invariants from gapped systems by using finite low temperatures. These systems are intrinsically fine-tuned, and therefore fragile to random disorder. We showed, however, that the topology of the critical point is robust against disorder that preserves criticality. The latter is shown by studying the entanglement entropy and the central charged associated with the critical point, which remains constant until the disorder is strong enough to probe other phases. In paper IV we explore the apparent similar topological features between critical systems and point-gapped systems. We interpolate between the two and show that some topological features of the non-Hermitian system, such as the invariants and the topology of the entanglement occupancy spectrum, can be understood from the related critical model. This relation can be exploited to study the topology of non-Hermitian systems using Hermitian quantum mechanics, as well as employing

the more developed topological classification of non-Hermitian systems to improve our understanding of topology on critical systems.

5.1 Outlook

There are several directions where the work in this thesis can be expanded upon. Regarding the study of the entanglement occupancy spectrum in gapped Hermitian systems, the literature is scarce in reference to the effects of interactions. In non-interacting systems the subsystem correlation matrix has the same information as the reduced density matrix. The spectrum of the reduced density matrix is known to be useful in the study of topology in strongly correlated systems. However, it is unclear how much information the correlation matrix retains when interactions is introduced. This might be useful since the correlation matrix is much easier to computed than the reduced density matrix even when interactions are introduced.

As for the study on critical systems, we provide a general method to extend topological invariants to critical systems, but we only applied it to one dimensional systems. Exploring which invariants one can introduce for two dimensional systems using this method is also interesting, since so far no invariant that has been defined gives the number of edge states directly.

Finally, regarding non-Hermitian systems, the physical interpretation of some of the results in this thesis needs a more closer look. In particular, the polarization studied in paper III is not well defined for point-gapped systems in the thermodynamic limit, which signals it to not being a proper physical quantity. This problem was, actually, shared with critical systems. In the latter case the polarization obtained is not the physical polarization, i.e. its changes do not result in measurable currents, but as discussed in paper III it is still measurable through interferometry experiments. So far, the bulk polarizations studied in non-Hermitian systems have not been shown to have a direct relation to transport properties. This would require to study the dynamics of non-Hermitian systems, which is a non-trivial problem due to the non-unitary time evolution.

Bibliography

[1] C. Ortega-Taberner, "Entanglement spectrum and the bulk polarization." Licentiate Thesis, Stockholm University, 2020.

[2] L. D. Landau, "On the theory of phase transitions," *Zh. Eksp. Teor. Fiz.*, vol. 7, pp. 19–32, 1937.

[3] L. LANDAU and E. LIFSHITZ, "Chapter xiv - phase transitions of the second kind and critical phenomena," in *Statistical Physics (Third Edition)* (L. LANDAU and E. LIFSHITZ, eds.), pp. 446–516, Oxford: Butterworth-Heinemann, third edition ed., 1980.

[4] K. v. Klitzing, G. Dorda, and M. Pepper, "New method for high-accuracy determination of the fine-structure constant based on quantized hall resistance," *Physical Review Letters*, vol. 45, pp. 494–497, Aug. 1980.

[5] D. J. Thouless, M. Kohmoto, M. P. Nightingale, and M. den Nijs, "Quantized hall conductance in a two-dimensional periodic potential," *Physical Review Letters*, vol. 49, pp. 405–408, Aug. 1982.

[6] D. C. Tsui, H. L. Stormer, and A. C. Gossard, "Two-dimensional magneto-transport in the extreme quantum limit," *Physical Review Letters*, vol. 48, pp. 1559–1562, May 1982.

[7] Q. Niu and D. J. Thouless, "Quantised adiabatic charge transport in the presence of substrate disorder and many-body interaction," *Journal of Physics A: Mathematical and General*, vol. 17, pp. 2453–2462, Aug. 1984.

[8] Q. Niu, D. J. Thouless, and Y.-S. Wu, "Quantized hall conductance as a topological invariant," *Phys. Rev. B*, vol. 31, pp. 3372–3377, Mar 1985.

[9] M. Kohmoto, "Topological invariant and the quantization of the Hall conductance," *Annals of Physics*, vol. 160, no. 2, pp. 343–354, 1985.

[10] F. D. M. Haldane, "Model for a quantum hall effect without landau levels: Condensed-matter realization of the "Parity Anomaly"," *Physical Review Letters*, vol. 61, pp. 2015–2018, Oct. 1988.

[11] W. P. Su, J. R. Schrieffer, and A. J. Heeger, "Soliton excitations in polyacetylene," *Physical Review B*, vol. 22, pp. 2099–2111, Aug. 1980.

[12] J. K. Asbóth, L. Oroszlány, and A. Pályi, "A short course on topological insulators," *Lecture Notes in Physics*, 2016.

[13] C. L. Kane and E. J. Mele, "Quantum spin Hall effect in graphene," *Physical review letters*, vol. 95, no. 22, p. 226801, 2005.

[14] C. L. Kane and E. J. Mele, "Z_2 topological order and the quantum spin hall effect," *Physical Review Letters*, vol. 95, p. 146802, Sept. 2005.

[15] A. W. W. Ludwig, "Topological phases: Classification of topological insulators and superconductors of non-interacting fermions, and beyond," *Physica Scripta*, vol. T168, p. 014001, Dec. 2015.

[16] A. P. Schnyder, S. Ryu, A. Furusaki, and A. W. W. Ludwig, "Classification of topological insulators and superconductors in three spatial dimensions," *Physical Review B*, vol. 78, p. 195125, Nov. 2008.

[17] X.-L. Qi and S.-C. Zhang, "Topological insulators and superconductors," *Reviews of Modern Physics*, vol. 83, pp. 1057–1110, oct 2011.

[18] A. Altland and M. R. Zirnbauer, "Nonstandard symmetry classes in mesoscopic normal-superconducting hybrid structures," *Physical Review B*, vol. 55, pp. 1142–1161, Jan. 1997.

[19] M. R. Zirnbauer, "Riemannian symmetric superspaces and their origin in random-matrix theory," *Journal of Mathematical Physics*, vol. 37, no. 10, pp. 4986–5018, 1996.

[20] S. Ryu, A. P. Schnyder, A. Furusaki, and A. W. Ludwig, "Topological insulators and superconductors: Tenfold way and dimensional hierarchy," *New Journal of Physics*, vol. 12, no. 6, p. 065010, 2010.

[21] A. Kitaev, "Periodic table for topological insulators and superconductors," *AIP Conference Proceedings*, vol. 1134, no. 1, pp. 22–30, 2009.

[22] R. Resta, "Theory of the electric polarization in crystals," *Ferroelectrics*, vol. 136, no. 1, pp. 51–55, 1992.

[23] R. Resta, "Macroscopic polarization in crystalline dielectrics: The geometric phase approach," *Reviews of Modern Physics*, vol. 66, pp. 899–915, July 1994.

[24] R. Resta, "Quantum-mechanical position operator in extended systems," *Physical Review Letters*, vol. 80, pp. 1800–1803, Mar. 1998.

[25] D. Vanderbilt and R. D. King-Smith, "Electric polarization as a bulk quantity and its relation to surface charge," *Physical Review B*, vol. 48, pp. 4442–4455, Aug. 1993.

[26] D. Vanderbilt, *Berry Phases in Electronic Structure Theory: Electric Polarization, Orbital Magnetization and Topological Insulators.* Cambridge: Cambridge University Press, 2018.

[27] R. D. King-Smith and D. Vanderbilt, "Theory of polarization of crystalline solids," *Physical Review B*, vol. 47, pp. 1651–1654, Jan. 1993.

[28] H. Watanabe and M. Oshikawa, "Inequivalent berry phases for the bulk polarization," *Physical Review X*, vol. 8, p. 021065, June 2018.

[29] X. G. WEN, "TOPOLOGICAL ORDERS IN RIGID STATES," *International Journal of Modern Physics B*, vol. 04, no. 02, pp. 239–271, 1990.

[30] M. Levin and X.-G. Wen, "Detecting topological order in a ground state wave function," *Physical Review Letters*, vol. 96, p. 110405, Mar. 2006.

[31] A. Kitaev and J. Preskill, "Topological entanglement entropy," *Physical Review Letters*, vol. 96, p. 110404, Mar. 2006.

[32] H. Li and F. D. M. Haldane, "Entanglement spectrum as a generalization of entanglement entropy: Identification of topological order in non-abelian fractional quantum hall effect states," *Physical Review Letters*, vol. 101, no. 1, p. 010504, 2008.

[33] M. Hermanns, A. Chandran, N. Regnault, and B. A. Bernevig, "Haldane statistics in the finite-size entanglement spectra of 1/m fractional quantum Hall states," *Physical Review B*, vol. 84, p. 121309, Sept. 2011.

[34] F. Pollmann, A. M. Turner, E. Berg, and M. Oshikawa, "Entanglement spectrum of a topological phase in one dimension," *Physical Review B*, vol. 81, p. 064439, Feb. 2010.

[35] I. Peschel, M. Kaulke, and Ö. Legeza, "Density-matrix spectra for integrable models," *Annalen der Physik*, vol. 8, no. 2, pp. 153–164, 1999.

Bibliography

[36] I. Peschel, "LETTER TO THE EDITOR: Calculation of reduced density matrices from correlation functions," *Journal of Physics A Mathematical General*, vol. 36, pp. L205–L208, Apr. 2003.

[37] I. Peschel and V. Eisler, "The conceptual background of density-matrix renormalization," in *Computational Many-Particle Physics* (H. Fehske, R. Schneider, and A. Weiße, eds.), pp. 581–596, Berlin, Heidelberg: Springer Berlin Heidelberg, 2008.

[38] Z. Huang and D. P. Arovas, "Edge states, entanglement spectra, and wannier functions in haldane's honeycomb lattice model and its bilayer generalization," *arXiv e-prints*, p. arXiv:1205.6266, May 2012.

[39] Z. Huang and D. P. Arovas, "Entanglement spectrum and Wannier center flow of the Hofstadter problem," *Physical Review B*, vol. 86, p. 245109, Dec. 2012.

[40] S. Ryu and Y. Hatsugai, "Entanglement entropy and the Berry phase in the solid state," *Physical Review B*, vol. 73, p. 245115, June 2006.

[41] N. P. Mitchell, L. M. Nash, D. Hexner, A. M. Turner, and W. T. M. Irvine, "Amorphous topological insulators constructed from random point sets," *Nature Physics*, vol. 14, pp. 380–385, jan 2018.

[42] A. Agarwala and V. B. Shenoy, "Topological insulators in amorphous systems," *Phys. Rev. Lett.*, vol. 118, p. 236402, Jun 2017.

[43] Y. Ando and L. Fu, "Topological crystalline insulators and topological superconductors: From concepts to materials," *Annual Review of Condensed Matter Physics*, vol. 6, 01 2015.

[44] F. Schindler, A. M. Cook, M. G. Vergniory, Z. Wang, S. S. P. Parkin, B. A. Bernevig, and T. Neupert, "Higher-order topological insulators," *Science Advances*, vol. 4, no. 6, p. eaat0346, 2018.

[45] R. Verresen, N. G. Jones, and F. Pollmann, "Topology and edge modes in quantum critical chains," *Physical Review Letters*, vol. 120, p. 057001, Jan. 2018.

[46] R. Verresen, "Topology and edge states survive quantum criticality between topological insulators," 2020.

[47] R. Verresen, R. Thorngren, N. G. Jones, and F. Pollmann, "Gapless topological phases and symmetry-enriched quantum criticality," *Physical Review X*, vol. 11, p. 041059, Dec. 2021.

[48] R. Thorngren, A. Vishwanath, and R. Verresen, "Intrinsically gapless topological phases," *Physical Review B*, vol. 104, p. 075132, Aug. 2021.

[49] O. Balabanov, D. Erkensten, and H. Johannesson, "Topology of critical chiral phases: Multiband insulators and superconductors," *Physical Review Research*, vol. 3, p. 043048, Oct. 2021.

[50] O. Balabanov, C. Ortega-Taberner, and M. Hermanns, "Quantization of topological indices in critical chains at low temperatures," *Physical Review B*, vol. 106, July 2022.

[51] Z. Gong, Y. Ashida, K. Kawabata, K. Takasan, S. Higashikawa, and M. Ueda, "Topological phases of non-hermitian systems," *Physical Review X*, vol. 8, p. 031079, Sept. 2018.

[52] K. Kawabata, K. Shiozaki, M. Ueda, and M. Sato, "Symmetry and topology in non-hermitian physics," *Physical Review X*, vol. 9, p. 041015, Oct. 2019.

[53] H. Zhou and J. Y. Lee, "Periodic table for topological bands with non-Hermitian symmetries," *Physical Review B*, vol. 99, p. 235112, June 2019.

[54] Z. Lin, H. Ramezani, T. Eichelkraut, T. Kottos, H. Cao, and D. N. Christodoulides, "Unidirectional invisibility induced by $\mathcal{PT}$-symmetric periodic structures," *Phys. Rev. Lett.*, vol. 106, p. 213901, May 2011.

[55] A. Regensburger, C. Bersch, M.-A. Miri, G. Onishchukov, D. Christodoulides, and U. Peschel, "Parity-time synthetic photonic lattices," *Nature*, vol. 488, pp. 167–71, 08 2012.

[56] B. Peng, Şahin Kaya Özdemir, M. Liertzer, W. Chen, J. Kramer, H. Yılmaz, J. Wiersig, S. Rotter, and L. Yang, "Chiral modes and directional lasing at exceptional points," *Proceedings of the National Academy of Sciences*, vol. 113, no. 25, pp. 6845–6850, 2016.

[57] H. Hodaei, A. Hassan, S. Wittek, H. Garcia-Gracia, R. Elganainy, D. Christodoulides, and M. Khajavikhan, "Enhanced sensitivity at higher-order exceptional points," *Nature*, vol. 548, pp. 187–191, 08 2017.

Bibliography

[58] W. Chen, S. Ozdemir, G. Zhao, J. Wiersig, and L. Yang, "Exceptional points enhance sensing in an optical microcavity," *Nature*, vol. 548, pp. 192–196, 08 2017.

[59] V. Kozii and L. Fu, "Non-hermitian topological theory of finite-lifetime quasiparticles: Prediction of bulk fermi arc due to exceptional point," 2017.

[60] T. Yoshida, R. Peters, N. Kawakami, and Y. Hatsugai, "Exceptional band touching for strongly correlated systems in equilibrium," *Progress of Theoretical and Experimental Physics*, vol. 2020, jul 2020.

[61] M. Kreibich, J. Main, H. Cartarius, and G. Wunner, "Realizing $\mathcal{PT}$-symmetric non-hermiticity with ultracold atoms and hermitian multiwell potentials," *Phys. Rev. A*, vol. 90, p. 033630, Sep 2014.

[62] A. Ghatak, M. Brandenbourger, J. van Wezel, and C. Coulais, "Observation of non-hermitian topology and its bulk-edge correspondence in an active mechanical metamaterial," *Proceedings of the National Academy of Sciences*, vol. 117, pp. 29561–29568, nov 2020.

[63] C. Yin, H. Jiang, L. Li, R. Lü, and S. Chen, "Geometrical meaning of winding number and its characterization of topological phases in one-dimensional chiral non-Hermitian systems," *Physical Review A: Atomic, Molecular, and Optical Physics*, vol. 97, p. 052115, May 2018.

[64] F. Alsallom, L. Herviou, O. V. Yazyev, and M. Brzezińska, "Fate of the non-Hermitian skin effect in many-body fermionic systems," 2021.

[65] Y. Ashida, Z. Gong, and M. Ueda, "Non-hermitian physics," *Advances in Physics*, vol. 69, no. 3, pp. 249–435, 2020.

[66] S. Masuda and M. Nakamura, "Relationship between the Electronic Polarization and the Winding Number in Non-Hermitian Systems," *Journal of the Physical Society of Japan*, vol. 91, p. 043701, Apr. 2022.

[67] S. Masuda and M. Nakamura, "The electronic polarization in the non-bloch band theory," 2022.

[68] E. J. Bergholtz, J. C. Budich, and F. K. Kunst, "Exceptional topology of non-Hermitian systems," *Reviews of Modern Physics*, vol. 93, p. 015005, Feb. 2021.

[69] F. K. Kunst, E. Edvardsson, J. C. Budich, and E. J. Bergholtz, "Biorthogonal bulk-boundary correspondence in non-hermitian systems," *Physical Review Letters*, vol. 121, p. 026808, July 2018.

[70] E. Edvardsson and E. Ardonne, "Sensitivity of non-Hermitian systems," *Physical Review B*, vol. 106, p. 115107, Sept. 2022.

[71] E. Edvardsson, F. K. Kunst, T. Yoshida, and E. J. Bergholtz, "Phase transitions and generalized biorthogonal polarization in non-Hermitian systems," *Physical Review Research*, vol. 2, p. 043046, Oct. 2020.

[72] N. Okuma and M. Sato, "Quantum anomaly, non-Hermitian skin effects, and entanglement entropy in open systems," *Physical Review B*, vol. 103, p. 085428, Feb. 2021.

[73] N. Okuma and M. Sato, "Non-hermitian skin effects in hermitian correlated or disordered systems: Quantities sensitive or insensitive to boundary effects and pseudo-quantum-number," *Physical Review Letters*, vol. 126, apr 2021.

[74] N. Okuma, K. Kawabata, K. Shiozaki, and M. Sato, "Topological Origin of Non-Hermitian Skin Effects," *Physical Review Letters*, vol. 124, p. 086801, Feb. 2020.

[75] L. Herviou, J. H. Bardarson, and N. Regnault, "Defining a bulk-edge correspondence for non-Hermitian Hamiltonians via singular-value decomposition," *Physical Review A*, vol. 99, p. 052118, May 2019.

[76] L. Herviou, N. Regnault, and J. H. Bardarson, "Entanglement spectrum and symmetries in non-Hermitian fermionic non-interacting models," *SciPost Physics*, vol. 7, p. 069, Nov. 2019.

[77] C.-K. Chiu, J. C. Y. Teo, A. P. Schnyder, and S. Ryu, "Classification of topological quantum matter with symmetries," *Reviews of Modern Physics*, vol. 88, p. 035005, Aug. 2016.

[78] B. A. Bernevig, T. L. Hughes, and S.-C. Zhang, "Quantum spin hall effect and topological phase transition in HgTe quantum wells," *Science*, vol. 314, pp. 1757–1761, dec 2006.

[79] M. KoÌnig, S. Wiedmann, C. BruÌne, A. Roth, H. Buhmann, L. W. Molenkamp, X.-L. Qi, and S.-C. Zhang, "Quantum spin hall insulator state in HgTe quantum wells," *Science*, vol. 318, pp. 766–770, nov 2007.

[80] I. Knez, R.-R. Du, and G. Sullivan, "Evidence for helical edge modes in inverted InAs/GaSb quantum wells," *Phys. Rev. Lett.*, vol. 107, p. 136603, Sep 2011.

[81] I. K. Drozdov, A. Alexandradinata, S. Jeon, S. Nadj-Perge, H. Ji, R. J. Cava, B. A. Bernevig, and A. Yazdani, "One-dimensional topological edge states of bismuth bilayers," *Nature Physics*, vol. 10, pp. 664–669, aug 2014.

[82] F. Reis, G. Li, L. Dudy, M. Bauernfeind, S. Glass, W. Hanke, R. Thomale, J. Schäfer, and R. Claessen, "Bismuthene on a SiC substrate: A candidate for a high-temperature quantum spin hall material," *Science*, vol. 357, pp. 287–290, jul 2017.

[83] L. Peng, Y. Yuan, G. Li, X. Yang, J.-J. Xian, C.-J. Yi, Y.-G. Shi, and Y.-S. Fu, "Observation of topological states residing at step edges of WTe2," *Nature Communications*, vol. 8, sep 2017.

[84] S. Tang, C. Zhang, D. Wong, Z. Pedramrazi, H.-Z. Tsai, C. Jia, B. Moritz, M. Claassen, H. Ryu, S. Kahn, J. Jiang, H. Yan, M. Hashimoto, D. Lu, R. G. Moore, C.-C. Hwang, C. Hwang, Z. Hussain, Y. Chen, M. M. Ugeda, Z. Liu, X. Xie, T. P. Devereaux, M. F. Crommie, S.-K. Mo, and Z.-X. Shen, "Quantum spin hall state in monolayer 1t'-WTe2," *Nature Physics*, vol. 13, pp. 683–687, June 2017.

[85] L. Fu, C. L. Kane, and E. J. Mele, "Topological insulators in three dimensions," *Physical Review Letters*, vol. 98, mar 2007.

[86] R. Roy, "Topological phases and the quantum spin Hall effect in three dimensions," *Physical Review B*, vol. 79, p. 195322, May 2009.

[87] J. E. Moore and L. Balents, "Topological invariants of time-reversal-invariant band structures," *Phys. Rev. B*, vol. 75, p. 121306, Mar 2007.

[88] D. Hsieh, D. Qian, L. Wray, Y. Xia, Y. S. Hor, R. J. Cava, and M. Z. Hasan, "A topological dirac insulator in a quantum spin hall phase," *Nature*, vol. 452, pp. 970–974, Apr. 2008.

[89] Y. Xia, D. Qian, D. Hsieh, L. Wray, A. Pal, H. Lin, A. Bansil, D. Grauer, Y. S. Hor, R. J. Cava, and M. Z. Hasan, "Observation of a large-gap topological-insulator class with a single dirac cone on the surface," *Nature Physics*, vol. 5, pp. 398–402, May 2009.

[90] Y. L. Chen, J. G. Analytis, J.-H. Chu, Z. K. Liu, S.-K. Mo, X. L. Qi, H. J. Zhang, D. H. Lu, X. Dai, Z. Fang, S. C. Zhang, I. R. Fisher, Z. Hussain, and Z.-X. Shen, "Experimental realization of a three-dimensional topological insulator, bi2te3," *Science*, vol. 325, pp. 178–181, July 2009.

[91] D. Hsieh, Y. Xia, D. Qian, L. Wray, F. Meier, J. H. Dil, J. Osterwalder, L. Patthey, A. V. Fedorov, H. Lin, A. Bansil, D. Grauer, Y. S. Hor, R. J. Cava, and M. Z. Hasan, "Observation of time-reversal-protected single-dirac-cone topological-insulator states in bi_2te_3 and sb_2te_3," *Phys. Rev. Lett.*, vol. 103, p. 146401, Sep 2009.

[92] Y. Ando, "Topological insulator materials," *Journal of the Physical Society of Japan*, vol. 82, p. 102001, oct 2013.

[93] M. Leijnse and K. Flensberg, "Introduction to topological superconductivity and majorana fermions," *Semiconductor Science and Technology*, vol. 27, p. 124003, nov 2012.

[94] A. Y. Kitaev, "Unpaired Majorana fermions in quantum wires," *Physics-Uspekhi*, vol. 44, pp. 131–136, Oct. 2001.

[95] V. Mourik, K. Zuo, S. M. Frolov, S. R. Plissard, E. P. A. M. Bakkers, and L. P. Kouwenhoven, "Signatures of majorana fermions in hybrid superconductor-semiconductor nanowire devices," *Science*, vol. 336, pp. 1003–1007, May 2012.

[96] X. Wan, A. M. Turner, A. Vishwanath, and S. Y. Savrasov, "Topological semimetal and fermi-arc surface states in the electronic structure of pyrochlore iridates," *Phys. Rev. B*, vol. 83, p. 205101, May 2011.

[97] M. Z. Hasan, S.-Y. Xu, I. Belopolski, and S.-M. Huang, "Discovery of weyl fermion semimetals and topological fermi arc states," *Annual Review of Condensed Matter Physics*, vol. 8, pp. 289–309, mar 2017.

[98] S. Matern and M. Hermanns, "Entanglement in 3D kitaev spin liquids," *Journal of Statistical Mechanics: Theory and Experiment*, vol. 2018, no. 6, p. 063101, 2018.

[99] M. Atala, M. Aidelsburger, J. T. Barreiro, D. Abanin, T. Kitagawa, E. Demler, and I. Bloch, "Direct measurement of the zak phase in topological bloch bands," *Nature Physics*, vol. 9, pp. 795–800, nov 2013.

[100] E. J. Meier, F. A. An, and B. Gadway, "Observation of the topological soliton state in the su–schrieffer–heeger model," *Nature Communications*, vol. 7, dec 2016.

Bibliography

[101] W. Shockley, "On the surface states associated with a periodic potential," *Phys. Rev.*, vol. 56, pp. 317–323, Aug 1939.

[102] J.-N. Fuchs and F. Piéchon, "Orbital embedding and topology of one-dimensional two-band insulators," *Physical Review B*, vol. 104, dec 2021.

[103] L. Fu, "Topological crystalline insulators," *Phys. Rev. Lett.*, vol. 106, p. 106802, Mar 2011.

[104] S. Pancharatnam, "Generalized theory of interference, and its applications," *Proceedings of the Indian Academy of Sciences - Section A*, vol. 44, pp. 247–262, 1956.

[105] Y. Aharonov and D. Bohm, "Significance of electromagnetic potentials in the quantum theory," *Physical Review*, vol. 115, pp. 485–491, Aug. 1959.

[106] M. V. Berry, "Quantal phase factors accompanying adiabatic changes," *Proceedings of the Royal Society of London. A. Mathematical and Physical Sciences*, vol. 392, no. 1802, pp. 45–57, 1984.

[107] J. Zak, "Berry's phase for energy bands in solids," *Physical Review Letters*, vol. 62, pp. 2747–2750, June 1989.

[108] P.-O. Löwdin, "Quantum theory of many-particle systems. I. Physical interpretations by means of density matrices, natural spin-orbitals, and convergence problems in the method of configurational interaction," *Physical Review*, vol. 97, pp. 1474–1489, Mar. 1955.

[109] F. Plasser, M. Ruckenbauer, S. Mai, M. Oppel, P. Marquetand, and L. Gonzalez, "Efficient and flexible computation of many-electron wave function overlaps," *J Chem Theory Comput.*, vol. 12, pp. 1207–1219, Mar. 2018.

[110] J. Song and E. Prodan, "AIII and BDI topological systems at strong disorder," *Physical Review B*, vol. 89, p. 224203, June 2014.

[111] I. Mondragon-Shem, T. L. Hughes, J. Song, and E. Prodan, "Topological criticality in the chiral-symmetric AIII class at strong disorder," *Physical Review Letters*, vol. 113, p. 046802, July 2014.

[112] A. Hayward, C. Schweizer, M. Lohse, M. Aidelsburger, and F. Heidrich-Meisner, "Topological charge pumping in the interacting bosonic Rice-Mele model," *Physical Review B*, vol. 98, p. 245148, Dec. 2018.

[113] D. J. Thouless, "Quantization of particle transport," *Physical Review B*, vol. 27, pp. 6083–6087, May 1983.

[114] N. Marzari and D. Vanderbilt, "Maximally localized generalized Wannier functions for composite energy bands," *Physical Review B*, vol. 56, pp. 12847–12865, Nov. 1997.

[115] S. Kivelson, "Wannier functions in one-dimensional disordered systems: Application to fractionally charged solitons," *Physical Review B*, vol. 26, pp. 4269–4277, Oct. 1982.

[116] R. B. Laughlin, "Anomalous quantum hall effect: An incompressible quantum fluid with fractionally charged excitations," *Phys. Rev. Lett.*, vol. 50, pp. 1395–1398, May 1983.

[117] F. D. M. Haldane, "Fractional quantization of the hall effect: A hierarchy of incompressible quantum fluid states," *Phys. Rev. Lett.*, vol. 51, pp. 605–608, Aug 1983.

[118] B. I. Halperin, "Theory of the quantized Hall conductance," *Helv. Phys. Acta*, vol. 56, pp. 75–102, 1983.

[119] A. Kitaev, "Anyons in an exactly solved model and beyond," *Annals of Physics*, vol. 321, no. 1, pp. 2–111, 2006.

[120] L. Balents, "Spin liquids in frustrated magnets," *Nature*, vol. 464, no. 7286, pp. 199–208, 2010.

[121] O. S. Zozulya, M. Haque, K. Schoutens, and E. H. Rezayi, "Bipartite entanglement entropy in fractional quantum Hall states," *Physical Review B*, vol. 76, p. 125310, Sept. 2007.

[122] H. Yao and X.-L. Qi, "Entanglement entropy and entanglement spectrum of the kitaev model," *Physical Review Letters*, vol. 105, p. 080501, Aug. 2010.

[123] X.-L. Qi, H. Katsura, and A. W. W. Ludwig, "General relationship between the entanglement spectrum and the edge state spectrum of topological quantum states," *Physical Review Letters*, vol. 108, p. 196402, May 2012.

[124] L. Fidkowski, "Entanglement spectrum of topological insulators and superconductors," *Physical Review Letters*, vol. 104, no. 13, p. 130502, 2010.

[125] A. Alexandradinata, T. L. Hughes, and B. A. Bernevig, "Trace index and spectral flow in the entanglement spectrum of topological insulators," *Physical Review B*, vol. 84, p. 195103, Nov. 2011.

Bibliography

[126] T. L. Hughes, E. Prodan, and B. A. Bernevig, "Inversion-symmetric topological insulators," *Physical Review B*, vol. 83, p. 245132, June 2011.

[127] M. P. Zaletel, R. S. K. Mong, and F. Pollmann, "Flux insertion, entanglement, and quantized responses," *Journal of Statistical Mechanics: Theory and Experiment*, vol. 2014, p. P10007, Oct. 2014.

[128] C. H. Lee and P. Ye, "Free-fermion entanglement spectrum through wannier interpolation," *Physical Review B*, vol. 91, feb 2015.

[129] S.-Q. Shen, *Topological Insulators: Dirac Equation in Condensed Matters*. No. 174 in Springer Series in Solid-State Sciences, Heidelberg ; New York: Springer, 2012.

[130] S. Kivelson, D.-H. Lee, and S.-C. Zhang, "Global phase diagram in the quantum hall effect," *Phys. Rev. B*, vol. 46, pp. 2223–2238, Jul 1992.

[131] D. E. Khmel'nitskii, "Quantization of hall conductivity," *Pis'ma Zh. Eksp. Teor. Fiz. 38*, vol. 38, pp. 454–458, Nov 1983.

[132] D.-H. Lee, S. Kivelson, and S.-C. Zhang, "Quasiparticle charge and the activated conductance of a quantum hall liquid," *Phys. Rev. Lett.*, vol. 68, pp. 2386–2389, Apr 1992.

[133] H. Levine, S. B. Libby, and A. M. M. Pruisken, "Electron delocalization by a magnetic field in two dimensions," *Phys. Rev. Lett.*, vol. 51, pp. 1915–1918, Nov 1983.

[134] R. B. Laughlin, "Levitation of extended-state bands in a strong magnetic field," *Phys. Rev. Lett.*, vol. 52, pp. 2304–2304, Jun 1984.

[135] D. M. Long, P. J. D. Crowley, and A. Chandran, "Coupled layer construction for synthetic hall effects in driven systems," *Phys. Rev. B*, vol. 106, p. 144203, Oct 2022.

[136] B. Fu, J.-Y. Zou, Z.-A. Hu, H.-W. Wang, and S.-Q. Shen, "Quantum Anomalous Semimetals," Mar. 2022.

[137] C.-E. Bardyn, L. Wawer, A. Altland, M. Fleischhauer, and S. Diehl, "Probing the topology of density matrices," *Physical Review X*, vol. 8, p. 011035, Feb. 2018.

[138] C. Holzhey, F. Larsen, and F. Wilczek, "Geometric and Renormalized Entropy in Conformal Field Theory," *Nuclear Physics B*, vol. 424, pp. 443–467, Aug. 1994.

[139] P. Calabrese and J. Cardy, "Entanglement Entropy and Quantum Field Theory," *Journal of Statistical Mechanics: Theory and Experiment*, vol. 2004, p. P06002, June 2004.

[140] P. Calabrese and J. Cardy, "Entanglement entropy and conformal field theory," *Journal of Physics A: Mathematical and Theoretical*, vol. 42, p. 504005, Dec. 2009.

[141] G. Refael and J. E. Moore, "Entanglement entropy of random quantum critical points in one dimension," *Phys. Rev. Lett.*, vol. 93, p. 260602, Dec 2004.

[142] P.-Y. Chang, J.-S. You, X. Wen, and S. Ryu, "Entanglement spectrum and entropy in topological non-Hermitian systems and nonunitary conformal field theory," *Physical Review Research*, vol. 2, p. 033069, July 2020.

[143] L.-M. Chen, S. A. Chen, and P. Ye, "Entanglement, non-hermiticity, and duality," *SciPost Phys.*, vol. 11, no. 1, p. 3, 2021.

[144] R. Modak and B. P. Mandal, "Eigenstate entanglement entropy in a PT-invariant non-Hermitian system," *Physical Review A: Atomic, Molecular, and Optical Physics*, vol. 103, p. 062416, June 2021.

[145] W. D. Heiss, "The physics of exceptional points," *Journal of Physics A: Mathematical and Theoretical*, vol. 45, p. 444016, oct 2012.

[146] R. Arouca, J. Cayao, and A. M. Black-Schaffer, "Exceptionally enhanced topological superconductivity," 2022.

[147] K. Kawabata, T. Bessho, and M. Sato, "Classification of exceptional points and non-hermitian topological semimetals," *Physical Review Letters*, vol. 123, aug 2019.

[148] G.-L. Zhang, D. Liu, and M.-H. Yung, "Observation of exceptional point in a PT broken non-hermitian system simulated using a quantum circuit," *Scientific Reports*, vol. 11, July 2021.

[149] D. Bernard and A. LeClair, "A classification of non-hermitian random matrices," in *Statistical Field Theories*, pp. 207–214, Dordrecht: Springer Netherlands, 2002.

[150] F. Scholtz, H. Geyer, and F. Hahne, "Quasi-Hermitian operators in quantum mechanics and the variational principle," *Annals of Physics*, vol. 213, pp. 74–101, Jan. 1992.

[151] H. B. Geyer, W. D. Heiss, and F. G. Scholtz, "The physical interpretation of non-Hermitian Hamiltonians and other observables," *Canadian Journal of Physics*, vol. 86, pp. 1195–1201, Oct. 2008.

[152] C. M. Bender, "Making sense of non-Hermitian Hamiltonians," *Reports on Progress in Physics*, vol. 70, pp. 947–1018, June 2007.

[153] C. M. Bender, "*PT*-symmetric quantum theory," *Journal of Physics: Conference Series*, vol. 631, p. 012002, July 2015.

[154] D. C. Brody, "Biorthogonal quantum mechanics," *Journal of Physics A: Mathematical and Theoretical*, vol. 47, p. 035305, dec 2013.

[155] T. Curtright and L. Mezincescu, "Biorthogonal quantum systems," *Journal of Mathematical Physics*, vol. 48, p. 092106, sep 2007.

[156] M. Wagner, F. Dangel, H. Cartarius, J. Main, and G. Wunner, "Numerical calculation of the complex berry phase in non-Hermitian systems," *Acta Polytechnica*, vol. 57, p. 470, Dec. 2017.

[157] S.-D. Liang and G.-Y. Huang, "Topological invariance and global Berry phase in non-Hermitian systems," *Physical Review A: Atomic, Molecular, and Optical Physics*, vol. 87, p. 012118, Jan. 2013.

[158] H. Shen, B. Zhen, and L. Fu, "Topological band theory for non-hermitian hamiltonians," *Physical Review Letters*, vol. 120, p. 146402, Apr. 2018.

[159] S. Yao and Z. Wang, "Edge States and Topological Invariants of Non-Hermitian Systems," *Physical Review Letters*, vol. 121, p. 086803, Aug. 2018.

[160] H. Jiang, C. Yang, and S. Chen, "Topological invariants and phase diagrams for one-dimensional two-band non-Hermitian systems without chiral symmetry," *Physical Review A: Atomic, Molecular, and Optical Physics*, vol. 98, p. 052116, Nov. 2018.

[161] N. Hatano and D. R. Nelson, "Localization Transitions in Non-Hermitian Quantum Mechanics," *Physical Review Letters*, vol. 77, pp. 570–573, July 1996.

[162] N. Hatano and D. R. Nelson, "Vortex pinning and non-Hermitian quantum mechanics," *Physical Review B*, vol. 56, pp. 8651–8673, Oct. 1997.

[163] N. Hatano and D. R. Nelson, "Non-Hermitian delocalization and eigenfunctions," *Physical Review B*, vol. 58, pp. 8384–8390, Oct. 1998.

[164] J. C. Budich and E. J. Bergholtz, "Non-hermitian topological sensors," *Phys. Rev. Lett.*, vol. 125, p. 180403, Oct 2020.

[165] E. Lee, H. Lee, and B.-J. Yang, "Many-body approach to non-Hermitian physics in fermionic systems," *Physical Review B*, vol. 101, p. 121109, Mar. 2020.

[166] L. Lu, J. D. Joannopoulos, and M. Soljačić, "Topological photonics," *Nature Photonics*, vol. 8, pp. 821–829, oct 2014.

[167] J. Doppler, A. A. Mailybaev, J. Bõhm, U. Kuhl, A. Girschik, F. Libisch, T. J. Milburn, P. Rabl, N. Moiseyev, and S. Rotter, "Dynamically encircling an exceptional point for asymmetric mode switching," *Nature*, vol. 537, pp. 76–79, jul 2016.

[168] A. J. Daley, "Quantum trajectories and open many-body quantum systems," *Advances in Physics*, vol. 63, pp. 77–149, mar 2014.

[169] M. B. Plenio and P. L. Knight, "The quantum-jump approach to dissipative dynamics in quantum optics," *Reviews of Modern Physics*, vol. 70, pp. 101–144, jan 1998.

[170] F. Roccati, G. M. Palma, F. Ciccarello, and F. Bagarello, "Non-hermitian physics and master equations," *Open Systems & Information Dynamics*, vol. 29, mar 2022.

[171] F. Minganti, A. Miranowicz, R. W. Chhajlany, and F. Nori, "Quantum exceptional points of non-hermitian hamiltonians and liouvillians: The effects of quantum jumps," *Physical Review A*, vol. 100, dec 2019.

[172] M. Naghiloo, M. Abbasi, Y. N. Joglekar, and K. W. Murch, "Quantum state tomography across the exceptional point in a single dissipative qubit," *Nature Physics*, vol. 15, pp. 1232–1236, oct 2019.

[173] T. Yoshida, R. Peters, N. Kawakami, and Y. Hatsugai, "Symmetry-protected exceptional rings in two-dimensional correlated systems with chiral symmetry," *Physical Review B*, vol. 99, mar 2019.

[174] K. Yang, D. Varjas, E. J. Bergholtz, S. Morampudi, and F. Wilczek, "Exceptional dynamics of interacting spin liquids," 2022.